MINISTRY OF NATIONAL EDUCATION

THE ANNALS OF "DUNAREA DE JOS" UNIVERSITY OF GALATI

Fascicle IX
METALLURGY AND MATERIALS SCIENCE

YEAR XXXII (XXXVII)
December 2014, no. 4

ISSN 1453-083X

2014
GALATI UNIVERSITY PRESS

EDITORIAL BOARD

Table of Contents

THE ANNALS OF "DUNAREA DE JOS" UNIVERSITY OF GALATI
FASCICLE IX. METALLURGY AND MATERIALS SCIENCE
N°. 4 – 2014, ISSN 1453 – 083X

INFLUENCE OF COOLING OIL ON THE SURFACE QUALITY OF THE ROLLED STRIP

Tamara RADU, Stela CONSTANTINESCU, Florentina POTECAȘU
"Dunarea de Jos" University of Galati, Romania
e-mail: tradu@ugal.ro

ABSTRACT

The excess of emulsion used in the lamination process leads to the formation of drops which in the annealing process forms spots of burned emulsion. It was also shown to cause formation areas with high carbon concentrations on the surface of the steel strips, after annealing. In the cold rolling process, the surface of the rolled strip is contaminated by cooling oil or emulsion and other chemical compounds, which could considerably influence the final quality of the strip.

The microscopic analysis of the spots of burned emulsion showed a complex phase structure resulting from the combustion rate through the interaction between the emulsion and the contaminating residues, as well as the one between the emulsion and the steel substrate.

KEYWORDS: rolling process, splices, scratches, plies, cooling oil

1. Introduction

In the cold rolling process, the surface of the rolled strip is contaminated by cooling oil or emulsion and other pollutants, which could considerably influence the final quality of the strip. Unfortunately, this will usually become visible only after subsequent operations such as annealing, galvanizing, phosphate or powder coating, etc. [1].

The emulsion is a system consisting of two liquid phases, one dispersed in the other. This is lubricating oil in water emulsion, in which different ingredients are introduced to ensure some characteristics and to improve others [2, 3]. In the case of the cold rolling process, the proper lubrication can facilitate: reduction of the thickness of hot rolled strips at acceptable rolling speed; control of heat losses; corrosion protection of the steel band that will be processed and also of the rolling equipment; obtaining quality surfaces of rolling thin strips [4, 5].

The classification of the defects of cold rolled strips can be done on two criteria [6, 7]:

- appearance and structure of the defect;
- technological step.

The experimental research aimed at identifying and explaining surface defects caused by oils used in cold rolling. These oils can reach the cold rolled and heat treatment process, decompose and burn causing the appearance of specific surface defects [8].

2. Experimental research

The methods of analysis used were:

- thermogravimetric analysis to assess the stability of emulsions and oil heat treatment applied on cold rolled thin strips;
- analysis of macroscopic surface defects;
- microscopic analysis of emulsion formation burnt spots.

The analysis of surface defects on thin steel strips produced by Galfinband S.A. led to the identification of several cases of production.

A primary cause of the occurrence of defects on the surface of very thin steel strips is the most common raw material. The identified raw material surface defects are: printing cylinder rolling folds of drawing up, scratches, splices (Fig. 1).

Surface defects caused by cooling emulsion occur mainly during the heat treatment when the emulsion used in excess generates spots of burned emulsion.

Emulsion and oil removal from steel strips can be done through several simple methods, which provide low removal efficiency.

One of these methods applied at Galfinband S.A. is carried out by means of the cloth scraper or stitched textile parts, which rapidly absorb the oil and/or emulsion. These scrapers are unusable in a short time. In addition, the release of textile fibers contributes thus to the staining of the strip and decreases its quality (for example, the occurrence of scratches on the strip surface).

Fig. 1. *Raw material surface defects (x1/1)*

The presence on the surface of the steel strip of fine iron oxides particles acting as a catalyst provides a highly favorable environment for the process of oil oxidation. During heat treatment, the products are reacted in the gaseous atmosphere of the heat treatment furnace and on the surface of the steel strip.

The annealing treatment was shown to cause the formation of areas with high carbon concentrations on the surface of strip.

3. Results and discussion

The rolling behavior of emulsions during heat treatment according to their degree of wear and temperature was determined by thermogravimetric analysis (Figure 2) and was set based on transformation temperatures and mass loss.

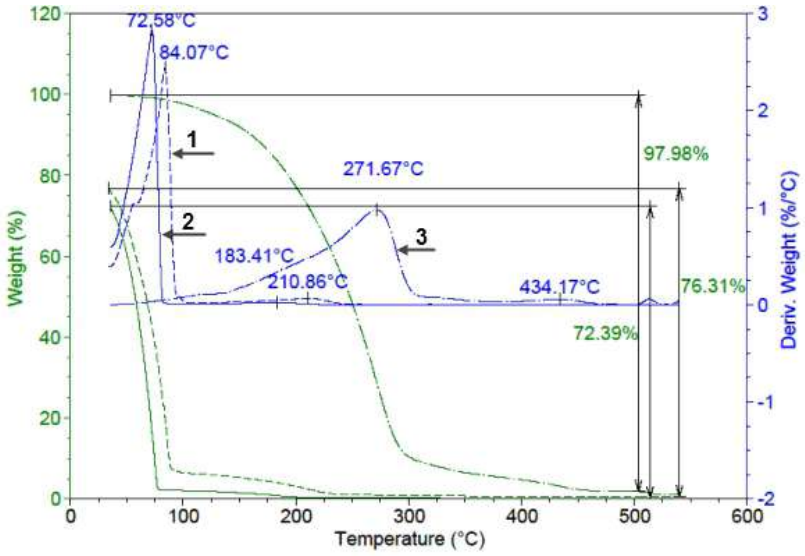

Fig. 2. *Analysis of emulsion stability according to temperature*
1 – used emulsion; 2 – fresh emulsion; 3 – mineral oil

For clean emulsion (oil 4.5% and water), mass loss is 76.31%. A temperature of 72.58 ºC corresponds to the maximum kinetics of water evaporation. The next inflection is at 183.41 ºC and corresponds to the maximum kinetics of lubricating oil mass loss. At temperatures above 200 ºC, no mass losses are registered. For used emulsion two transformation temperatures were observed, and a total mass loss of 76.31%. A temperature of 84.07 ºC corresponds to the maximum kinetics of the water evaporation process and a temperature of 210.86 ºC corresponds to the lubricating oil. At temperatures above 350 ºC mass losses are insignificant.

Note that the transformation temperatures of emulsions and oil are under the heat treatment temperature and therefore the mentioned transformations occur during heat treatment. Weight loss shows that residues will remain on the board even higher with more waste emulsion.

Carbonaceous residues that remain on the surface of the strip after rolling must be strictly limited because of their negative influence on all subsequent processing stages [9]. Research has shown that increasing the degree of contamination of the emulsion by recirculation and wear can generate an amount of carbon residue up to 8 mg/m^2. During heat treatment, residual products are reacted further with

the gaseous products, the heat treating furnace atmosphere and with the surface of the steel strip, causing the formation of areas of high carbon concentration on the surface of the strip, subjected to the annealing process [10].

The presence on the surface of the steel strip of fine iron oxide particles acting as a catalyst leads to a highly favorable environment for oil oxidation [11].

Emulsion spots and burned emulsion are emulsion cracked residues deposited on the surface of the steel strip after cold rolling and heat treatment.

Emulsion spots are easily recognized with the naked eye. They are dark and of irregular shape, spread on the cold rolled strip surface and heat treated as seen in Fig. 3.

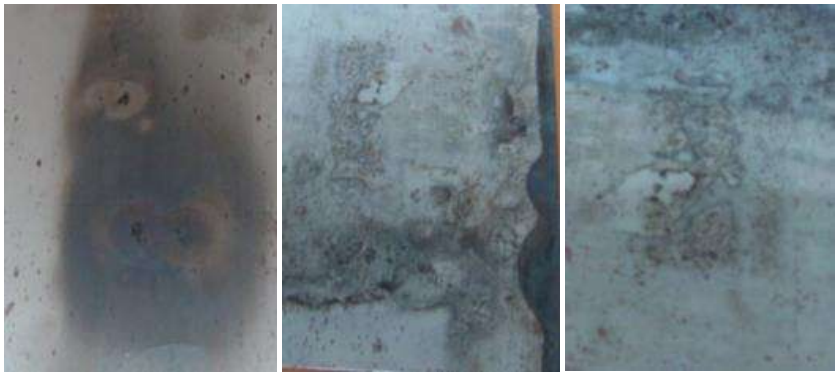

Fig. 3. *Burned emulsion on the surface of the heat treated strip (x1/10)*

The burned emulsion spots on the surface of the cold-rolled steel strip are caused by cracked emulsion residues from the thermal treatment of annealing. These residues are the result of unevaporated emulsion during annealing, which occurs due to an excess of emulsion on the cold rolled strip.

The microscopic analysis of defects was performed only on the heat treated steel strip [12].

The defects observed in the highest proportion on heat-treated steel bands are burned emulsion spots. The microscopic analysis of such black spots showed a complex phase structure of the resulting residues from the combustion rate. This is due to both emulsion interactions with contaminating residues, as well as due to the emulsion interacting with steel support.

It was also found that, as explained above, the main cause of the formation of this defect is emulsion excess [10]. In Figure 4 it can be seen that the emulsion starts to stain a large drop that flowed on the surface of the steel forming radiating streams.

The spot droplet formed is dense and dark and the area where they spread is diffuse, without allowing compactness to reveal the steel bracket that appears white. At a magnification higher than 100, it can be seen that the core of started emulsion stain has also a heterogeneous structure showing black and gray burnt areas and less brown burnt areas. Large drops of emulsion are formed due to several causes.

Emulsion spots are formed from singular and excessively high drops and will have nearly circular shapes (Fig. 5a). Burned emulsion spots come from several neighboring droplets whose small streams flow intertwined, forming less compact large spots (Fig. 5b).

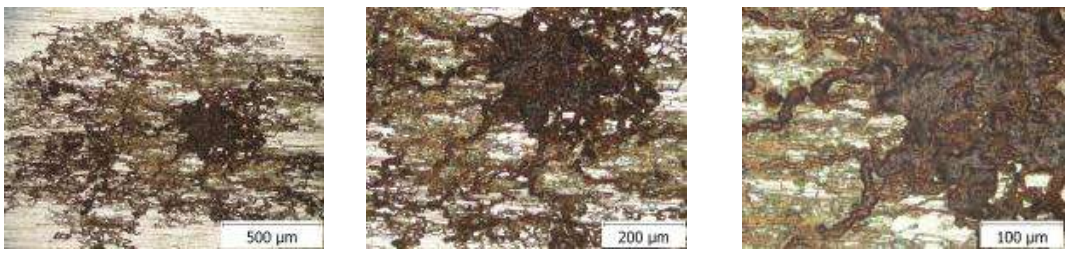

Fig. 4. *Formation of emulsion spots at different magnifications*

We also observed atypical distributions compared to those listed above, as shown in Figure 6. These spots, very diffuse and difficult to see with the naked eye, are formed from the excess of emulsion accumulated on bumps during the cold rolling process.

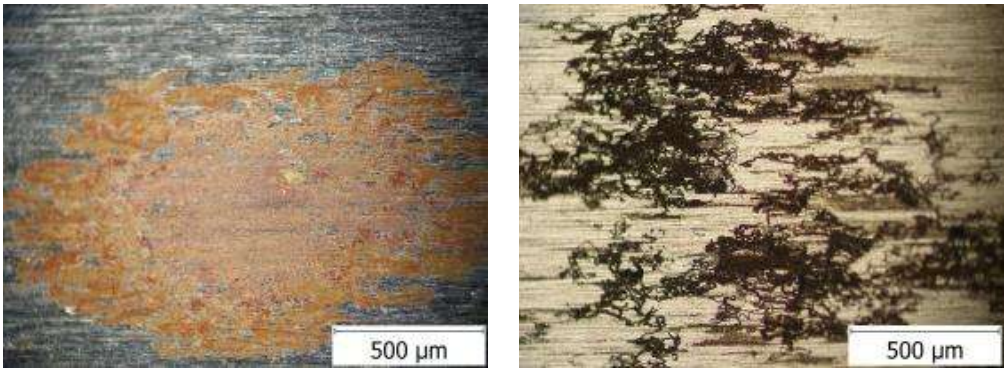

a b

Fig. 5. *Aspects of burned emulsion spots*
a - compact spots; b - less compact spots

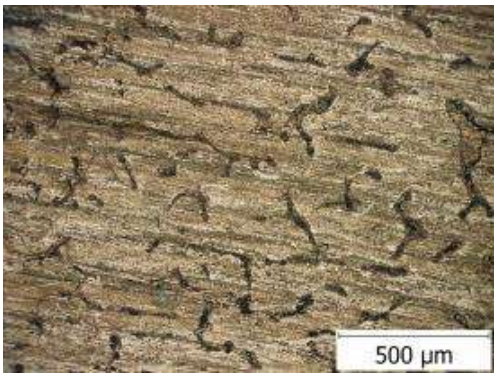

Fig. 6. *Spots of burned emulsion with atypical forms*

Figure 7 shows the structure of a burned emulsion spot with areas of corrosion of steel support (rust) areas that formed carbon or combustion ash (light gray) and areas of black burned emulsion.

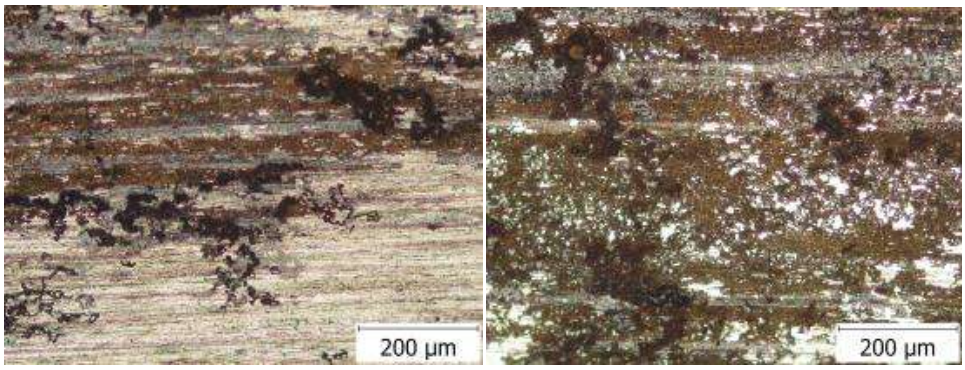

Fig. 7. *Spot of burned emulsion with rust*

Emulsion spots intimately associated with rust are shown in Figure 8a. Corrosive attack with singular formation of iron oxides in rolling direction can be seen in Figure 8b.

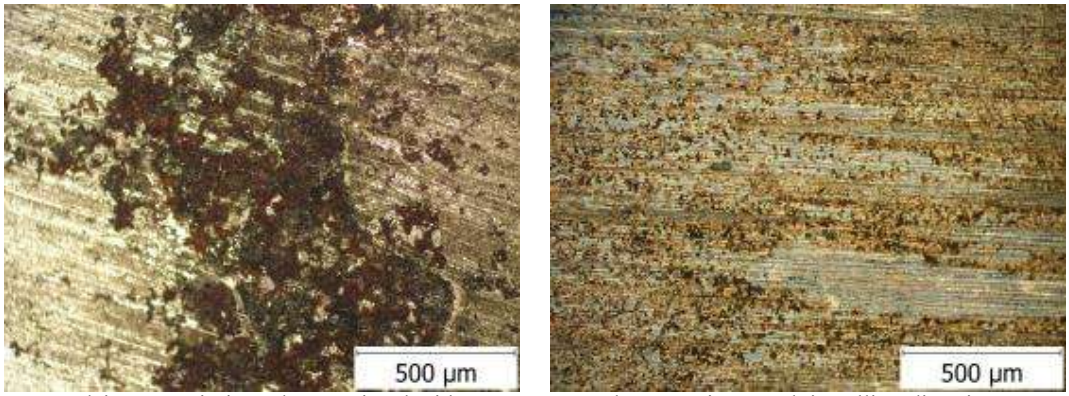

a. Emulsion spots intimately associated with rust b. Corrosive attack in rolling direction

Fig. 8. *Spot of burned emulsion with rust*

4. Conclusions

The microscopic analysis of spots of burned emulsion showed a complex phase structure resulting from the combustion rate, due to the interaction of the emulsion with contaminating residues and with the steel substrate. Spot emulsion usually starts from a large drop that falls on the surface of the steel forming radiating streams. Spot drops are dense and dark and the area where they spread is diffuse, without allowing compactness to reveal the steel support. At magnification higher than 100, it can be seen that the core of started emulsion stain also has a heterogeneous structure showing both burnt black areas, as well as gray and slightly burnt areas.

Carbonaceous residues that remain on the surface of the strip after rolling must be strictly limited because they negatively influence all subsequent stages of processing. Research has shown that increasing the degree of contamination of the emulsion by recirculation and wear can generate an amount of carbon residue up to 8 mg/m^2.

The excess of emulsion used in the lamination process leads to the formation of drops which in the annealing process form spots of burned emulsion. It was also shown to cause formation areas with high carbon concentrations on the surface of the steel strips, after annealing.

Acknowledgement

The authors thanks Prof. dr. chem. V. Musat, for performing the thermal analysis, DSC, in the laboratory of Chemical Nanotechnology, "Dunarea de Jos" University of Galati.

References

[1]. ***, www.uvbtechnik.cz.
[2]. M. Raulf, T. Brixius, H. Duchaczek, *Optimisation of rolling lubricants for improved operation of cold rolling mills (Optilub),* 2009.
[3]. P. Pathak, S. K. Jha, A. Singh, *Tribological Approach for Improvement in Productivity and Quality of Flat Rolled Steel Products: A Review*, International Journal of Technical Research (IJTR), Vol. 1, Issue 1, Mar-Apr 2012.
[4]. Tamara Radu, Anişoara Ciocan, *Behaviour of cold rolling emulsions in the obtaining process of steel strips*, International conference, UGALMAT 2014, 29 -30 May, Galati, Romania.
[5]. Lucica Balint,Maria Vlad,Dumitru DimaIoan, Simion Balint, *Characterization of the emulsions used for cold rolling steel strips with the view of their valorisation*, 14th Geoconference SGEM 2014, Albena, Bulgaria, p. 43-51, 2014.
[6]. *,** Defect Catalog Extract http://www.slideshare.net.
[7]. *,** Defects Atlas *for surface defects on Cold Rolled Steel*, www.iitk.ac.in.
[8]. *,** *Atlas de defecte de suprafata a benzilor laminate la rece*, Arcelor Mittal.
[9]. F. Potecasu, *Stiinta si ingineria materialelor* - Galati, Editura Europlus Galati – ISBN 973 –7845 –10–2, ISBN 978 –973 - 7845 –10-8, 2006.
[10]. S. R. Schmid, W. D. Wilson, *Lubrification mechanisms for oil-in-water emulsions*, Lubrification Engineering, vol. 52, 2, p. 168-175, 1996.
[11]. T. Radu, A. Ciocan, F. Potecaşu, S. Constantinescu, L. Balint, C. Eni, *Influence of cold rolling emulsion on the steel strips surface quality*, Symposium of Croatian Metallurgical Society "SHMD 2014", Rev. Metallurgy, vol. 53, Br./No. 3, Str./p. 289-432.
[12]. K. Hyunok, K. Nimet, *Friction and lubrication*, Sheet Metal Forming Fundamentals 20.

THE ANNALS OF "DUNAREA DE JOS" UNIVERSITY OF GALATI
FASCICLE IX. METALLURGY AND MATERIALS SCIENCE
N°. 4 – 2014, ISSN 1453 – 083X

METAL HEATING FURNACE WITH FLUE GAS CONDENSATION. A THERMOECONOMIC ANALYSIS

Daniela PANĂ[a], Ion V. ION[b], Marcel DRĂGAN[b]
"Dunarea de Jos" University of Galati, Romania
[a]Department of Engineering Sciences and Management
[b]Department of Thermal Systems and Environmental Engineering
e-mail: daniela.pana@ugal.ro

ABSTRACT

The heat treating furnaces are one of the largest energy consumers in the manufacturing sector and therefore many techniques to improve their energy efficiency have been developed. One of them focuses on the recovery of the heat contained in exhaust gases and its use to preheat combustion air/charge or to generate steam. The maximum amount of recovered heat is obtained when the flue gases are cooled down below dew point temperature in order to recover the latent heat of water vapor in flue gases. The use of a condensing economizer in a 70 t/h heat treating furnace allows the decrease of the cost of heated metal bars by 0.32%, which means a cost saving of 158 lei/h.

KEYWORDS: furnace, exergy, efficiency, heat recovery

1. Introduction

The heat treating furnaces operate with low efficiency due to the high temperature at which the flue gases have to leave the furnace (higher than the load temperature). That is why the largest amount of the heat supplied in the heating process is wasted in the form of sensible and latent heat contained by the exhaust gases.

This wasted heat by exhaust gases depends mainly on the design and operation of the heating equipment. A significant reduction of this waste can be obtained by heat recovery in order to preheat the load or combustion air or to generate steam. The amount of heat to be recovered from exhaust gases depends on the temperature at which the flue gases are cooled down. After the preheating of load or combustion air, or the steam generation, the exhaust gases usually have a temperature of about 200 °C. At this temperature the exhaust gases still contain a large amount of heat which can be recovered by cooling them down below the dew point in order to recover both the sensible and the latent heat of water contained in flue gases.

The dependence of the enthalpy of flue gases on temperature is almost linear when the temperature is above the dew pint temperature and has a parabolic profile for temperatures below the dew point (Fig. 1).

In this paper the thermoeconomic analysis of a 70 t/h heat treating furnace with flue gases condensation for steam generation is performed.

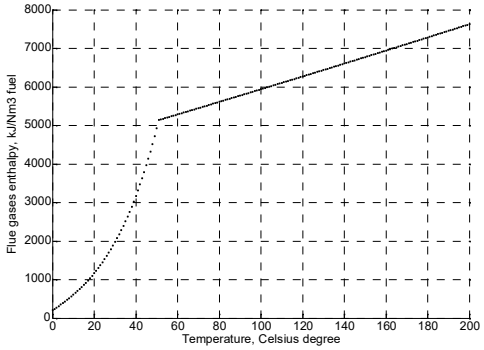

Fig. 1. *Enthalpy of flue gases vs temperature (natural gas, stack air excess λ=1.4)*

2. Enthalpy of flue gases

The enthalpy of flue gases is calculated with the following equations:

- for temperatures above dew point: eq. (1);
- for temperatures below dew point: eq. (2);

$$h_{fg}(T) = m_{CO_2} h_{CO_2}(T) + m_{N_2} h_{N_2}(T) + m_{O_2} h_{O_2}(T) + m_{SO_2} h_{SO_2}(T) + m_{H_2O}\left[h_{H_2O}(T) + h_l\right] \text{ [kJ/Nm}^3\text{ fuel]} \quad (1)$$

$$h_{fg}(T) = m_{CO_2} h_{CO_2}(T) + m_{N_2} h_{N_2}(T) + m_{O_2} h_{O_2}(T) + m_{SO_2} h_{SO_2}(T) + m_{H_2Osat}\left[h_{H_2O}(T) + h_l\right] + \left(m_{H_2O} - m_{H_2Osat}\right) c_{pW} \cdot T \text{ [kJ/Nm}^3\text{ fuel]} \quad (2)$$

where:

$m_{CO_2}, m_{H_2O}, m_{N_2}, m_{O_2}, m_{SO_2}$ - mass of CO_2, H_2O, N_2, O_2 and SO_2 in flue gases;

$h_{CO2}(T)$, $h_{SO2}(T)$, $h_{H2O}(T)$, $h_{N2}(T)$, $h_{O2}(T)$ – enthalpy of CO_2, SO_2, H_2O, N_2 and O_2 corresponding to temperature t, [kJ/kg];

h_l– latent heat of water vapour, [kJ/kg]; h_l = 2502 kJ/kg.

m_{H_2Osat} - mass of water vapour in flue gases at saturation temperature T_s:

$$m_{H_2Osat} = x_{fgs} \cdot m_{fgd} \text{ [kg water/ Nm}^3\text{ fuel]} \quad (3)$$

$$m_{fgd} = m_{CO_2} + m_{O_2} + m_{N_2} + m_{SO_2} \text{ [kg dfg/Nm}^3\text{ fuel]} \quad (4)$$

x_{fgs} – absolute humidity of flue gases at saturation:

$$x_{fgs} = 0.622 \frac{p_s}{p_{dfg}} \quad (5)$$

$$p_{dfg} = 1.013 \cdot 10^5 \frac{V_{CO2} + V_{O2} + V_{N2} + V_{SO2}}{V_{ga}} \quad (6)$$

$$p_s = 610.78 \cdot e^{17.2694 \frac{t}{(t+238.3)}} \quad (7)$$

c_{pw}– specific heat of liquid water, [kJ/kg·K]

$$c_{pw} = 2820 + 11.82 \cdot T - 0.03502 \cdot T^2 + 0.00003599 \cdot T^3 \quad (8)$$

The dew temperature of flue gases can be calculated by the following equation [1]:

$$T_d = 1000 / \left[2.20732 - 2.117187 \cdot 10^{-1} \ln m - 2.166605 \cdot 10^{-3} (\ln m)^2 + 1.619692 \cdot 10^{-4} (\ln m)^3 + 4.8998 \cdot 10^{-5} (\ln m)^4 + 3.691725 \cdot 10^{-6} (\ln m)^5 + 1.619692 \cdot 10^{-4} (\ln m)^3 + 4.8998 \cdot 10^{-5} (\ln m)^4 + 3.691725 \cdot 10^{-6} (\ln m)^5\right] \text{ [K]} \quad (9)$$

$$m = \frac{p_{H_2O}}{10};\ p_{H_2O} = 1.013 \cdot 10^5 \frac{V_{H_2O}}{V_{ga}} \quad (10)$$

The heat recovered from the flue gases is given by the following equation:

$$\dot{Q}_r = B\left[h_{fg}(T_1) - h_{fg}(T_2)\right], \text{ [kW]} \quad (10)$$

where:

B – fuel flow rate, Nm³/s; $h_{fg}(T_1)$, $h_{fg}(T_2)$ – enthalpy of flue gases corresponding to temperature t_1 at condenser inlet, and to temperature t_2 at condenser outlet, respectively, kJ/Nm³ fuel.

3. Description of heat treating furnace

The furnace is schematically shown in Fig. 2. It comprises the combustion chamber, air preheater, heat-recovery steam generator, condensing economizer, air fan, feed water pump and exhauster.

The fuel used is natural gas with the following composition:

CH_4=97.7%, C_2H_6=0.5%, C_3H_8=0.35, C_4H_{10} =0.15, N_2=0.8%, H_2S =0.35, CO_2=0.15% and the lower heating value of 35888 kJ/Nm³. The furnace heating capacity is 70 t/h. Its operation parameters are shown in Table 1.

Table 1. *Operation data of the furnace*

Parameter	Value
Natural gas flow rate	0.412 Nm³/s
Combustion air flow rate	4.13 Nm³/s
Air fan power	250 W
Exhauster power	100 W
Feed water pump power	10 W
Saturated team pressure	12 bar
Excess air coefficient at stack	1.54
Dew point of flue gases	51 °C
Temperature of flue gases before condensing economizer	157 °C
Temperature of exhaust gases	40 °C

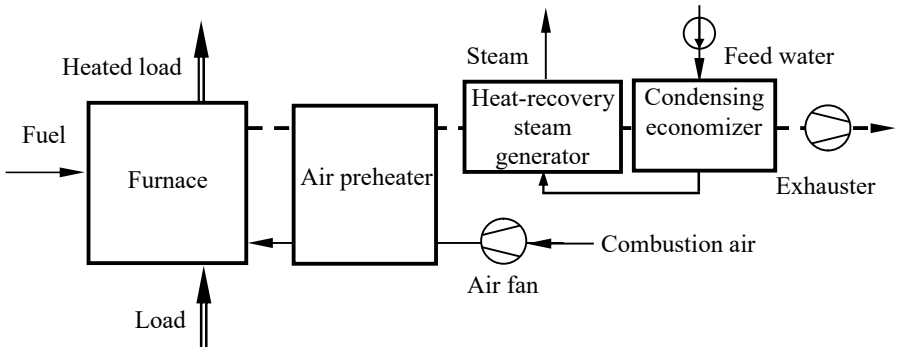

Fig. 2. *Schematic diagram of the furnace*

4. Thermoeconomic analysis

The exergetic cost of the products heated into the furnace is calculated using the following exergetic cost balance equations written for steady state operation, lei/s:

$$\dot{C}_{sf,e} = \dot{C}_f + \dot{C}_{sf,i} + \dot{C}_{el} + \dot{C}_w - \dot{C}_{steam} + \\ + \dot{C}_{environ} + \dot{Z}^{CI}_{furnace} + \dot{Z}^{OM}_{furnace} \quad (11)$$

where:

$\dot{C}_f$ - fuel cost rate: $\dot{C}_f = c_{e,f} \cdot \dot{E}_f$, lei/s;

$c_{e,f}$ - exergetic cost of fuel, lei/kJ (Tab. 2);

$\dot{E}_f$ - fuel exergy flow rate, kJ/s;

$\dot{C}_{sf,i}$ - cost rate of metal bars at furnace inlet;

$\dot{C}_w$ - feed water cost rate: $\dot{C}_w = c_{e,w} \cdot \dot{E}_w$;

$c_{e,w}$ - exergetic cost of feed water (Tab. 2);

$\dot{E}_w$ - feed water cost rate;

$\dot{C}_{el}$ - electricity cost rate: $\dot{C}_{el} = (W_w + W_{Ex} + W_{ac}) c_{el}$;

W_w, W_{Ex}, W_{ac} - power of feed water pump, exhauster, and combustion air fan;

c_{el} - electricity specific cost;

$\dot{C}_{st}$ - steam cost rate: $\dot{C}_{st} = G_{st} \cdot c_{e,st} \cdot e_{st}$;

G_{st} - steam flow rate;

$c_{e,f}$ - exergetic cost of steam, (Tab. 2);

e_{st} - steam exergy;

$\dot{Z}^{CI}_{furnace}$ - cost rate associated with capital investment calculated according to [2].

The purchase cost of the heat-recovery steam generator is calculated using the following equation [3]:

$$Z_{HRSG} = C_1 \left[\left(\frac{\Phi_E}{(\Delta TLM)_E} \right)^{0.8} + \left(\frac{\Phi_{EV}}{(\Delta TLM)_{EV}} \right)^{0.8} \right] + \\ + C_2 \dot{m}_{st} + C_3 \dot{m}_g^{1.2} \quad (12)$$

$\dot{m}_g$, $\dot{m}_{st}$ - steam and flue gas mass flow rate, kg/s;

ΔTLM - log mean temperature difference;

Φ_E, Φ_{EV} – heat flow rate transferred in economiser and evaporator respectively;

C_1 = 12712 lei/(kW/K)$^{0.8}$; C_2 = 41165 lei/(kg/s); C_3 = 2292 lei/(kg/s)$^{1.2}$;

$\dot{Z}^{OM}_{furnace}$ - cost rate associated with operation and maintenance of the furnace;

$\dot{C}_{env}$ - cost rate due to environmental pollution and energy taxes;

Table 2. *Costs associated with furnace operation*

Cost rate of cold metal bars	14.088 lei/s
Exergetic cost of fuel	$2.440 \cdot 10^{-5}$ lei/kJ
Exergetic cost of feed water	$1.170 \cdot 10^{-3}$ lei/kJ
Electricity specific cost	$7.970 \cdot 10^{-5}$ lei/kJ
Exergetic cost of steam	$5.820 \cdot 10^{-5}$ lei/kJ
Cost rate associated with capital investment without condensing economizer	$1.580 \cdot 10^{-3}$ lei/s
Cost rate associated with capital investment with condensing economizer	$1.583 \cdot 10^{-3}$ lei/s
Cost rate associated with operation and maintenance of furnace	$4.88 \cdot 10^{-3}$lei/s

The purchase cost of condensing, calculated by equation (11) leads to a slight increase of the cost rate associated with capital investment from $1.580 \cdot 10^{3}$ lei/s to $1.583 \cdot 10^{-3}$ lei/s.

By using the condensing economizer, the recovered heat from flue gases is equal to 1562.21 kW. The temperature of exhaust gases decreases in this way from 157 °C to 40 °C.

The flue gas condensation allows for the increase of the steam flow rate from 1.94 kg/s to 2.49 kg/s. The steam cost rate increases from 0.186 lei/s to 0.233 lei/s leading to the decrease of exergetic cost of the heated metal bars from 0.002856 lei/kJ to 0.002847 lei/kJ.

The cost of the heated metal bars decreases from 0.8387 lei/kg to 0.8360 lei/kg, which means a cost saving of 158 lei/h.

4. Conclusions

Condensing heat exchangers to recover the heat contained in flue gases generated especially by the natural gas burners are widely used.

Combustion type furnaces used to heat treat metal have low energy efficiency because of heat losses in different areas and forms, especially with exhaust gases.

In the studied case, the use of a condensing economizer allowed for the recovery of 1562.21 kW from flue gases which led to the increase of the steam flow rate from 1.94 kg/s to 2.49 kg/s and therefore the increase of the steam cost rate from 0.186 lei/s to 0.233 lei/s. In this way the cost of heated metal bars decreases from 0.8387 lei/kg to 0.8362 lei/kg. The achieved cost saving is 158 lei/h.

Acknowledgement

This work has been funded by the TEMPUS Programme of the European Union through the project „Development of Training Network for Improving Education in Energy Efficiency – ENERGY" (530379-TEMPUS-1-2012-1-LV-TEMPUS-JPCR).

References

[1]. Pop G. M., ş.a., *Îndrumar. Tabele, nomograme şi formule termotehnice*, Ed. Tehnică, Bucureşti, 1987.

[2]. Bejan A., Tsatsaronis G., Moran M., *Thermal Design and Optimization*, Wiley, New York, 1996.

[3]. Kotas I. J., *The exergy method of thermal plant analysis*, Exergon Publishing Company UK Ltd., London, 2012.

[4]. Iliev I., *Heat exchangers*, Ruse, Academic publishing centre of Ruse University, 2013.

[5]. Iliev I., *Heat waste recovery from corrosive flue gas streams*, Proceedings of the 2nd International Conference of Thermal *Equipment,* Renewable Energy and Rural Development - TE-RE-RD 2013, 20-22 June, Romania, PRINTECH, p. 61-66, 2013.

[6]. Iliev I., Kaloyanov N., Gramatikov P., Kamburova V., Terziev A., Palov I., Stefanov S., Sirakov K., *Energy Efficiency and Energy Management Handbook*, Bulgaria Energy Efficiency for Competitive Industry Financing Facility (BEECIFF): Project Preparation, Capacity Building and Implementation Support. Sofia, Ministry of Economy, Energy and Tourism ("MoEET"), 2012.

[7]. Mullinger P., Jenkins B., *Industrial and Process Furnaces. Principles, Design and Operation*, Butterworth-Heinemann, 2008.

[8]. Trinks W., Mawhinney M. H., Shannon R. A., Reed R. J., Garvey J. R., *Industrial Furnaces,* Sixth Edition, John Wiley & Sons, 2004.

[9]. Hasanuzzaman M., Rahim N. A., Hosenuzzaman M., Saidur R., Mahbubul I. M., Rashid M. M., *Energy savings in the combustion based process heating in industrial sector*, Renewable and Sustainable Energy Reviews, Vol. 16, Issue 7, p. 4527-4536, 2012.

THE ANNALS OF "DUNAREA DE JOS" UNIVERSITY OF GALATI
FASCICLE IX. METALLURGY AND MATERIALS SCIENCE
N°. 4 – 2014, ISSN 1453 – 083X

FABRICATION OF ULTRAFINE LOW CARBON METALLIC MULTILAYER BY ACCUMULATIVE ROLL BONDING

Carmela GURĂU, Gheorghe GURĂU, Lidia GURĂU, Petrică ALEXANDRU
"Dunarea de Jos" University of Galati, Romania
e-mail: carmela.gurau@ugal.ro

ABSTRACT

The effect of grain refinements by Accumulative Roll Bonding (ARB) was investigated on low carbon steel. Optical microscopy (OM) and microhardness tests were used to check the phase changes and hardness before and after ARB. A combined technique between cold rolling and ARB was used to obtain the changes of grain size under 1 μm. Metallographic analysis reveals the change of low carbon microcrystalline one compared to the ultrafine one with increased hardness resulted from straining by ARB. The severe plastic deformation (SPD) processing of bulk metals is not straightforward due to several differences in the final microstructure at several material length scales. The plastic deformation behavior of the final material depends on many microstructural aspects, one of them being grain refinement up to amorphization caused by ARB.

KEYWORDS: metallic multilayer, low carbon, roll bonding

1. Introduction

Grain refinement of metallic materials by severe plastic deformation (SPD) has been widely studied in various alloys. The fundamentals of nanostructure formation in metals by SPD have been discussed extensively [1-4]. Accumulative Roll Bonding (ARB) is one of the SPD methods that have been used to produce bulk amorphous and nanostructured materials [5-9]. During deformation by ARB, a sample is subjected to high-friction conditions without any lubricant between materials and rolls, which may cause a large amount of redundant shear strain near the sheet surface. The repetition of cutting, stacking and roll-bonding in the ARB leads to grain refinement of the sample, producing a nanostructured material with improved mechanical properties [10]. The purpose of the present study is to promote a combination between classic rolling and ARB. The effect of these two types of processes on microstructure evolution was studied. The observation of the effect of ARB on other alloys or composites was discussed [11]. Despite many reports on the positive effect of bulk nanostructured metals produced by SPD on mechanical properties, detailed mechanisms of these effects have not been clarified yet [7]. It is also reported that SPD application resulted in improved corrosion resistance [4]. Grain refinement and amorphization induced by ARB may change the structural properties of low carbon steel thus further improving its performance. In this study, thin layered low carbon steel was fabricated and the effects of the structural and mechanical properties change of ARB were investigated.

2. Materials and methods

This section describes the starting microstructure of steel, the fabrication process and structure evolution as a function of rolling passes in the layered composites to a final mean layer thickness of 50 μm.

The starting materials in this study were 5 mm thick X60 steel plates with the nominal composition presented in Table 1:

Table 1. *Chemical composition of X60 steel plates*

C	Mn	Si	P	S	Al	Ti	V	Nb	N_2
0.05	1.60	0.28	0.015	0.005	0.035	0.28	0.013	0.085	0.0058

The low carbon microalloyed steel was deformed by cold rolling followed by three cycles of ARB (a thickness reduction of 99.01%) at room temperature, without lubrication and without any intermediate annealing. The rolling was performed on a quarto rolling stand, with 30 mm diameter work rolls. The equipment is operated using a DC power supply of 4.5 kW that provides high torque at low speeds, with thyristor. The thyristor drive allows for fine adjustment of speed. The cold rolled plates were cleaned with acetone and wire-brushed in preparation for bonding by accumulative roll bonding (ARB). The bonded material was cut in half and the process of surface cleaning, stacking, and roll bonding was iterated in order to produce samples having experienced couple amounts of cumulative strain. Using this technique, fine-layered steel was fabricated.

The deformation degree achieved in the ARB process was calculated with the following equation: $\varepsilon=1-1/2^n$, where n is the number of ARB cycles.

Optical micrographs were recorded using an OLIMPUS microscope, equipped with a video camera. QCapture software was used for micrograph capture. Hardness tests were made using a PMT-3-type instrument, equipped with a digital camera. Image capture and the processing of fingerprint measurements were performed using OPTIKA VIEW software. Prior to microstructural analysis and hardness tests, the samples were prepared according to the metallographic standard.

3. Results and discussion

The X60 steel samples were initially cold rolled at room temperature. This produced a strongly textured plate, whose normal direction is nearly aligned with the deformation axis. As a final preparation the cold rolled plates were preceded by three ARB steps. The material underwent further straight rolling; the plates were then cut, stacked in twos and roll-bonded together at room temperature using a single high-strain rolling pass of approximately 50% reduction. Roll-bonding was performed on the same rolling mill as in the classic process.

Figure 1 shows the optical micrograph of the specimens in initial hot rolled state (Figure 1a) and subjected to 43 cold rolled steps (Figure 1b). The microstructure of the samples in initial state and after cold rolling is made up of ferrite and pearlite, specific to low carbon steels. The hot deformed grains are ferrite with few strings pearlite grains arranged in linear arrays. During the rolling process, the grains are strongly elongated in the rolling direction until lamellar boundary appears. While deformation increases, a large number of grains are distorted and refined and fibrous structure produced for clear preferred orientation [10]. In the case of cold rolling, recrystallization processes do not occur, because deformation occurs below the recrystallization temperature and is accompanied by hardening. The deformed specimen became crystallographically textured (Figure 1b) and fibrous structure is produced.

The main factors influencing the excellent deformability of steel are the size and the distribution of its structural constituents and its purity and homogeneity, incurring very large plastic strain (95.6%) without any cracks or breaks. The finer the grain size, the more likely it is that more grains appear with favorable orientation to enter the plastic deformation and to improve plasticity.

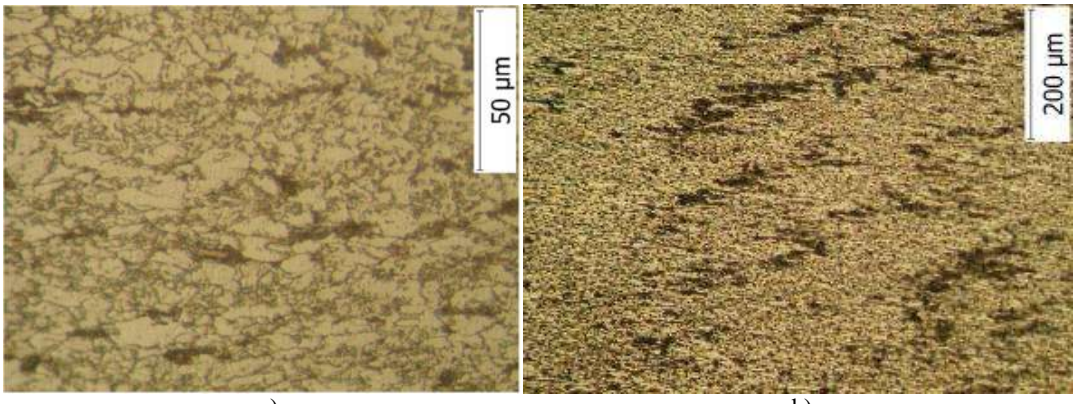

a) b)

Fig. 1. *Optical micrograph of the steel sample (a) in initial state and (b) after cold rolling in 43 passes with 95.6% degree of deformation*

After cold rolling in 43 passes, the ribbon was degreased, cut into sheets and brushed. Immediately after surface treatment, in order to avoid oxidation on the surface, the sandwich samples, composed by two sheets overlapped, are subjected to concurrent rolling. The ARB process was repeated 3 times at room temperature. Figure 2 shows the macrostructure of the mechanically polished samples after 1, 2 and 3 ARB cycles. The resulting layered severe plastic deformation has the following total reduction [%]/number of layers/average layer thicknesses [μm]: 50/2/220, 75/4/110, and 87.5/8/55.

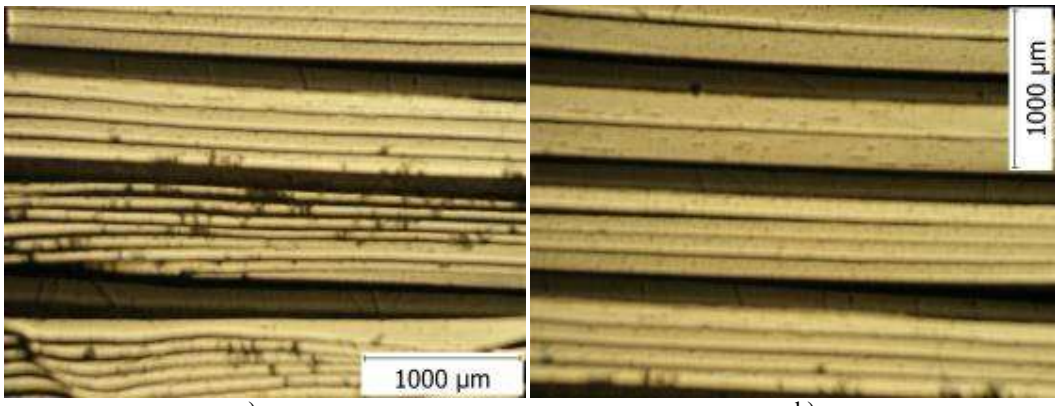

a) b)

Fig. 2. *Macrostructure of ARB samples in longitudinal and transversal section (a) 2 and 4 layers and (b) 4 and 8 layers*

Corresponding to Figure 2, as the number of ARB cycles increased, strain increased and the thickness of steel layers decreased. Unlike in the classic process, the rolling in the ARB process is not just a deformation process, being accompanied by a bonding process. The layers are joined together by rolling on the strength of the interfaces prepared preliminarily. The rolls and the surface of the samples are not lubricated, owing to the high friction between them caused by a large amount of redundant shear strain [9-11]. In order to obtain appropriate bonding, high pressure is required concomitantly with intense friction rolling conditions. The repetition of cutting, stacking and roll-bonding in the ARB leads to grain refinement of the sample, producing ultrafine grained structure.

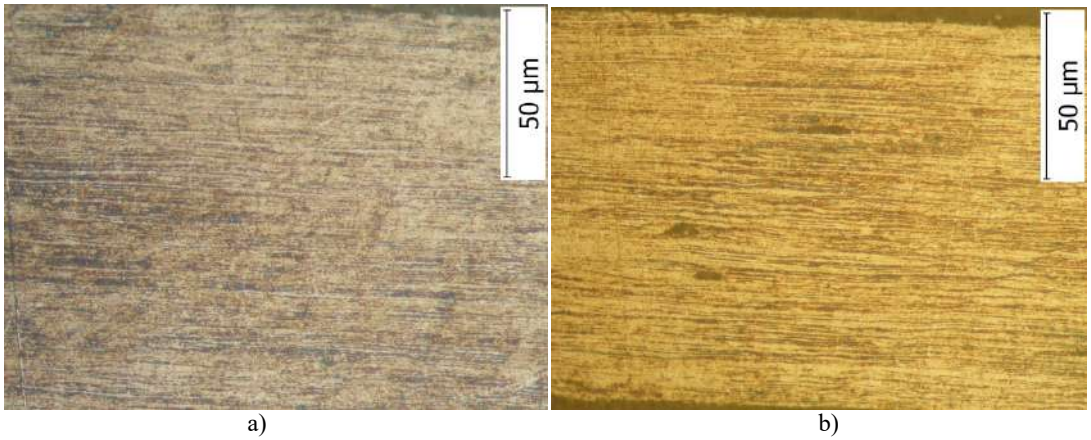

a) b)

Fig. 3. *Optical micrographs of ARB low carbon samples:(a) 2 layers and (b)4 layers*

In the case of two layers, for the first roll-bonding, grain refinement and elongated grain microstructure on rolling direction as a direct effect of ARB strains can be observed (Figure 3a). Also, it can be highlighted the role of increase of trend dislocation and agglomeration within subgrains leading to a subdivision of the microstructure. The size of subgrains falls below one micron and limits the dislocations orientation. Finally, microstructure evolves into a multilamellar structure that exists

between cells, subgrains [11]. The lamellar appearance and boundary ambiguity manifest stronger when rolling 4 layers in package. The crystalline grains loss of orientation is emphasized by the increased number of boundaries with large angles. This indicates the crystalline grain size reduction induced by severe plastic deformation [11].

The most grain refinement was experienced in the case of the samples which underwent severe plastic deformation by cold rolling and 3 ARB cycles, having 8 layers with about 50 μm thickness. The microstructural aspect is specific to ultrafine grained alloys. Figure 4 highlights fine distorted grains and very dense areas. Figure 4b illustrates large areas were neither lamellar grains nor boundaries are observable, after repeated metallographic etch. These areas resemble amorphous structures.

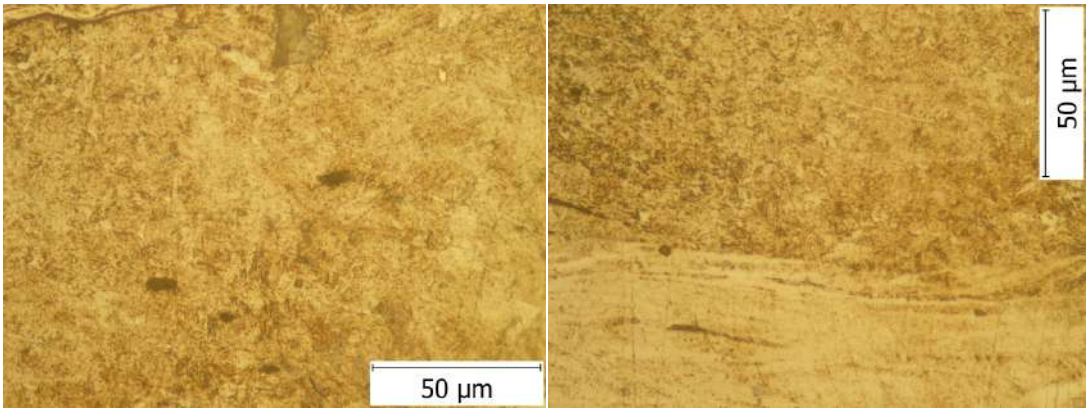

a) b)

Fig. 4. *Optical micrographs of ARB low carbon 8-layered samples: longitudinal section (a) and transversal section (b)*

Figure 5 shows microhardness variation of microalloyed low carbon steel after hot rolling in initial state (IS), 43 passes cold rolled (9CR) and a different number of ARB cycles (one pass CR+ARB, two passes CR+2ARB and three passes CR+3ARB). The curve reveals that the increase in the number of ARB cycles results in the number of layers increasing the microhardness of steel. The largest increase of the hardness value occurred after 43 passes, cold rolling correlated with refinement of grain and hardening. During the ARB second pass, microhardness had a sharp rise of approximately 800 MPa.

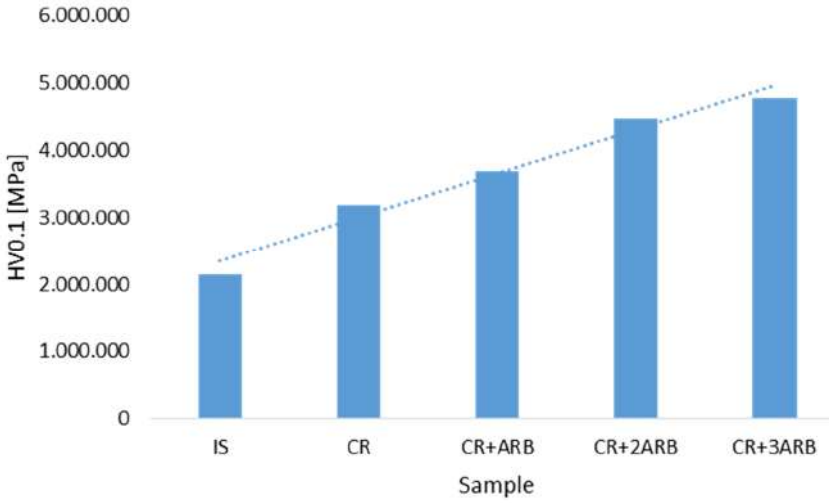

Fig. 5. *Microhardness variation*

4. Conclusion

The effect of cold rolling (CR) followed by accumulative roll bonding (ARB) was investigated on low carbon steel. The evaluation of the structure and hardness properties of multilayered steel during different cycles of process leads to the following conclusions:

1. Low carbon steels can be processed by cold rolling followed by three ARB cycles at room temperature, without any intermediate annealing.
2. The deformation degree achieved in the case of cold rolling was 95.6% without any cracks or breaks. The total reduction after 3 ARB cycles was 87.5%, with a few observable cracks.
3. Starting from a fibrous structure obtained by cold rolling with high deformation, after ARB the structure became ultra-fine grained.
4. As the number of ARB cycles and the number of layers increase, the microhardness of steel increases; in the second cycle, microhardness had a sharp rise.

Further investigations should be carried on to find better bonding methods.

References

[1]. Y. T. Zhu, T. G. Langdon, *The fundamentals of nanostructured materials processed by severe plastic deformation*, JOM 56, p. 58-63, 2004.

[2]. R. Valiev, *Nanostructuring of metals by severe plastic deformation for advanced properties*, Nat. Mater., 3, p. 511-516, 2004.

[3]. A. P. Zhilyaev, T. G. Langdon, *Using high-pressure torsion for metal processing: fundamentals and applications*, Prog. Mater. Sci., 53, p. 893-979, 2008.

[4]. A. Azushima, *Severe plastic deformation (SPD) process for metals*, CIRP Annals Manufacturing Technology, 37, p. 216-735, 2008.

[5]. M. Eizadjou, A. Kazemi Talachi, H. Danesh Manesh, H. Shakur Shahabi, K. Janghorban, *Investigation of structure and mechanical properties of multilayerd Al/Cu composite produced by accumulative roll bonding (ARB) process*, Composites Science and Technology, 68, p. 2003-2009, 2008.

[6]. Tsuji N., Saito Y., Lee S. H., Minamino Y., *ARB and other new techniques to produce bulk ultrafine grained materials*, 2003.

[7]. Saito Y., Tsuji N., Utsunomiya H., Sakai T., Hong R. G., *Ultra-fine grained bulk aluminium produced by accumulative roll-bonding (ARB) process*, Scripta Materialia, 39, 9, p. 1221-1227, 1998.

[8]. Saito Y., Utsunomiaya H., Tsuji N., Sakai T., *Novel ultra-high straining process for bulk materials-development of the accumulative roll-bonding (ARB) process*, Acta Materialia, 47, 2, p. 579-583, 1999.

[9]. Lee S. H., Saito Y., Tsuji N., Utsunomiya H., Sakai T., *Role of shear strain in ultragrain refinement by accumulative roll-bonding (ARB) process*, Scripta Materialia, 46, 4, p. 281-285, 2002.

[10]. N. Kamikawa, T. Sakai, N. Tsuji, *Effect of redundant shear strain on microstructure and texture evolution during accumulative roll-bonding in ultralow carbon IF steel*, Acta Materialia, 55, p. 5873-5888, 2007.

[11]. Marko Knezevic, Thomas Nizolek, Milan Ardeljan, Irene J. Beyerlein, Nathan A. Mara, Tresa M. Pollock, *Texture evolution in two-phase Zr/Nb lamellar composites during accumulative roll bonding*, International Journal of Plasticity, 57, p. 16-28, 2014.

THE ANNALS OF "DUNAREA DE JOS" UNIVERSITY OF GALATI
FASCICLE IX. METALLURGY AND MATERIALS SCIENCE
N°. 4 – 2014, ISSN 1453 – 083X

EVOLUTIONARY PERSPECTIVES ON ENERGY CONSUMPTION OF RAW MATERIALS TO ENSURE ENERGY PRODUCTION IN THE EU-28

Mariana Carmelia DRAGOMIR[a], Aurel Gabriel SIMIONESCU[b]
[a]"Dunarea de Jos" University of Galati, Cross-border Faculty of Humanities, Economics and Engineering, Cahul, the Republic of Moldova
[b]"Constantin Brâncoveanu" University of Piteşti, Faculty of Administrative Sciences and Communication Brăila
e-mail: dragomircarmelia@gmail.com

ABSTRACT

A clear analysis of the electricity production and consumption sector in the EU 28 offers firstly the possibility of knowing the final energy consumption for each segment (industry, households, trade, services and transports). The final energy consumption for the industrial sector decreased during the2001-2012 period, from 330872/1000 tons of oil equivalent to 282316/1000 tons of oil equivalent, while, if the transport sector is considered, an increase can be observed in consumption over the same period, from 348636/1000 tons of oil equivalent to 351080/1000 tons of oil equivalent. Although greenhouse gas emissions from energy used decreased during the analyzed period from 98.8 tons CO_2e to 91.4 tons CO_2e, a special attention must be paid to the energy production from unconventional sources. As regards the primary production of energy from renewable sources between 2001 and 2012, an increase was observed in solar power, from 16.4/1000 tons of oil equivalent to 5781/1000 tons of oil equivalent, and in wind energy, from 2296/1000 tons of oil equivalent to 17692/1000 tons of oil equivalent.

KEYWORDS: conventional energy, greenhouse gas, non-conventional energy

1. Introduction

To ensure a sustainable future in a constantly developing Europe it is particularly important to keep a balance between energy consumption and emissions of greenhouse gases. In 2010, the European Commission established five "themes" for 2020 ("Europe 2020, a European strategy for smart, sustainable and inclusive growth"): employment, research and innovation, climate change and energy, education and combating poverty. These targets require a number of steps and directions to obtain the established results.

2. The final energy consumption in different sectors

The "20/20/20" objectives regarding the climate/energy assumed by the EU first require a different approach to energy consumers regardless of their nature [1].

The final energy consumption in industry between 2001 and 2012 in the 28 member states of the EU decreased from 330872/1000 tons of oil equivalent (toe) to 282316/1000 toe. The lowest amount is 269814/1000 tons of oil equivalent in 2009, when the economic crisis strongly influenced all activities in the field. After this year, a slow, gradual rise can be observed. The average EU-28 final energy consumption in industry over the analyzed period was 313558/1000 toe, the three countries with the highest consumption being: Germany – 59222/1000 toe, Italy – 36018/1000 toe, and France – 34537/1000 toe [2].

Among the countries with the lowest power consumption are: Estonia – 650/1000 toe, Cyprus – 315/1000 toe, and Malta – 48/1000 toe [3]. In the 2001-2012 period, the average amount of energy consumed by Romania is 8858/1000 toe and it is observed from the annual progress analysis that the smallest amount consumed is that of 2009, only 6518/1000 toe, almost by 50% less than in the 2002-2005 period.

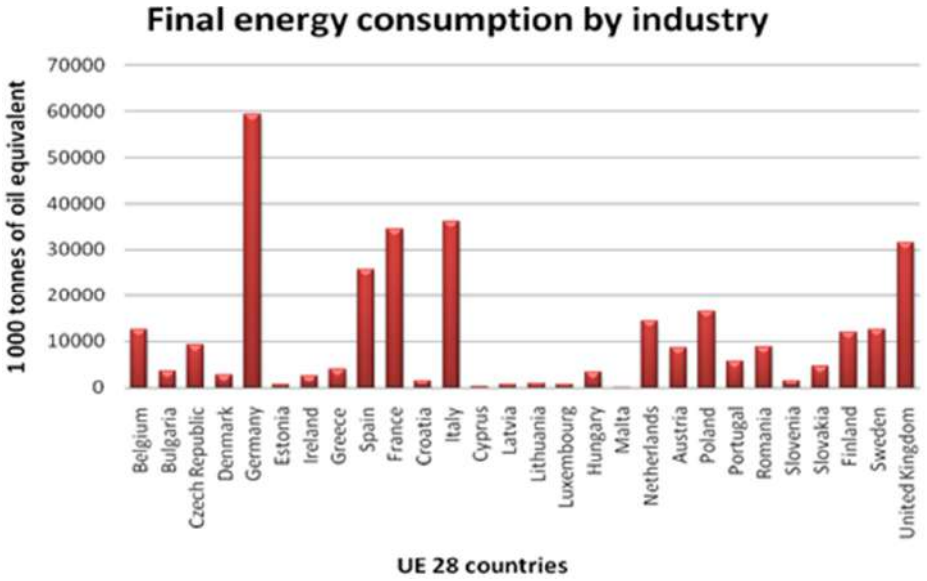

Fig. 1. *Final energy consumption by industry in EU-28*

Drastic measures are required for climate challenges and also for resource usage. The local and the central public administration should prepare a number of measures to reduce these impacts in the following period.

The heavy dependence on fossil fuels and the inefficient use of raw materials are found in their prices, affecting the economic security and simultaneously causing the increase of climate changes. The competition for natural resources and for improving the quality of life will be emphasized by the world population growth from 6 to 9 billion [4].

The final energy household consumption is influenced by the population of that country, the first ranked being: Germany, with a consumption of 95476/1000 toe, France – 72900/1000 toe and England – 61009/1000 toe [5]. The final energy trade and services consumption is also linked to population. Romania ranks 10 among the countries with the highest final energy consumption, with an average of 10084/1000 toe for the period 2001-2012.

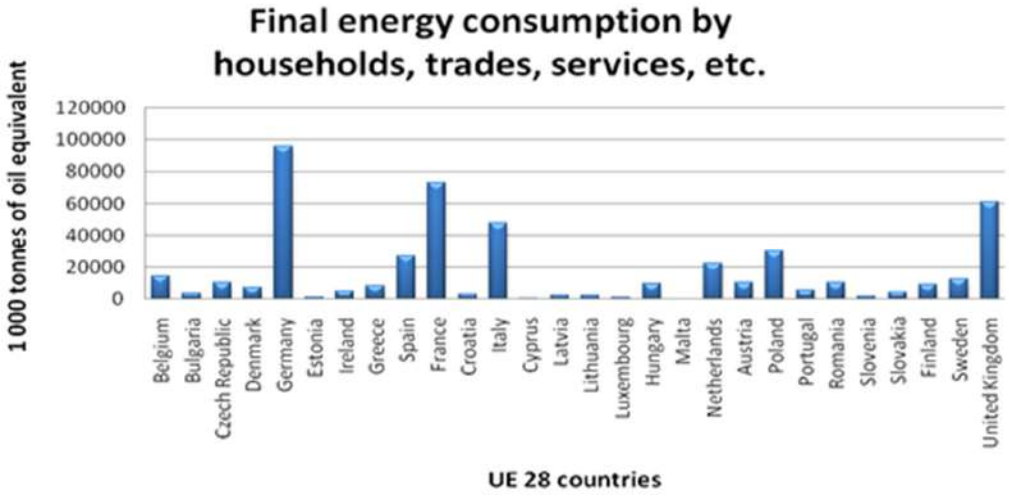

Fig. 2. *Final energy consumption by population, trade and services in EU-28*

A significant objective included in the 2020 strategy refers to the modernization of the transport sector and thereby the reduction of carbon dioxide emissions contributing to competitiveness [6].The local and central authorities will benefit from a number of facilities for a rapid development of the infrastructure of an electrical mobility network, efficient traffic management, more efficient transportation vehicles, the supervision of CO_2 emission reduction for road vehicles, aviation and naval sectors, etc. Simultaneously, the strategy aims to promote the use of European green cars, including electric and hybrid vehicles. This set of measures can be realized through the application of innovative technologies, through a series of support measures that include research, development and innovation, establishing common standards and the development of infrastructure required throughout the EU [7].

The urban dimension of transport is responsible fora large part of greenhouse gas emissions in the environment.

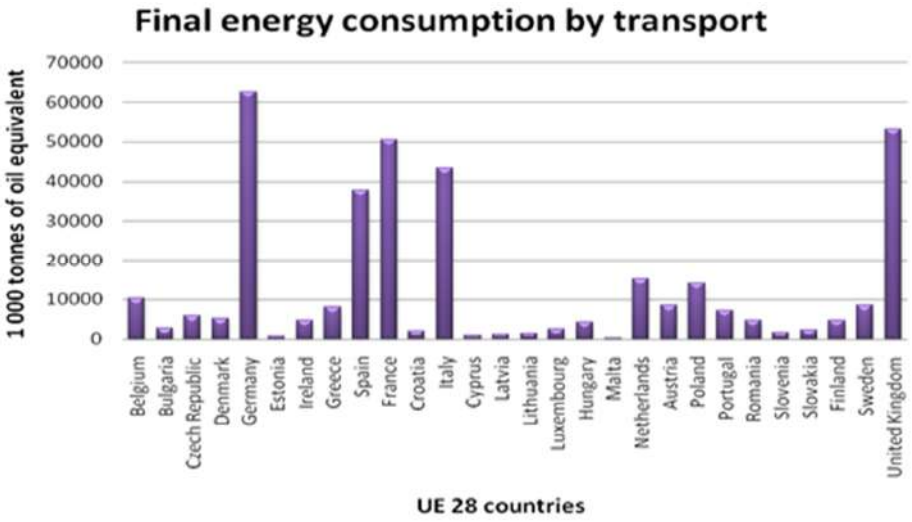

***Fig. 3**. Final energy consumption by transport in EU-28*

In the EU-28, from 2001 to 2012, the largest amount of power consumed by the transport sector was recorded in Germany – 62571/1000 toe, England – 53164/1000 toe, and France – 50536/1000 toe. The average consumption of Romania in that period was 4791/1000 toe, a value quite close to that of Ireland – 4832/1000 toe and of Finland – 4714/1000 toe. The smallest amount of energy used by the transportation sector is in: Cyprus – 989/1000 toe, Estonia – 768/1000 toe and Malta – 237/1000 toe [8].

The application of the strategy regarding the climate changes and energy production and consumption throughout the EU requires a number of investments in key-infrastructure by the cross-border energy and transport networks and also in the application of low-carbon technologies. It is extremely important, in the next period, to find a common solution in response to the challenges posed by the climate changes.

One of the major targets set out in the 2020 Strategy refers to the reduction of greenhouse gas emissions by at least 20% compared to 1990 levels or by 30%, increasing to 20% the share of renewable energy in the final consumption and a 20% increase in energy efficiency. By reaching the energy targets, according to the studies, the EU imports of oil and gas could fall by 60 billion € in 2020. Achieving the EU target, that 20% of the energy used to come from renewable sources, could allow for the creation of over 600 000 jobs in the EU and, if we add the objective of 20% energy efficiency, there are over 1 million new jobs. Additionally, the European energy market integration may result in a GDP growth of 0.6% -0.8% [9].

The EU-28 average intensity of greenhouse gas emissions from energy consumption for 2001-2012 was 95 tons of CO_2e. The highest average was: 103 tons of CO_2e in Bulgaria, 101 tons in Croatia and 100 tons in Malta. The value of our country was above the European average, 96 tons of CO_2e, but we have to point out that the trend is decreasing, with lower values in 2009-2011, followed by a slow growth in 2012. All these values reflect the degree of energy usage in various sectors and the ecological characteristics of machinery, equipment and vehicles.

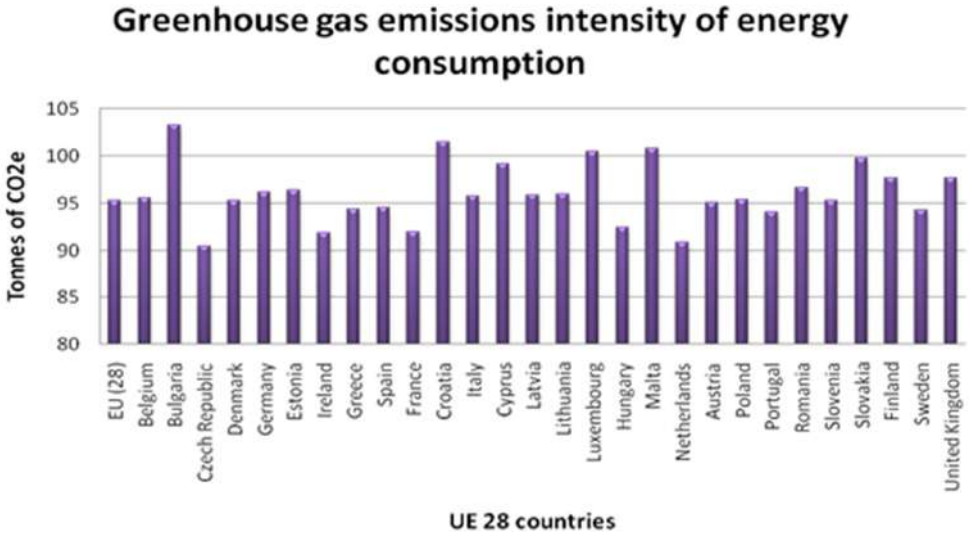

Fig. 4. *Intensity of greenhouse gas emissions from energy consumption in EU-28*

From the analyzed period it can be clearly seen that, as more investments were made in upgrading the equipment, the obtained values of greenhouse gas emissions were lower, and the clearest examples are the Czech Republic – 90 tons of CO_2e, Netherlands – 90 tons and Ireland – 91 tons [10].

Europe must achieve a higher efficiency in terms of resource usage by 2020 by supporting the transition to a low carbon economy and increasing the usage of renewable energy. All these measures will help decouple economic growth from the use of conventional resources.

3. Renewable and gross final energy consumption

During 2001–2012, the share of renewable energy in the gross final energy consumption in the EU-28 was 11%, with significant differences between the first and the last countries, and it has increased steadily since 2001. The highest percentage of energy from renewable sources is in Norway – 62%, Sweden – 45%, Latvia – 32%. Romania ranks 8 in the 28 EU Member States, with an average of 20% energy from renewable sources in the gross final energy consumption. Denmark has the same percentage, 20%.

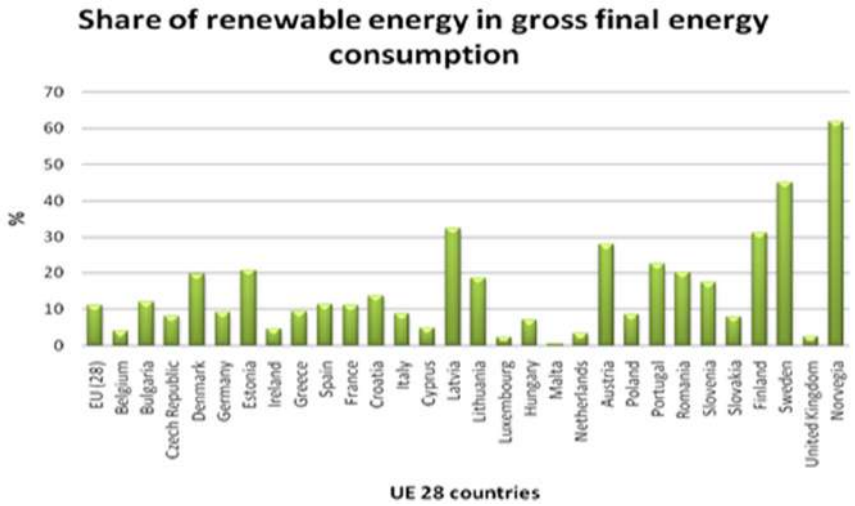

Fig. 5. *Share of renewable energy in the gross final energy consumption in EU-28*

In the share of renewable energy in final energy consumption, Hungary has only 7%, while Netherlands has only 3%. The last three places in this chapter are occupied by UK– 3%, Luxembourg – 2% and Malta – 1%. These values are proportional to the size and population of each country. The share of renewable energy in the final energy consumption varies between countries from 60% to 1 in some cases [11].

The European directives on renewable energy include, among others, the Directive on promoting the electricity from renewable energies and the Directive on promoting biofuels [12]. The number of policies adopted at national level increased after the adoption of the 2008 climate and energy package, which imposed a target of 20% of the total final energy consumption.

It has to be accepted that the application of renewable technologies depends largely on the geographical and socio-economic context situation of each Member State. EU Member States have the possibility to determine the measures that will be adopted in the electricity and heat field, to achieve the 20% of the objective.

Most of the renewable energy fields have experienced an accelerated growth since 2001. A major increase was recorded in photovoltaic solar energy in Germany, from 10/1000 toe in 2001 to 2268/1000 toe in 2012. The same extremely ascending trend was recorded in Italy, with an increase from 1/1000 toe to 1621/1000 toe, Spain – from 2/1000 toe to 704/1000 toe. For the Czech Republic, Belgium and Greece the proportion of primary production of photovoltaic energy has increased since 2008 from 1/1000 toe to about 180/1000 toe.

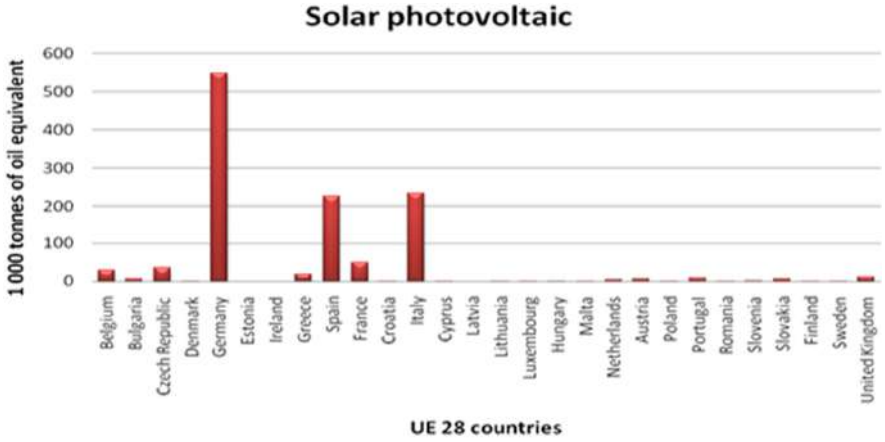

Fig. 6. *Renewable energy (solar photovoltaic technology) in EU-28*

In Romania a feeble growth can be seen starting with 2011, from 0.1/1000 toe photovoltaic primary production to 0.7/1000 toe photovoltaic primary production in 2012. Also, starting with 2011, a rise was observed in the percentage for Poland, Croatia and Lithuania, reaching, at the end of 2012, 0.1/1000 toe Estonia, Ireland and Latvia do not use solar photovoltaic energy.

The photovoltaic solar energy market is dependent on developments from Germany, which remains the world leader in the production of photovoltaic cells. In Germany this evolution is influenced by favorable policy framework, while Italy and Spain have seen this progress due to their favorable geographical context.

The evolution of primary production from wind power has seen a growth rate as upward as the wind energy in most EU-28 countries. During the period2001-2012 the primary production of wind energy varies from 2757/1000 toe to 0 in some cases. The most significant progress has been made by Germany, from 899/1000 toe to 4356/1000 toe, Spain – from 581/1000 toe to 4253/1000 toe and England – from 83/1000 toe to 1683/1000 toe.

In Romania and Bulgaria, the primary production of wind power was nonexistent until 2003, after which Bulgaria had an increase of 0.1/1000 toe to 105/1000 toe in 2012, and in the case of Romania between 2007 and2012, the amount of wind power increased from 0.3/1000 toe to 227/1000 toe. From the 28 countries, only Malta and Slovenia remain without primary production of wind energy. It is observed that most Member States have managed to increase their primary production of wind energy in response to new EU targets set for 2020 [13].

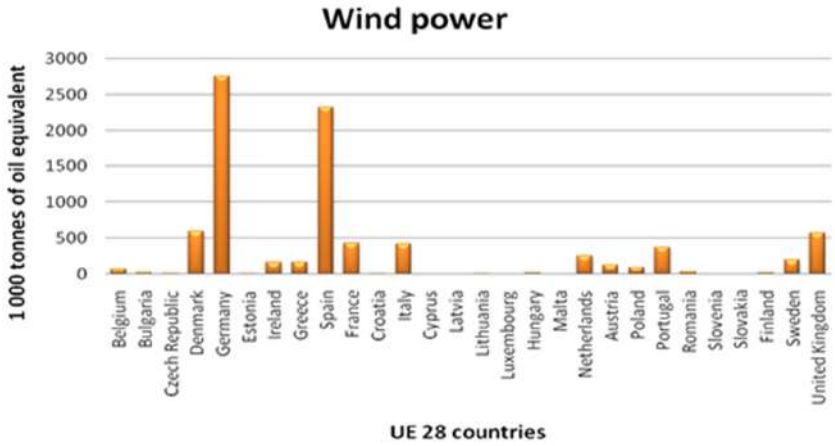

Fig. 7. *Renewable energy (wind power) in EU-28*

The renewable energy production is dominated by the large hydro plants (> 10 MW), which produced over two thirds of the EU-27's the renewable energy in the analyzed period. The greatest amount of hydroelectric power is produced in Sweden, 5779/1000 toe, on an average for the period 2001-2012.

During this period, in France and Italy, there have been decreases in hydro power production, from 6413/1000 toe to 5048/1000 toe in France and from 3829/1000 toe to 3438/1000 toe in Italy. Notable progress has been made by Bulgaria, from 149/1000 toe in 2001 to 277/1000 toe in 2012, and Estonia, which has increased the amount from 0.6/1000 toe to 3.6/1000 toe. Spain has halved the amount of energy, from 3515/1000 toe to 1766/1000 toe. In Romania the production decreased from 1283/1000 toe to 1037/1000 toe in 2012 [14].

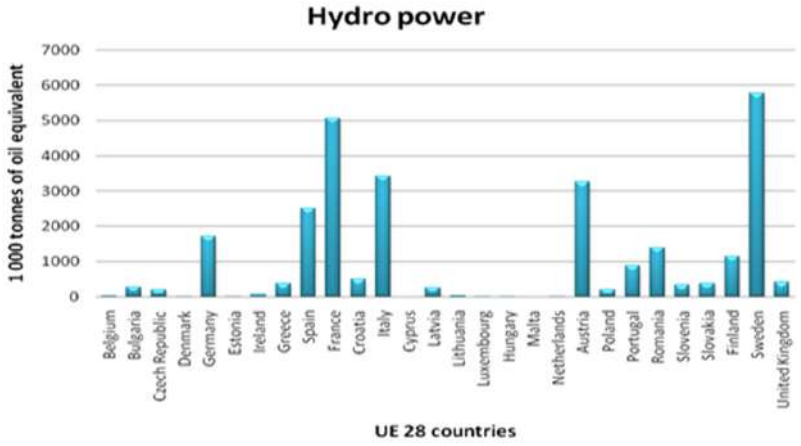

Fig. 8. *Renewable energy (hydropower) in EU-28*

The development of micro hydro power plants has been limited since 2006 by the constraints imposed by the Water Framework Directive. The fluctuations in hydropower production were mostly caused by the climate change, which led to low precipitation and prolonged droughts.

4. Conclusions

The rhythm of the exploitation of primary energy resources, the risk of their decreasing in a few decades, rising energy prices, also the increasing of the amount of imported energy resources and also a more significant climate change lead to the idea that renewable energy sources (solar, wind power, hydro-electricity) are the only real alternatives to fossil fuels.

In the near future, energy consumption will be particularly controlled and directed by carefully monitoring of the energy efficiency and through the diversification of primary energy sources. An increasing energy efficiency can be achieved by

reducing specific energy consumption for the same product, service or process, without affecting the quality of the product, service or process.

The reduction of environmental pollution, the maintenance of raw material and energy reserves are the main targets of energy efficiency analysis. A sustainable society is based primarily on an increase in the efficiency of energy usage, the increase of energy security by limiting the dependence on resources from outside the EU.

Acknowledgement

The work of Carmelia Mariana Dragomir was supported by Project SOP HRD - PERFORM /159/1.5/S/138963, project co financed from ESF of EC, the Romanian Government, and "Dunarea de Jos" University of Galati.

References

[1]. *,** *Europe 2020 - A strategy for smart, sustainable and inclusive growth* – Brussels (2010).
[2]. Commission of the European Communities, *Communication from the Commission -The support of electricity from renewable energy sources – Brussels*, COM (2005) 627 final.
[3]. Commission of the European Communities - Communication from the Commission to the European Council and the European Parliament, *An Energy Policy for Europe {Sec (2007) 12} Brussels*, Com (2007) 1 Final.
[4]. Edenhofer O., Pichs-Madruga R., Sokona Y., Seyboth K., Matschoss P., Kadner S., Zwickel T., Eickemeier P., Hansen G., Schlömer S., von Stechow C., *IPCC Special Report on Renewable Energy Sources and Climate Change Mitigation. Prepared by Working Group III of the Intergovernmental Panel on Climate Change*. Cambridge University Press, Cambridge, United Kingdom and New York (2012), NY, USA, p. 1075.
[5]. Environmental indicator report 2012, *Ecosystem resilience and resource efficiency in a green economy in Europe EEA*, Copenhagen (2012).
[6]. European Environment Agency, *European Union emission inventory report 1990–2010 under the UNECE Convention on Long-range Transboundary Air Pollution (LRTAP),* **(**2012).
[7]. Eurostat News Releases on the internet: http://ec.europa.eu/eurostat/ Accessed on July 2014.
[8]. http://epp.eurostat.ec.europa.eu/tgm/table.do?tab=table&init=1&plugin=1&language=en&pcode=tsdcc310, accessed on July 2014.
[9]. *,** http://ec.europa.eu/geninfo/legal_notices_en.htm, Accessed on July 2014.
[10]. WBGU, *World in Transition – Future Bioenergy and Sustainable Land Use*, German Advisory Council on Global Change (WBGU), Earthscan, London, UK, (2009).
[11]. *,** *Romanian Energy Strategy for the period 2007 to 2020 updated for the period 2011-2020.*
[12]. Territorial Agenda of the European Union in 2020, *Towards a smart, sustainable and inclusive of Diverse Regions*, May 2011 in Gödöllő, Hungary.
[13]. UNEP, *Global Trends in Sustainable Energy Investment 2009: Analysis of Trends and Issues in the Financing of Renewable Energy and Energy Efficiency*. United Nations Environment Programme, Paris, France (2009).
[14]. REN21, *Renewables 2010 Global Status Report. REN21 Renewable Energy Policy Network for the 21st Century*, Paris, France. Reprinted with permission from REN21, (2010).

THE ANNALS OF "DUNAREA DE JOS" UNIVERSITY OF GALATI
FASCICLE IX. METALLURGY AND MATERIALS SCIENCE
No. 4 – 2014, ISSN 1453 – 083X

CHARACTERIZATION OF ARCHAEOLOGICAL OBJECTS COMING FROM MOLDOVIAN SETTLEMENTS IN THE XIVTH CENTURY

Mihaela POTECAȘU, Marian BORDEI
"Dunarea de Jos" University of Galati
e-mail: mbordei@ugal.ro

ABSTRACT

This paper presents the characterization, from the materials science point of view, of an object found in an archaeological vestige of the 14th century.

The object studied (an iron nail used in constructions) proves that the inhabitants of those lands were very good craftsmen, capable of performing useful products for everyday life, who worked with precision, ingenuity and ability.

The analysis of the archaeological relic led to the conclusion that plastic deformation was achieved by successive cycles of hammering (driving) applied after repeated heating meant to enable the material to regain its deformability so that, through low repeated deformation, it could finally reach the requested shape.

The process is revealed by microstructural analysis and by the value obtained for hardness.

KEYWORDS: nail, plastic deformation, strings oxides, archaeology

1. Introduction

Despite the fact that the processing of raw materials was complex and difficult, the craft of iron processing originated in the earliest times of human existence and continuously improved with the development of human society. In what regards the exploitation of iron and brass, the written documents of the fourteenth and fifteenth centuries contain little information, but supplemented by archaeological testimonies. Archaeological excavations have revealed man-made tools: hammers, anvils, pliers, chisels, household items (knives, locks, keys), objects for construction (nails, chisels), or parts of weapons and harness.

The techniques used in the production of iron tools and objects in the 14th-15th centuries were: casting, hot and cold processing, heat treatments.

The ore rock was taken to pieces using crowbars, and the pieces were broken with hammers (later hydraulically); the ore was previously crushed, washed and sorted, then, before being introduced into the furnace, it was roasted to remove water and ferrous components. From the mineral thus prepared, the iron reduction followed using the procedures documented in the 9th-13th centuries in an oval oven-furnace built partially in the ground, the inner walls being coated with clay "with a siliceous refractory facing". After placing the ore and charcoal in layers, and sometimes adding pieces of limestone (lime), the preparatory operations were over and the burning process that followed was maintained by air currents using bellows. In the oven, temperatures were between 1300 and 1450 °C. This type of furnace, as evidenced by the findings at Ghelar (9th-10th centuries), Hlincea (11th century), partly to Bucov (10th century) and Barlad (11th-12th centuries), similar to that discovered in other European countries about the same time, continued to be used in the Romanian countries in the 14th and 15th centuries [1, 2].

If, in early feudalism, extractive metallurgy was not separated from processing metallurgy (e.g. Bucov, 10th-11th centuries), starting with the 14th century the process of separation emerges, certified by the workshops where the iron objects were made (e.g. Zimnicea), but which do not contain any trace (pieces of ore, slag) resulting from the reduction of mining operations. The object processing was done at a temperature of about 1000 °C, as the craftsmen of that period knew how to make steel (research revealed the existence of a 0.370 carbon steel in the metal paste with a rather homogeneous structure) for steel blades (swords, knives) [1, 3].

Cold working operations that include modeling by "hammering", cutting, stamping, drilling, incision, bending, twisting, cold riveted joint are used in particular for working bands, bars, thin sheet and wire. Hot working operations include: bonding, bending, twisting, drilling. These techniques are used, in particular, for heavy parts so that, together with the

cold working techniques, they form an assembly which allows obtaining multiple types of objects made of iron or its alloys with carbon. The different hardening procedures ensured the hardness and resistance of the processed iron objects. The skill of the autochthonous craftsmen regarding hardness is demonstrated by the fact that all the pieces found are hardened; moreover, the hardness is not uniform but it is differently executed only on the active parts of the piece.

There are some cases considered extraordinary for the technologies in that period or at least incompletely elucidated scientifically. One such example is the "dacian nail" found in the Dacian sanctuary at Racoş (Romania). According to the analysis carried out by the physicist Andrei Vartic at the Institute of Metallurgy in Balti (Rep. of Moldova), this one dates back over 2,000 years and is assigned to the Dacian culture. The Nail, considered an "ancient miracle" consists of 99.97% pure alpha iron without traces of impurities (carbon compounds remaining from processing), which leads to the conclusion that it could have been done by techniques and under conditions inexistent during that period.

Further research conducted in Leningrad and Moscow can lead to the conclusion that the protection is given by three molecular layers: first layer (surface) - Magnetic "Fe_3O_4"; second layer - Iron Oxide "FeO"; third layer - alumo silicates [4]. The Dacian nail is found at the cedar doors of St. Catherine's Monastery in Sinai.

The study of this work was done on a metal nail originating in an archaeological vestige from the 14th century and pursued its characterization: determination of chemical composition, metallographic analysis and hardness determination.

2. Results and discussions

The chemical composition of the sample was determined using a portable metal analyzer (X-ray fluorescence spectrometer Innov-X Systems brand) and is presented in Table 1.

Table 1. *Chemical composition of the studied object*

Object	*Chemical composition* **(%)**			
	C	**Mn**	**Si**	**Al**
Nail	0.10	0.13	0.084	0.026

A first finding of the macrostructural analysis carried out on the studied object is the advanced state of degradation of the object and the penetration of oxide films in the thickness of the product as seen in the microstructural analysis performed in the longitudinal section of the object (Figure 1).

In Figure 1, using the 100X microscope increase, uncontested evidence is found regarding the degradation mechanism and damage on the analyzed object under the action of chemical agents in the external environment from chemical (especially electrochemical) reactions which started from the nail surface to its core (process known as rust of iron).

The areas analyzed showed that object-environment interaction in time evolved unevenly and non-simultaneously.

Thus, after the appearance of destruction, highly complex phenomena of corrosion are observable, i.e. corrosion both continuous (because the entire metal-environment interface showed destructive action of aggressive environment) and local (because the destruction occurs in depth pin, mostly in certain areas with greater instability).

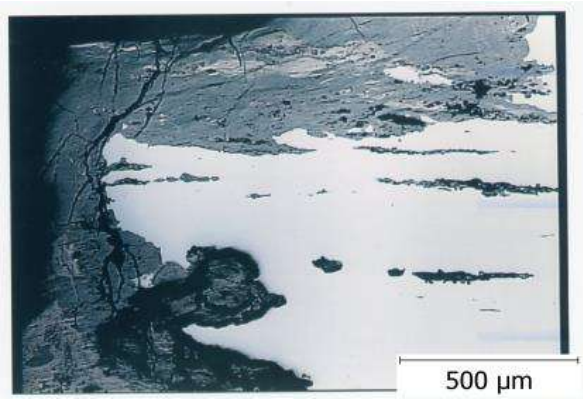

Fig. 1. *Nail microstructure in longitudinal section in the end section (no metallographic attack) magnification x100*

The macrostructural analysis of the studied object shows that the continuous corrosion process evolved over the centuries and the nail oxidation in the atmosphere led to its dressing in layers of brown and black iron oxide (the so-called iron rust).

According to the literature [5, 6], it is known that, in the first stage of iron oxidation, FeO is formed, ferrous oxide, which is stable only in the absence of oxygen. When the atmospheric oxygen appears, the iron oxide is converted into iron hydroxide ($Fe_2O_3H_2O$) and FeO (OH), in two phases:

- phase 1, corresponding to a large excess of oxygen;
- phase 2, characterized by an amount of insufficient oxygen that slows down the oxidation process.

Depending on the rust color, 3 type scan be distinguished:

1. White rust $Fe(OH)_2$, which is formed by the reaction

$$Fe+2H_2O \rightarrow Fe(OH)_2+H_2$$

This type of rust quickly changes through oxidation into brown rust; that is why it is so rarely observed.

2. Brown rust occurs from the reaction

$$4Fe(OH)_2+O_2 \rightarrow 4FeO\cdot OH+2H_2O$$

3. Black rust consists of ferrous and ferric oxide (also called magnetite because of its magnetic properties) and is considered the most stable form of iron oxide. It forms on the metal surface a protective layer with homogeneous and adherent structure. The reaction proceeds as follows:

$$2FeO\cdot OH+Fe(OH)_2 \rightarrow Fe_3O_4+2H_2O$$

The microstructural aspect of Figure 1 shows that local corrosion has several aspects:

• punctiform corrosion, located on small surfaces (corrosion points);

• under subsurface corrosion, starting at the surface but preferably extending below the metal surface, which causes metal swelling and peeling (corrosion bags);

• corrosion spots, distributed on relatively large areas, but of small depth;

• intercrystalline corrosion, characterized by the selective destruction of the metal on the edge of the crystals;

• transcristalline corrosion, a typical local corrosion at which the corrosive destruction of the mechanical stresses is determined by the direction of stretching.

Characteristic of this type of corrosion is that cracks do not propagate only at the crystal's edge but they actually transit them.

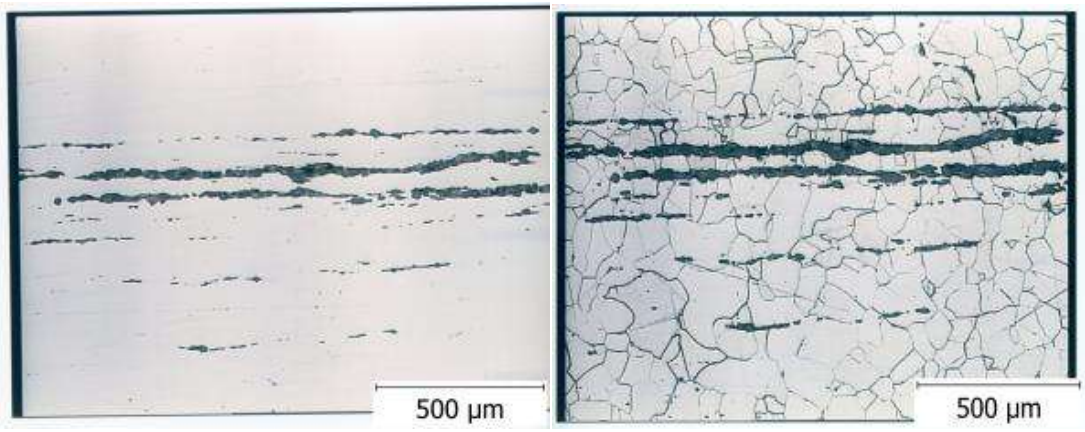

Fig. 2. *Nail microstructure in longitudinal zone in the end section (a - metallographic attack-free, b - with metallographic attack), magnification x 100*

On the metallographic sample attack (NITAL reagent 2%), the microstructural analysis carried out in longitudinal section shows a structure made of a ferritic matrix with tertiary cementite separation and small pearlite amounts (in agreement with the content of 0.1% C determined by the fluorescence spectrometer).

On the sample without metallographic attack, the microstructural analysis performed in longitudinal section shows the fibering inclusions and corrosion preferentially developed in the metallic base mass of the pin on these strings of inclusions. In Figure 2b the pin microstructure in longitudinal section towards the end (the outer edge of the nail) shows only a ferrite and tertiary cementite structure (F + Fe3CIII), indicating a low carbon content (less than 0.0218%), i.e. advanced decarburization due to successive heating cycles necessary to achieve the object by

plastic deformation. Here, the crystalline grains are coarser compared to grains from the center section. This decarburization is confirmed by the very low hardness 110-120 HB, compared to values of 140-145 HB towards the center area of the nail longitudinal section with finer granulation and where pearlite grains are also present. The ferrite in the base mass of the analyzed object is a light hardened ferrite of manganese and silicon atoms dissolved by substitution in the iron network (Table 1).

3. Conclusions

• The analyzed object comes from an archaeological relic of 14th century Moldovan settlements.

• The Analysis of the object (iron nail) led to the conclusion that plastic deformation was achieved by successive cycles of hammering (driving) applied after repeated heating meant to enable the material to regain its deformability so that, by low repeated deformation, to obtain finally the desired shape.

• Repeated heating (probably in fire) had the effect of decarburization emphasized in the surface layer.

• The microstructure consists of ferrite and tertiary cementite on the surface of the object (decarburized zone) and ferrite with tertiary cementite separations and small amounts of perlite in the core of the object.

• Hardness varies according to the microstructure from 110-120 HB to the outer edge of the studied object in longitudinal section to 150-155 HB to the center.

• The studied object (iron nail) proves that people from Moldovan lands were very good craftsmen, capable of performing useful products for everyday life, who worked with precision, ingenuity and ability.

References

[1]. Dinu C. Giurescu, *Ţara Românească în sec. XIV-XV*, Ed. Stiintifica, Bucuresti, 1973.
[2]. Şt. Olteanu, Const. Şerban, *Meşteşugurile din Ţara Românească şi Moldova în evul mediu*, Bucureşti, 1969.
[3]. Nicolae Maghiar, Şt. Olteanu, *Din istoria mineritului în România*, Bucureşti, 1970.
[4]. *,** http://dacia.8m.net/Diverse/Cuiul_dacic/cuiul_dacic.html.
[5]. Edith Beral, Mihai Zapan, *Chimie Anorganică (ediţia IV)*, Editura Tehnică, Bucureşti 1977.
[6]. P. Spacu, Constanţa Gheorghiu, Marta Stan, Maria Brezeanu, *Tratat de Chimie Anorganică (volumul III)*, Editura Tehnică, Bucureşti 1978.
[7]. Valeriu Sărbu, Paul Damian, Oana Damian, Emilian Alexandrescu, Stănică Pandrea, Elvira Safta, Alexandru Niculescu, *Aşezări din zona Căscioarele-Greaca–Prundu – mileniile I î.Hr. – I d. Hr.*, Editura Istros, Brăila 1996, p. 139.
[8]. Ana Doniga, Florentina Potecaşu, Ovidiu Dima, *Obiecte din fier provenite din aşezările geto-dacice din zona Căscioarele–Greaca*, Monografii arheologice III, Editura Istros, Brăila 1996.
[9]. Cociş Sorin, *Fibule în formă de ancoră. Tipologie, cronologie, arie de răspândire, modă, ateliere*, în Ephemeris Napocensis, XIV – XV, p. 123-166, 2004-2005.

THE ANNALS OF "DUNAREA DE JOS" UNIVERSITY OF GALATI
FASCICLE IX. METALLURGY AND MATERIALS SCIENCE
N°. 4 – 2014, ISSN 1453 – 083X

STUDY ON THE RHEOLOGY OF CORN OIL SUBJECTED TO FORCED OXIDATION

Liviu Cătălin ŞOLEA, Romică CREŢU
"Dunarea de Jos" University of Galati
e-mail: catalin.solea@ugal.ro

ABSTRACT

This paper reflects a study on the rheology of corn oil in unoxidized state, subjected to forced oxidation treatment. Using the Rheotest2 system, the variation of dynamic viscosity with temperature and shear rate, using oxidized and non-oxidized corn oil, was determined. The oils were heated to 110 °C and 120 °C and the temperature was maintained for 5 to 10 hours. The experiments showed the decrease of dynamic viscosity with temperature and shear rate. The oxidation process causes a sharp increase in the dynamic viscosity of the oxidized corn oil for 10 hours at 120 °C. The measurement of the dynamic viscosity of the oils subjected to the oxidation process is an indicator of the degree of oxidative degradation of vegetable oils.

KEYWORDS: corn oil, lubrication, biodegradable, shear rate, viscosity, oxidation

1. Introduction

Currently, 50% of all lubricants used in the world end up in the environment, by total loss, volatility or major accidents. Before the year 2000, 95% of these materials were based on mineral oils. Due to their ecotoxicity and low biodegradability, they constitute a considerable threat to the environment, although they are efficient lubricants, with good tribological properties [1]. Biodegradable oils are, at the moment, a high achievement in the field of lubrication in equipment and machinery mainly working under conditions that may result in environmental pollution. Lately, the emphasis is on the use of vegetable oils as the basis of biodegradable lubricants. The rheological properties of vegetable oils depend on many factors, including temperature, shear rate, concentration, density, pressure, time of application, chemical properties, additives and catalysts, molecular weight, degree of unsaturation of fatty acids, melting point [2-6]. Most research has been directed to study the effects of temperature, shear rate, concentration and pressure. The most important factor affecting viscosity is temperature. The viscosity of oils and fats decreases with the increase of temperature [7-10]. Wan Nik, Ani, Masjuki and Eng Giap [11] evaluated the effects of shear rate and temperature on the rheological properties of vegetable oils from sun flower, corn, canola, coconut and superolein.

2. Experimental results

Viscosity was determined with the help of a Rheotest 2 system, shear rates ranging between 3.3 s^{-1} and 80 s^{-1}, the test temperatures being between 40 °C and 80 °C (determinations were done for each step of 10 °C, in this range).

To perform forced oxidation, a system was built, as presented in Figure 1. It consists of: 1 - air pump, 2 - air flow meter, 3 - air filter, 4 - tube with oil sample, 5 - thermostatic bath. For each oxidation test, 25 ml of oil were used. The flow rate of air introduced into the oil sample was 20 l/h.

Fig. 1. *Oxidation equipment*

The corn oil was oxidized at temperatures of 110 ºC and 120 ºC for 5 hours and 10 hours. The results obtained are presented in Figures 2-5. They

show variations in dynamic viscosity depending on the shear rate corresponding to the test temperatures of 40 ºC and 80 ºC.

2.1. Dynamic viscosity changes depending on shear rate

At both temperatures and periods of oxidation, as well as test temperatures, dynamic viscosity decreases when the shear rate increases. The decrease in dynamic viscosity is much more accentuated at low shear rates.

Corn oil oxidation at 110 ºC and 120 ºC for 5 hours and 10 hours causes increases in the dynamic viscosity of the oils in comparison with unoxidized oil, a phenomenon observed at both temperatures.

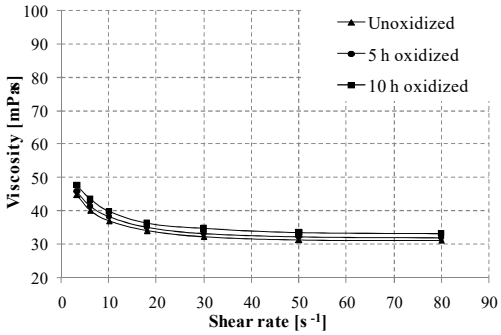

Fig. 2. *Variation of viscosity with shear rate, at 40 ºC, for corn oil oxidized at 110 ºC*

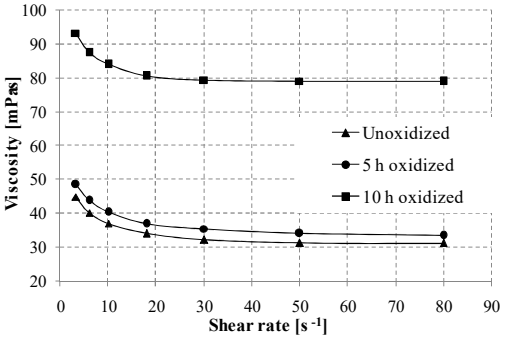

Fig. 3. *Variation of viscosity with shear rate, at 40 ºC, for corn oil oxidized at 120 ºC*

A large increase in dynamic viscosity can be observed with an increase in the oxidation period, from 5 hours to 10 hours. The largest increase in dynamic viscosity is recorded at a temperature of oxidation of 120 ºC, for oil oxidized for 10 hours, the temperature of the test being of 40 ºC.

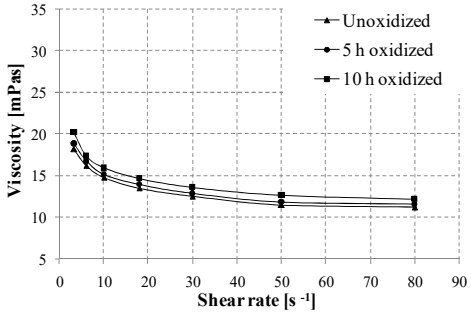

Fig. 4. *Variation of viscosity with shear rate, at 80 ºC, for corn oil oxidized at 110 ºC*

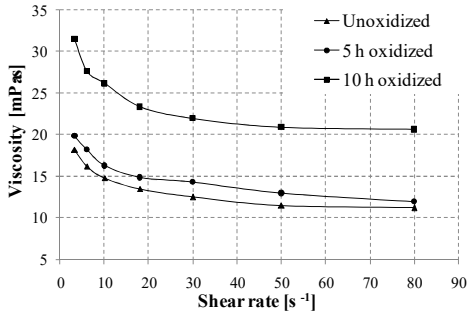

Fig. 5. *Variation of viscosity with shear rate, at 80 ºC, for corn oil oxidized at 120 ºC*

By increasing the test temperature from 40 ºC to 80 ºC, a less significant increase of the dynamic viscosity could be noticed.

2.2. Dynamic viscosity changes depending on temperature

In Figures 6-9 the dynamic viscosity changes depending on temperature were represented, for corn oils oxidized at temperatures of 110 ºC and 120 ºC for 5 hours and 10 hours, corresponding to shear rates of 6 s^{-1} and 50 s^{-1}.

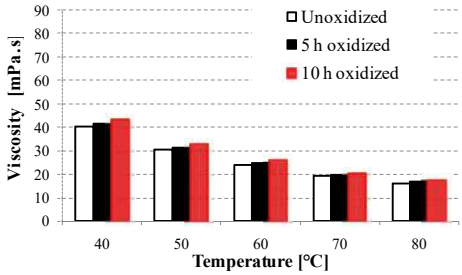

Fig. 6. *Variation of viscosity with temperature, at 6^{-1} shear rate, for corn oil oxidized at 110 ºC*

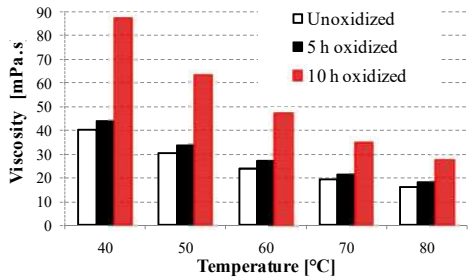

Fig. 7. *Variation of viscosity with temperature, at 6^{-1} shear rate, for corn oil oxidized at 120 ºC*

For both temperatures and periods of oxidation, as well as shear rates, the dynamic viscosity decreases with the increase in the temperature at which the oils have been tested.

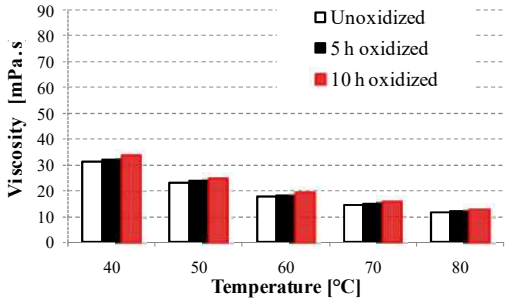

Fig. 8. *Variation of viscosity with temperature, at 50^{-1} shear rate, for corn oil oxidized at 110 ºC*

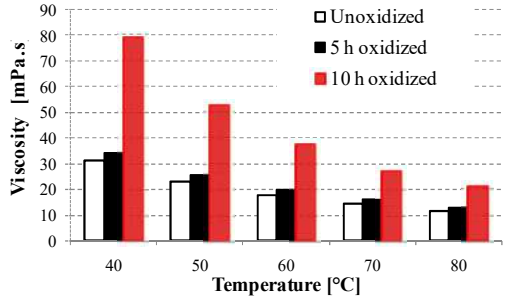

Fig. 9. *Variation of viscosity with temperature, at 50^{-1} shear rate, for corn oil oxidized at 120 ºC*

Corn oil oxidation at a temperature of 110 ºC for 5 and 10 hours, tried to shear rates of 6 s^{-1} and 50 s^{-1}, does not cause significant increase in dynamic viscosity in comparison to unoxidized oil.

The increase in the temperature of the oxidation from 110 ºC to 120 ºC leads to a strong rise in the dynamic viscosity of the oil oxidized for 10 hours. Tested at a temperature of 40 ºC, the viscosity of the oil oxidized for 10 hours at a temperature of 110 ºC and a shear rate of 6 s^{-1} is 8.1% higher than that of unoxidized oil, while after 5 hours of oxidation, the viscosity increased by only 3.1%. At the same test temperature, the viscosity of the oil oxidized for 10 hours at a temperature of 120 ºC and a shear rate of 6 s^{-1} is 117.7% higher than that of unoxidized oil, while after 5 hours of oxidation, the viscosity increased by only 8.8 %. In the case of the test temperature of 80 ºC, the viscosity of the oil oxidized for 10 hours at a temperature of 110 ºC and a shear rate of 6 s^{-1} is 7.3% higher than that of unoxidized oil, while after 5 hours of oxidation, the viscosity increased by only 3.5%.

At the same temperature of the test, the viscosity of the oil oxidized for 10 hours at a temperature of 120 ºC and a shear rate of 6 s^{-1} is 70.7% higher than that of unoxidized oil, while after 5 hours of oxidation, the viscosity increased by only 12.5%.

In the case of corn oil oxidized for 10 hours at a temperature of 110 ºC and a shear rate of 6 s^{-1}, the increase in the temperature of the test from 40 ºC to 80 ºC causes a decrease in the dynamic viscosity by 60.1%, while for the shear rate of 50 s^{-1}, the decrease is 62.2% (comparable with that recorded at a shear rate of 6 s^{-1}).

Increasing the oxidation temperature to 120 ºC for the corn oil oxidized for 10 hours, the percentage variation in dynamic viscosity, between the temperatures of 40 ºC and 80 ºC, is 68.46% for the shear rate of 6 s^{-1} and 73.6% for the shear rate of 50 s^{-1}.

To support our results regarding the variation in viscosity depending on temperature, the Andrade equation (1) and the Azian equation (2) [12-16] were used:

$$\ln \eta = \ln A + \frac{B}{T} \quad (1)$$

$$\ln \eta = A + \frac{B}{T} + \frac{C}{T^2} \quad (2)$$

where T is the absolute temperature and A, B and C are material constants.

The rheological parameters of the Andrade and Azian equations as well as the correlation coefficients are presented in Tables 1 and 2.

It should be noted that the resulting correlation coefficients are higher for the Azian equation (values between 0.99954 and 0.99996). This equation approximates very well the experimental results, and can be used to determine the variation of the dynamic viscosity of the vegetable oils depending on their temperature.

3. Conclusions

This study focuses on the variation of dynamic viscosity with temperature and shear rate for corn oil in unoxidized state, as well as oxidized for 5 and 10 hours at 110 °C and 120 °C.

It was noted that the viscosity decreases with increasing shear rate and temperature. A significant decrease in viscosity is recorded at low shear rates. During the process of forced oxidation, there occurs a formation of hidroperoxides which causes the appearance of non-volatile compounds (dimers, trimers and compounds of high molecular weight), the result being the increase of the oil's viscosity. The largest increases in dynamic viscosity were observed at a temperature of oxidation of 120 ºC maintained for 10 hours.

The measurement of the dynamic viscosity of the oils subjected to the oxidation process could be an indicator of the degree of oxidative degradation of vegetable oils. To study the change of dynamic viscosity depending on temperature, the Andrade and Azian equations were used to determine the rheological parameters and the correlation coefficients. From the analysis of the latter, there were noted values of the correlation coefficients closer to 1 when using the Azian equation. This equation gives the best approximation on the experimental data and can be used to assess the change in the dynamic viscosity of oils depending on temperature variation.

Table 1. *Parameters of the Andrade equation*

Shear rate [s^{-1}]	***Parameters***		***lnA***	***B***	***Correlation coefficients***
6	*Unoxidized*		-4.39013	$2.5252 \cdot 10^3$	0.9986
	Oxidized at 110 ºC	*5 h*	-4.35212	$2.5228 \cdot 10^3$	0.9982
		10 h	-4.42020	$2.5602 \cdot 10^3$	0.9987
	Oxidized at 120 ºC	*5 h*	-4.08455	$2.4592 \cdot 10^3$	0.9989
		10 h	-5.7845	$3.2101 \cdot 10^3$	0.9997
50	*Unoxidized*		-5.3312	$2.7406 \cdot 10^3$	0.9991
	Oxidized at 110 ºC	*5 h*	-5.2907	$2.7373 \cdot 10^3$	0.9991
		10 h	-5.0489	$2.6734 \cdot 10^3$	0.9987
	Oxidized at 120 ºC	*5 h*	-5.0166	$2.6698 \cdot 10^3$	0.9988
		10 h	-7.4141	$3.6826 \cdot 10^3$	0.9991

Table 2. *Parameters of the Azian equation*

Shear rate [s^{-1}]	***Parameters***		***A***	***B***	***C***	***Correlation coefficients***
6	*Unoxidized*		6.4875	$-4.7087 \cdot 10^3$	$1.2 \cdot 10^6$	0.99992
	Oxidized at 110 ºC	*5 h*	7.8593	$-5.5983 \cdot 10^3$	$1.347 \cdot 10^6$	0.99987
		10 h	5.6859	$-4.1607 \cdot 10^3$	$1.115 \cdot 10^6$	0.99985
	Oxidized at 120 ºC	*5 h*	3.2163	$-2.3961 \cdot 10^3$	$0.805 \cdot 10^6$	0.99954
		10 h	3.7262	$-2.7621 \cdot 10^2$	$1.039 \cdot 10^6$	0.99985
50	*Unoxidized*		3.9037	$-3.41 \cdot 10^3$	$1.019 \cdot 10^6$	0.99981
	Oxidized at 110 ºC	*5 h*	3.9961	$-3.4387 \cdot 10^3$	$1.025 \cdot 10^6$	0.99984
		10 h	6.0421	$-4.7026 \cdot 10^3$	$1.224 \cdot 10^6$	0.99992
	Oxidized at 120 ºC	*5 h*	5.4683	$-4.3031 \cdot 10^3$	$1.156 \cdot 10^6$	0.99994
		10 h	5.8371	$-5.129 \cdot 10^3$	$1.462 \cdot 10^6$	0.99996

References

[1]. Schneider M., Smith P., *Plant Oil in Total Loss & Potential Loss Applications*, Finall Report, 2002.

[2]. Revwolinski C., Shaffer D. L., *Sunflower oil diesel fuel: lubrication system contamination*, JAOCS, 62, p. 1120-1124, 1985.

[3]. Rosana F. T. L., Carlos H. M., Edimir, M. B., *A new approach to evaluate temperature effects on rheological behavior of formate-base fluids*, J. Energy Resour. Technol., 124, p. 141-144, 2002.

[4]. Chen D. H., Hong L., Nie X. W., Wang X. L., Tang X. Z., *Study on rheological properties and relaxational behavior of poly(dianilinephosphazene)/low-density polyethylene blends*, Eur. Polym. J., 39, p. 871-876, 2003.

[5]. Georgopoulos T., Larsson H., Eliasson A. C., *A comparison of the rheological properties of wheat flour dough and its gluten prepared by ultracentrifugation*, Food Hydrocolloids, 18, p. 143-151, 2004.

[6]. Igwe I. O., *The effects of temperature on the viscosity of vegetable oils in solution*, Ind. Crop. Prod., 19, p. 185-190, 2004.

[7]. Eromosele C. O., Paschal N. H., *Short communication characterization and viscosity parameters of seed oils from wild plants*,Bioresour. Technol., 86, p. 203-205, 2003.
[8]. Hasan S. W., Ghannamb M., Esmail N., *Heavy crude oil viscosity reduction and rheology for pipeline transportation*, Fuel, 89, p. 1095-1100, 2010.
[9]. Quinchia L. A., Delgado M. A., Franco J. M., Spikes H. A., Gallegos C., *Low temperature flow behavior of vegetable oil-based lubricants,* Industrial Crops and Products, 37, p. 383-388, 2012.
[10]. Quinchia L. A., Delgado M. A., Valencia C., Franco J. M., Gallegos C., *Viscosity modification of different vegetable oils with EVA copolymer for lubricant applications,* Ind. Crop. Prod., 32, p. 607-612, 2010.
[11]. Wan Nik W., Ani F. N., Masjuki H. H., Eng Giap S. G., *Rheology of bio-edible oils according to several rheological models and its potential as hydraulic fluid*, Industrial Crops and Products, 22, p. 249-255, 2005.
[12]. Rodenbush C. M., Hsieh F. H., Viswanath D. S., *Density and viscosity of vegetable oils*, J. Am. Oil Chem. Soc., p. 76-141, 1999.
[13]. Krisnangkura K., Yimsuwan T., Pairintra R., *An empirical approach in predicting biodiesel viscosity at various temperatures*, Fuel, p. 85-107, 2006.
[14]. Esteban B., Riba J. R., Baquero G., Rius A., Puig R., *Temperature dependence and viscosity of vegetable oils*, Biomass and Bioenergy, 42, p. 164-171, 2012.
[15]. Perez A. T., *Characterisation of the rheological properties of lubricants for EHL film thickness prediction*, TriboUK, Imperial College, London, 2010.
[16]. Azian M. N., Kamal A. A. M., Panau F., Ten W. K., *Viscosity estimation of triacylglycerols and of some vegetable oils based on their triacylglycero composition*, J. Am. Oil Chem. Soc., 78:1001, 2001.

THE ANNALS OF "DUNAREA DE JOS" UNIVERSITY OF GALATI
FASCICLE IX. METALLURGY AND MATERIALS SCIENCE
N°. 4 – 2014, ISSN 1453 – 083X

COMPUTER VISION SYSTEM FOR DETECTION OF PASSENGER SLEEPING STATE FOR ADVANCED DRIVER ASSISTANCE SYSTEMS

Ionel PETREA, Florin Bogdan MARIN
"Dunărea de Jos" University of Galaţi, Romania
e-mail: florin.marin@ugal.ro

ABSTRACT

The goal of this research is to develop an in-vehicle computerized system able to warn the driver, to assess the passenger's state of sleeping in order to avoid affecting the driver psychologically and induce drowsiness. This new feature proposed for Advanced Driver Assistance System might increase car safety by mitigation or avoidance of accidents.

KEYWORDS: computer vision**,** passenger fatigue detection, Advanced Driver Assistance System

1. Introduction

Every year in Europe more than 40000 casualties and 1.3 million injuries are caused by car accidents [1]. The advances in passive safety have reached their limits regarding consumption conditions, as traditional materials are used for manufacturing safety components. Also, passive safety has limits concerning speed due to the huge amount of deceleration to human body. The safety potential of further improvements in passive safety features is limited. However, Advanced Driver Assistance Systems (ADASs) have the potential to significantly reduce the number of road accidents, mitigate and moreover reduce accident casualties and victims. An ADAS is a vehicle control system that uses different sensors (e.g. camera, radar, laser, vision) to improve traffic safety by assisting and warning the driver in potentially dangerous traffic situations. Nowadays an ADAS can even autonomously intervene in case of dangerous situations.

There are many ADAS systems [2–9] concerning issues such as traffic sign recognition, forward collision warning, lane warning departure, parking assistance, etc. Nearly 80 percent of all crashes involve driver inattention or sleepy state [10].

Drowsiness appears in situations of fatigue and it may be produced by several factors such as sleep disorders, medications, and even the fact that the right passenger is sleeping during a long, especially night, drive, as stressed by psychological studies [1].

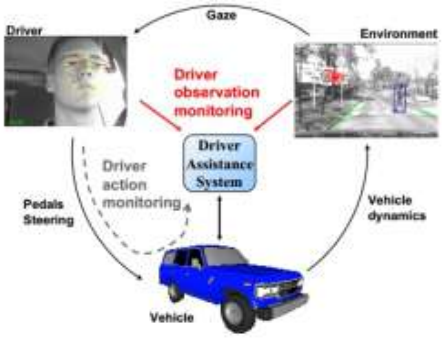

Fig. 1. *Principle of driver drowsiness warning systems* [11]

It has been revealed that drowsiness causes between 10% and 20% of traffic accidents with casualties and injured drivers [12]. Other authors [13] estimate that 30% of all traffic accidents have been caused by drowsiness. According to recent road safety surveys, fatigued driving is a common cause of accidents in Canada.

The main concern related to drivers falling asleep is their high crash rate. Fatigue and sleepiness are typically shown in the driver's facial expression and affect eye movement, gaze orientation, and head and body movement (Fig. 1). Such visual cues are analyzed by various computer vision techniques for the detection of fatigue [13-19]. There are research groups dealing with occupant posture analysis but only for airbag activation and not for detection of sleepiness.

Starting from a psychological study [1], this paper proposes a new feature for ADAS, aiming for the real-time detection of sleep onset in a fatigued passenger. Sleep onset is one of the most important consequences regarding high causalities as shown by statistics all over the world.

One of the reasons for driver sleep onset is the co-driver state of sleep. Therefore, unlike previous related work, we separate the issue of driver sleep onset from the right passenger sleep onset and we consider a major influence the physiological state of fatigue of the right passenger (co-driver in case of truck transport). This allows us to formulate our approach as an event-detection problem. Real-time performance is achieved by focusing on a multiple visual cue (eye-state, movement, face position), and by a custom-designed template-matching algorithm for passenger state detection.

The system proposed offers a non-invasive and low-cost alternative to electrode-based measures of fatigue. The approach proposed tracks eye and body motion from video data acquired with one camera placed on the dashboard of the car. In terms of simplicity, the hardware architecture is similar to another approach mentioned above concerning driver sleep detection. However, their scope lies in monitoring the visual attention of the driver, which is different from occupant fatigue.

The proposed algorithm is designed for on-line data processing: when detecting that the occupant is sleeping, it will activate a warning audio alarm to inform the passengers in the car.

2. Technique proposed

Experimental results were acquired using the Logitech C170 placed on dashboard as webcam (Fig. 3), and the Acer NoteBook 1.6 GHz with 1 GB RAMas processing unit. The video sequences were acquired at 20 frames per second. The proposed approach was implemented in Microsoft Visual C++ and OPenCV library. Figure 2 shows the general algorithm to detect passenger sleeping state. While preliminary tests have shown that the proposed approach works well in the in-vehicle environment, all results reported here have been obtained using offline video.

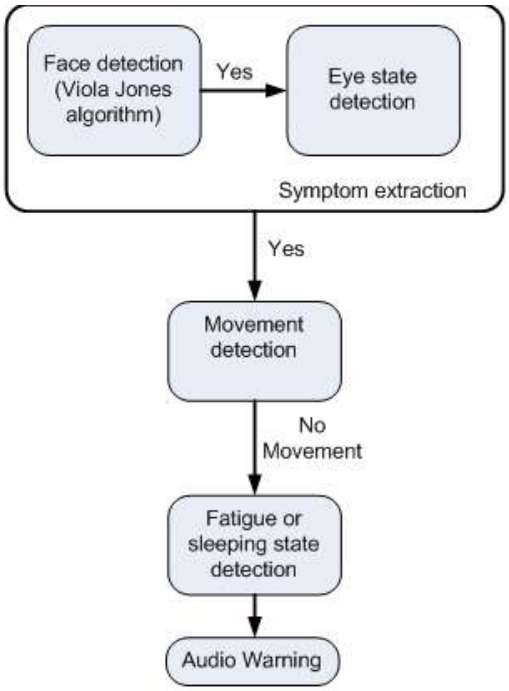

Fig. 2. *General algorithm used for passenger sleeping state*

The well-knownViola-Jones face detection algorithm is used for face detection, and once face is detected, the last 100 seconds are considered for movement detection in order to decide if the passenger is sleeping. The Viola-Jones machine learning-based approach is concerned with face detection using a number of training samples. This algorithm benefits from using algorithm for object detection, which uses very simple features named Haar-like features. In this algorithm, many numbers of Haar-like features are extracted from the image samples, and a number of effective features are selected using AdaBoost algorithm. The data base for training was used from OpenCv library. Due to the simple extracted features and selection of the best features, this algorithm is relatively fast and robust. Compared to the case of driver sleeping detection, the passenger detection is an easier task as the warning may be delayed dozens of seconds whereas in the first case 2 or 3 seconds is the upper limit to avoid an accident. The developed system monitors the driver's body position in the car and quantifies the body movement by a position into the space (x,y), a head yawn. We also quantify the level of closed eye vs open eye by taking into consideration the degree of modification for a period of time (100 seconds) (Fig. 4 and Fig. 5). The more the driver is moving his body, including his head, the higher the head activity variable. When the variable indicating body

movement is zero, the detection of closed eye for more than 60 seconds and head yawn position, a gentle sound alarm is issued.

Fig. 3. *Positioning of the web camera on dashboard*

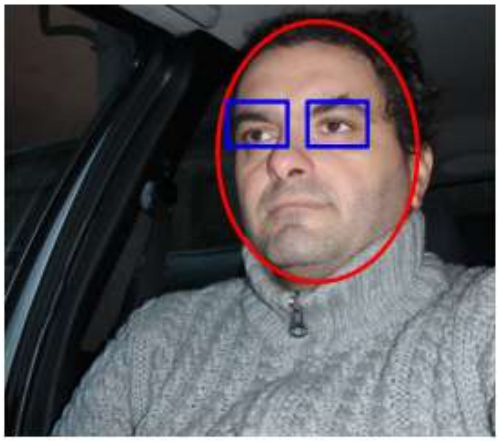

Fig. 4. *Face detection and eye opened detection*

Fig. 5. *Face detection and eye closed detection*

The proposed approach also features an on-line calibration step in order to improve eye detection and allow the user to adjust the parameters of the proposed system.

Table 1. *Statistics concerning detected features*

No of video sequences	50 – total 3h
Open Eye detection	85%
Closed Eye detection	60%
Face detection	90%
Movement detection	30%
Sleeping state detection	3%

Real-time performance was achieved by focusing on several visual cues (face detection, eye-state, body movement).

4. Conclusions

The present study has shown the potential use of a new ADAS feature – monitoring car occupant sleeping state in order not to psychologically affect the driver. Computer vision technique as a tool to assess the passenger sleeping state is a very effective non-intrusive solution. The presented method is an alternative feature to the driver sleeping on state detection and further enhances driving safety and also improves ADAS features. This represents a significant advance in the application of computer vision to ADAS.

References

[1]. Walter H. Moog, A. O. K. Baden-Württemberg, *et al.*, *Hellwach am Steuer - Bestandsaufnahme der Situation von Lastkraftwagenfahrern und Vorschläge zur Prävention von Sekundenschlaf am Steuer*, 2011.

[2]. S. E. Shladover, *Review of the state of development of advanced vehicle control systems*, Vehicle System Dynamics, 24 (6–7), p. 551-595, 1995.

[3]. S. Tsugawa, M. Aoki, A. Hosaka, K. Seki, *A survey of present IVHS activities in Japan*, Control Engineering Practice, 5 (11), p. 1591-1597, November 1997.

[6]. A. Vahidi, A. Eskandarian, *Research advances in intelligent collision avoidance and adaptive cruise control*, IEEE Trans. on Intelligent Transportation Systems, 4 (3), p. 143-153, September 2003.

[7]. R. Bishop, *Intelligent Vehicle Technology and Trends*, Artech House, Norwood, MA, USA, 2005.

[8]. P. L. Zador, S. A. Krawchuk, R. B. Voas, *Automotive collision avoidance system (ACAS) program. Final Report*, DOT HS 809 080, National Highway Traffic Safety Administration, Washington, DC, USA, August 2000, http://www-nrd.nhtsa.dot.gov/departments/nrd-12/pubs_rev.html.

[9]. H. M. Jagtman, V. A. W. J. Marchau, T. Heijer, *Current knowledge on safety impacts of Collision Avoidance Systems (CAS)*, In P. M. Herder and W. A. H. Thissen, editors, Proc. of the 5th International Conference on Technology, Policy and Innovation, Delft, June 26-29, 2001.

[10]. ***, *The 100-Car Naturalistic Driving Study, Phase II - Results of the 100 Car Field Experiment*, Report No. DOT HS 810 593, April 2006.
[11]. Luke Sebastian Fletcher, *An Automated Co-driver for Advanced Driver Assistance Systems*: *The next step in road safety*, A thesis submitted for the degree of Doctor of Philosophy at the Australian National University
[12]. Dong W., Wu X., *Driver fatigue detection based on the distance of eyelid*, In: IEEE Int. Workshop VLSI Design & Video Tech., Suzhou, China, 2005.
[13]. Fletcher L., Petersson L., ZelinskyA., *Driver assistance systems based on vision in and out of vehicles*, In: IEEE Proceedings of Intelligent Vehicles Symposium, p. 322-327, 2003.
[14]. Bergasa L. M., Nuevo J., Sotelo M. A., Barea R., Lopez M. E., *Real-time system for monitoring driver vigilance*, IEEE Trans. Intell. Transp. Syst., 7 (1), p. 63-77, 2006.
[15]. Cheng S. Y., Park S., Trivedi M. M., *Multiperspective and multimodal video arrays for 3d body tracking and activity analysis*, Comput. Vis. Image Underst., Special Issue on Advances in Vision Algorithms and Systems Beyond the Visible Spectrum, 106 (2-3), p. 245-257, 2007.
[16]. Cheng S. Y., Trivedi M. M., *Turn-intent analysis using body pose for intelligent driver assistance*, IEEE Pervasive Comput., 5 (4), p. 28-37, 2006.
[17]. Doshi A., Trivedi M. M., *Investigating the relationships between gaze patterns, dynamic vehicle surround analysis, and driver intentions*, In: IEEE Intelligent Vehicles Symposium, 2009.
[18]. Trivedi M. M., Cheng S. Y., Childers E., Krotosky S., *Occupant posture analysis with stereo and thermal infrared video: Algorithms and experimental evaluation*, IEEE Trans. Veh. Technol., Special Issue on In-Vehicle Vision Systems, 53 (6), p. 1698-1712, 2004.
[19]. Wu J., Trivedi M. M., *An eye localization, tracking and blink pattern recognition system: Algorithm and evaluation*, ACM Trans. Multimedia Comput. Commun. Appl., 6 (2), 2010.
[20]. Zhu Y., Fujimura K., *Head pose estimation for driver monitoring*, In Intelligent Vehicles Symposium, p. 501-506, June 2004.
[21]. Zhu Z., Fujimura K., Ji Q., *Real-time eye detection and tracking under various light conditions*, InETRA '02: Proceedings of the Symposium on Eye Tracking Research & Applications, p. 139-144, ACM Press, 2002.

THE ANNALS OF "DUNAREA DE JOS" UNIVERSITY OF GALATI
FASCICLE IX. METALLURGY AND MATERIALS SCIENCE
N°. 4 – 2014, ISSN 1453 – 083X

STUDY ON THE REFRACTORY MATERIAL USED FORTHE WEAR LAYER OF THE TUNDISH

Beatrice TUDOR
"Dunarea de Jos" University of Galati
e-mail: btudor@ugal.ro

ABSTRACT

The continuous casting of steel is a modern and efficient process for the production of semi-finished products required for the other components of steel industry. In order to improve the quality of continuous cast slebs and to reduce costs, I have carried out a study on the refractory materials used in the tundish. This study highlights the advantages which result from the application of improved technology for the achievement of continuously cast semis.

KEYWORDS: refractory, tundish, continuous casting, macroscopic analysis

1. Introduction

The continuous casting process of steel is now recognized by all professionals as a process which, besides productivity and efficiency, offers quality improvement.

The conditions that determine the continuous casting product are the result of several combined influences of metallurgy, thermotechnics and machine building. Of a particular importance among these conditions is the solidification process of the slebs in the continuous casting plant.

The continuous casting of steel is a modern and efficient process for the production of semi-finished products required for the other components of steel industry.

Upgrading and refurbishment of the continuous casting machines are considering improving the business of manufacturing, cost reduction per tonne of steel slabs, reducing defects and increasing competitiveness of manufactured products.

Getting good results in continuous casting is mainly conditioned by the following factors:

- synchronization of the activity with LD steelworks which provide steel for casting;
- maintenance of the casting machine and related facilities in perfect working order, especially by applying preventive maintenance;
- existence of operating and maintenance personnel, trained and disciplined in all departments;
- ensuring the materials and spare parts needed.

2. The role of the tundish in continuous casting

The tundish is designed as an intermediate assembly between the ladle and the crystallizer, serving to distribute the liquid steel in the crystallizer and to prevent temperature losses, and allowing coarse impurities to rise to the surface of the metal bath.

A special role of the distributor is to protect the jet of steel against the secondary reoxidation and gas uptake.

The tundish must also allow for precise control of the flow of steel in the crystallizer and provide enough storage capacity for changing the pot in the case of sequential casting.

During the steel flowing in the tundish, various phenomena occur which can result in products of lower quality:

- the steel jet distributed by the protection tube favors turbulence and waves on the surface of the metal bath. These turbulences destroy the surface of the metal bath which is covered with dust coating and slag, along with inclusions captured, and direct them to the crystallizer through immersion tubes. In the same time, this break in the flow of coating at the metal bath allows the steel to be exposed to strongly oxidizing atmosphere.

• the strong jet of the steel, which is focused by the jet protection tube, causes the erosion of the refractory lining of the tundish;

• the process of filling of the tundish leads to splashing (sprinkling) with steel and entrainment of air bubbles.

For a continuous reduction of the costs and for eliminating non-metallic inclusions in the cast steel, in addition to constructive modifications of the tundish, the refractory material lining was replaced.

To highlight the need to replace the material the tundish is made of and the economic efficiency resulting from this substitution, I have made a comparison between the old technology of making fabric tundish with KERMAG LTD 90 and the new technology that uses material TUNDEX 160AS. Consequently, the study highlights the advantages of using the new material.

3. Methods used to create the distributor

3.1. Version A-tundish with KERMAG LTD90

In version A, the tundish of gunite with KERMAG LTD90 is used to make a refractory lining at the tundish with a greater resistance to the number of castings, using two types of refractory concrete. The composition and properties are presented in Tables 1 and 2.

Table 1. *Chemical composition of the materials for concrete*

Material	Al_2O_3	Fe_2O_3	CaO
ULTRACAST BSR	84.3%	max 0.9%	max 0.5%
PHLOX 1560 SR	59.1%	max 1.1%	max 2.2%

Table 2. *Properties of the materials for concrete*

Materials	Grain max.[mm]	Density [t/m³]	Temperature max. [° C]	Quantity of water [l/100kg]	Rock for the manufacturing
ULTRACAST BSR	5	3.03	1680	4.5-6	bauxite
PHLOX 1560 SR	5	2.6	1650	6.5-8	andalusite

Pouring concrete is accompanied by vibration, for better compaction of the walls. Hardening of the concrete lasts 24 hours, and then the formwork is removed. Drying continues for 72 hours in the open air before placing the tundish under the dryer, after which drying is running according to the drying diagram (Figure 1).

The liner of the wear was made with shotcrete KERMAG LTD90.

The composition and properties for making the lining of the wear by guniting are shown in Tables 3 and 4.

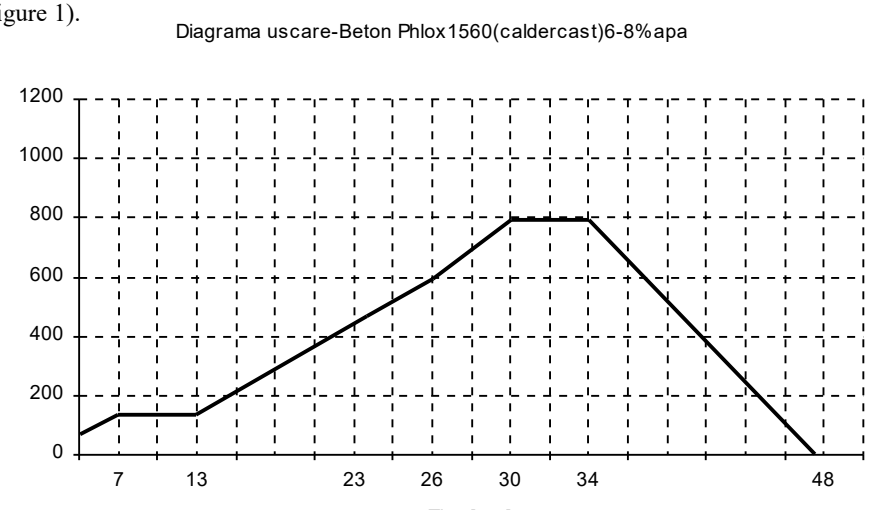

Fig. 1. *Drying diagram of the concrete, Phlox 1560*

Table 3. *Chemical composition of the material-KERMAG LTD 90*

Material	MgO	CaO	Al_2O_3	Fe_2O_3	$Si\ O_2$
KERMAG LTD 90	89.3%	2%	max 1.2%	max 0.4%	max 0.5%

Table 4. *Properties of the material KERMAG LTD-90*

Material	Grain max. [mm]	Density [t/m³]	Temperature max. [°C]	Quantity of water [l/100kg]
KERMAG LTD 90	1.2	3.03	1650	17-21

Guniting begins with filling all depressions, then filling hearth and continues with the walls of the tundish from top to bottom. To obtain a quality wear layer, plastering materials must provide a good grip at the walls, must not slip on the walls and must not react with the refractory mass. The deposited layer will have a thickness of 25-35 mm at the walls and 35-45 mm at the hearth (Figure 2).

After guniting, the tundish is left to dry in the open for at least 30 minutes, then it is forced dried with gas, according to the drying diagram (Figures 3 and 4).

Fig. 2. *Tundish with shotcrete*

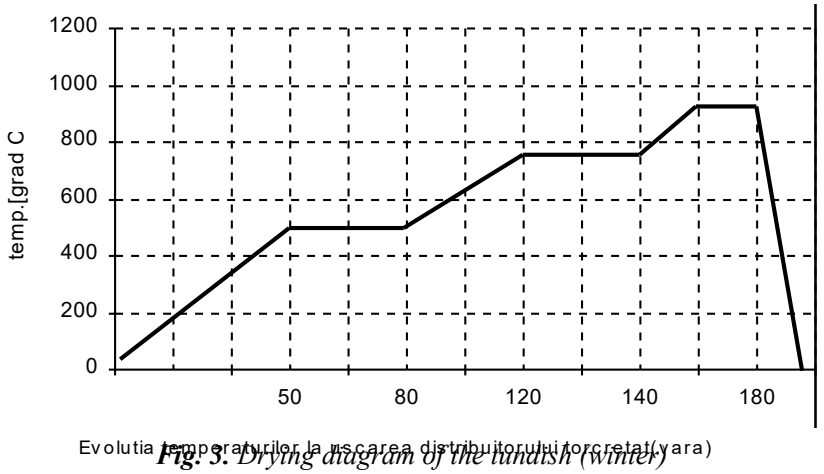

Fig. 3. *Drying diagram of the tundish (winter)*

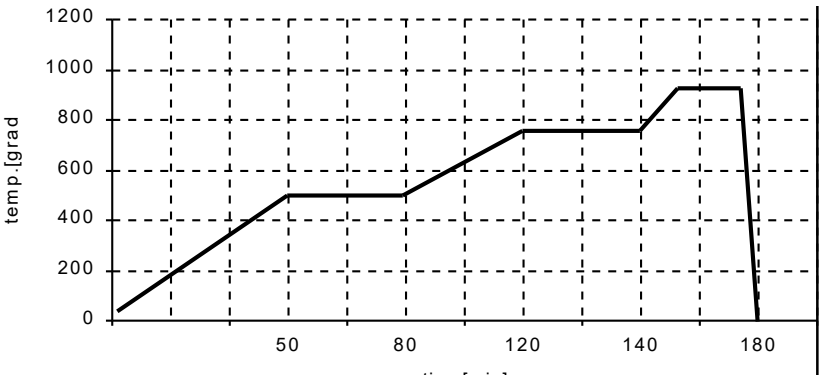

Fig. 4. *Drying diagram of the tundish (summer)*

The degree of drying is checked by measuring the temperature of the refractory shotcrete or concrete, with special thermocouples.

Fig. 5. *Tundish gunited after drying*

3.2. Version B-tundish with TUNDEX 160AS

The wear lining of the tundish was achieved with Tundex 160AS, with the chemical composition shown in Table 5.

The Tundex 160AS material will be poured into the space created between the formwork and the permanent masonry, at about 50 mm from the top edge of the wall, taking care not to obstruct the outlet of the tundish.

To obtain a quality wear layer, plastering materials must provide a good grip at the walls, must not slip on the walls and must not react with the refractory mass. The deposited layer will have a thickness of 25-35 mm at the walls and 35-45 mm at the hearth.

After completing these operations, the drying with gas is carried out according to the diagram in Figure 6.

Table 5. *The chemical composition of the TUNDEX 160 AS*

Material	MgO	Si O_2	CaO	Fe_2O_3	Al_2O_3	C	Density
TUNDEX 160 AS	60-65%	25-28%	1-2%	5-7%	1-2%	2-3%	1.5-1.7 g/cm^3

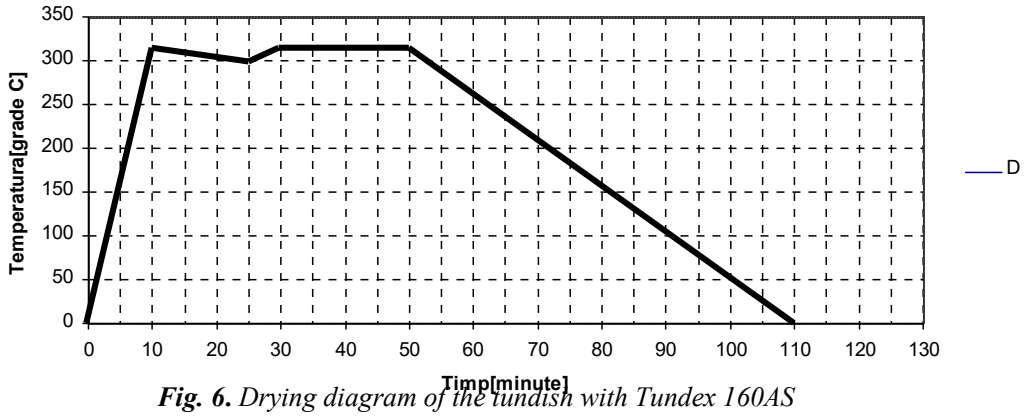

Fig. 6. *Drying diagram of the tundish with Tundex 160AS*

Fig. 7. *Tundish with Tundex 160 AS after drying*

4. Macroscopic analysis of the materials used for the tundish

The macroscopic analysis of the refractory materials used in both embodiments of the tundish highlighted this wear according to the number of castings.

The studied material samples were taken before and after casting, from the top of the tundish lining, the place where the contact with the metal bath erodes the material.

The photos were taken with the optical microscope NEOPHOT 2 with digital acquisition of the image and soft Optika Vision Lite2.1.

4.1. Analysis of KERMAG LTD90 samples (A version)

Before casting:

Fig. 8. *Macrostructure of the KERMAG LTD90 sample before casting (calibration 63x stereomicroscope)*

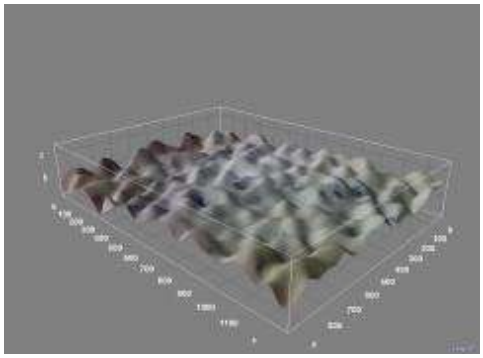

Fig. 9. *3D image of the KERMAG LTD90 sample before casting*

After casting:

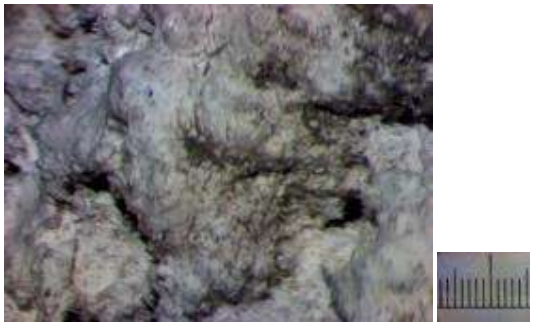

Fig. 10. *Macrostructure of the KERMAG LTD90 sample after casting (calibration 63x stereomicroscope)*

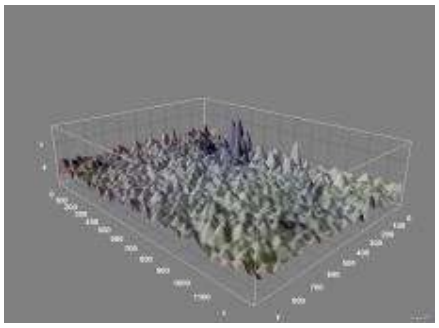

Fig. 11. *3D image of the KERMAG LTD90 sample after casting*

4.2. Analysis of TUNDEX 160 AS samples (B version)

Before casting:

Fig. 12. *Macrostructure of the TUNDEX 160 AS sample before casting (calibration 63x stereomicroscope)*

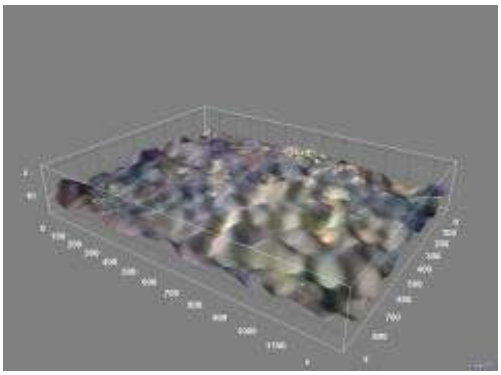

Fig. 13. *3D image of the TUNDEX 160 AS sample before casting*

After casting:

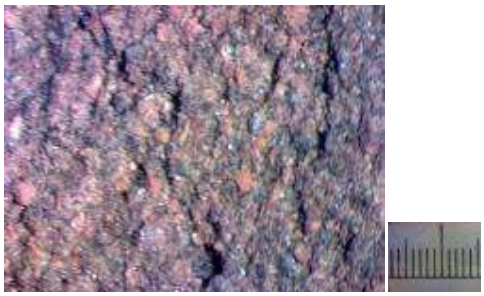

Fig. 14. *Macrostructure of the TUNDEX 160 AS sample after casting (calibration 63x stereomicroscope)*

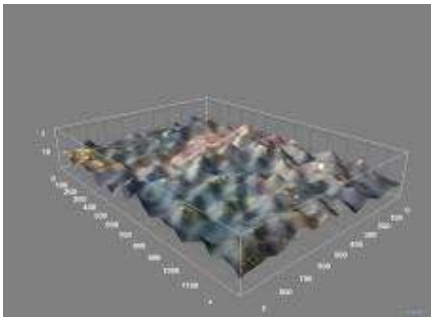

Fig. 15.*3D image of the TUNDEX 160 AS sample after casting*

5. Conclusions

The improvement of the casting technology by replacing the material for the wear layer led to greater protection of the lining, the default of the duration of use of the tundish was higher, these resisted to casting for a larger number of charges: 1700 with TUNDEX 160 AS versus 1000 charges with KERMAG LTD 90.

The analysis of the macrostructures and the 3D images of the sample materials TUNDEX 160AS and KERMAG LTD 90 showed a less worn surface after casting at the TUNDEX 160 AS material, and fewer non-metallic inclusions in the cast slabs.

Increasing the number of castings in the tundish leads to a more efficient casting process by using a smaller number of tundish, respectively 5 to 8. The preparation of the tundish cycle is shortened from 4 to 12 hours, there is economy of gas, electricity and labor.

There is also lower consumption of natural gas because the drying temperature of this material is 320 ºC, compared to the wet material that requires a temperature of 900 °C, resulting in less drying time: 50 minutes compared to 180 minutes for the tundish that does not require additional heating before casting begins.

The new material used shows at the end of the casting process a surface with less roughness, in the slabs casting.

The absence of water in the material composition led to a lower risk of expansion and greater occupational safety.

References

[1]. Irving W. R., *Continuous Casting of Steel*, Institute of Materials, Cambridge, 1993.
[2]. Butnariu I., Geantă V., ş.a., *Turnarea continuă a semifabricatelor de oţel*, Editura Tehnică, Bucureşti, 2000.
[3]. *,** *Casting and Solidification of Steel*, IPC Science and Technology Press Ltd, Guildford, Luxembourg, November, 1977.
[4]. *,** *Continous Casting Ceramics*, Firma Foseca, 1984.

THE ANNALS OF "DUNAREA DE JOS" UNIVERSITY OF GALATI
FASCICLE IX. METALLURGY AND MATERIALS SCIENCE
N°. 4 – 2014, ISSN 1453 – 083X

MICROSTRUCTURAL CHARACTERISTICS OF SINTERED POWDER METALLURGY ALLOYS

Mihaela MARIN, Florentina POTECAŞU, Octavian POTECAŞU
"Dunarea de Jos" University of Galati
e-mail: mihaela.marin@ugal.ro, fpotec@ugal.ro

ABSTRACT

The purpose of this paper is to study the influence of processing parameters on the microstructural characteristics of sintered powder metallurgy alloys. The specimens were produced from atomised iron powders with different sizes (<45, 45-63, 63-100, 100-150, >150 μm). They were compacted at pressures of 600 MPa and sintered for 30 minutes and 120 minutes at 1150 ºC, respectively. The porosity of the sintered samples was analyzed according to their microstructural characteristics and chemical composition.

KEYWORDS: powder metallurgy, porosity, sintering, microstructure

1. Introduction

Powder metallurgy (P/M) is a metal processing technique of production of metal powders and their consolidation into components with near net shape, helping in this way to save time, energy, material, labor and money [1-3].

In conventional P/M, metal powders are mixed, compacted into molds and sintered in different atmospheres. The products obtained by powder metallurgy (P/M) are widely used, especially in the automotive industry.

One of the main problems in powder metallurgy products is the presence of porosity, but this can be viewed as a consequence of this technique. The porosity in these products can be classified into two types: open and closed porosities. In closed porosity, the pores are isolated within the material and to the external surface of the sample. In open porosity, the pores are represented as a network of pores that are connected one with another and also to the external surface of the sample.

Sometimes, porosity is deliberately produced in the component to meet certain requirements such as filters or bearings. Porosity has influence on the mechanical properties of P/M alloys [4-11].

In this paper, the microstructural characteristics of iron based powder metallurgy alloys were studied.

2. Experimental procedure

Two types of iron powders (P_1 and P_2) produced by the water atomization method in irregular shape were used. The chemical composition of the powders is given in Table 1. The powders were mixed with 1% zinc stearate. The mixed powders were uniaxially compacted in a universal mechanical testing machine at a pressure of 600 MPa to produce cylindrical specimens with the dimensions of 8× 6 mm. After pressing, the compacts were subjected to sintering. The sintering temperature was approximately 1,150 °C.

Two types of treatment cycles were used: the first, with a sintering time of 30 minutes and the second, with the sintering time of120 minutes. Following sintering, the sintered density of the alloys was measured using the geometrical method and image analysis techniques.

Table 1. *Chemical composition of analyzed powders*

Powder type	C	Cu	Ni	Mo
P_1	<0.01	0.09	0.05	0.01
P_2	<0.01	1.50	4	0.50

3. Results and discussion

3.1. Microstructure and density

In Figs. 1 and 4 are presented the optical micrographs of the specimens to analyze the pore size, morphology, and distribution. Also, in Figs. 2 and 5, a 3D view of the surface using Image Jis presented. In the sample with the lowest density, P_1, the pores appeared to be larger and more irregular than the pores in the sample with the highest density,

P_2. The higher fraction of porosity, as well as the larger, more irregular pores for sample P_1 with the lowest density are observable.

The green and sintered densities of the samples were determined from weight and dimensional measurements, which were accurate within the ±0.01 g and ±0.001 mm ranges, respectively (Table 2).

The density of a green part (ρ_g) is calculated by the following relation:

$\rho_g = (m_g / v_g)$, where, m_g is the mass of the green part and v_g is the volume of the green part.

The density of a sintered part (ρ_s) is calculated by the relation:

$\rho_s = (m_s / v_s)$ where, m_s is the mass of the sintered part and v_s is the volume of the sintered part.

3.2. Porosity measurements

Porosity is determined by a couple of processing variables such as: type and amount of alloying elements, powder size distribution, green and sintered density of compacts, temperature and sintering time [6-8].

The usual method for porosity measurement of powder metallurgy products is by density technique. The total porosity of the green compact, in volume percent, is calculated using the following equation: $P_t = 100\ (1 - \rho_s/\rho_t)\ [\%]$ where, ρ_s, ρ_t and ρt are the sintered density and theoretical density.

The second method for porosity measurement was using a specialized software for digital image processing, *ImageJ.* By applying filters and adjustments, the software allows the detection of the pores (black areas) and the measurement of their area as percentage.

The porosity measurements of the sintered alloys, achieved using the sintered density technique and by digital image analysis, are shown in Table 2. The porosity measured using image analysis was higher than that resulted from the use of the density technique, because only open porosity is considered in the image analysis technique, whereas closed porosity is not taken into account.

The porosity measured by image analysis software – *Image J* - is depicted in Figs. 3 and 6. Due to the prolonged time of sintering in cycle 2, the pores are smaller and the total porosity is decreasing comparing with cycle 1. Porosity decreases with increasing time.

Table 2. *Green and sintered density*

Powder type	Cycle treatment	Green density, (g/cm^3) ρ_g	Sintered density, (g/cm^3) ρ_s	Porosity from sintered density (%)	Porosity from image analysis (%)
P_1	30 min.	6.91	6.93	12.05	14.14
P_2	30 min.	6.95	6.98	11.42	13.29
P_1	120 min.	6.92	7.03	10.78	13.03
P_2	120 min.	6.96	7.10	9.89	10.53

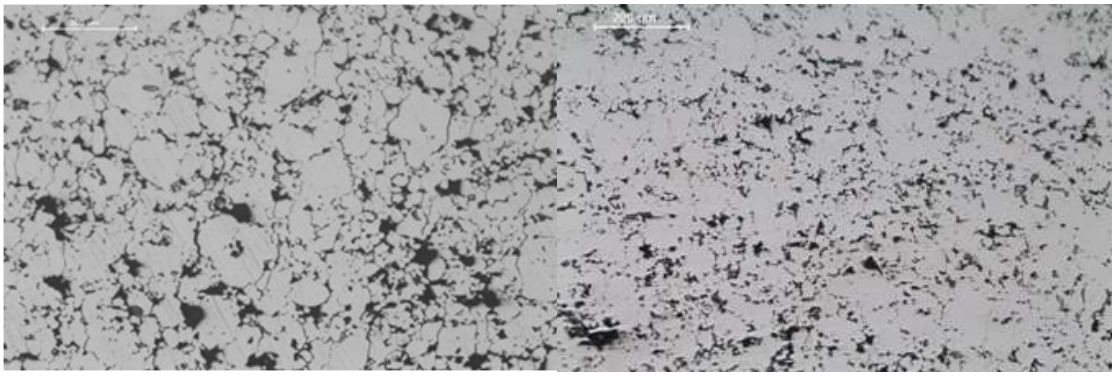

a) b)

Fig. 1. *Optical micrographs of polished surface of samples in cycle 1 of sintering (30 minutes): a) P_1; b) P_2*

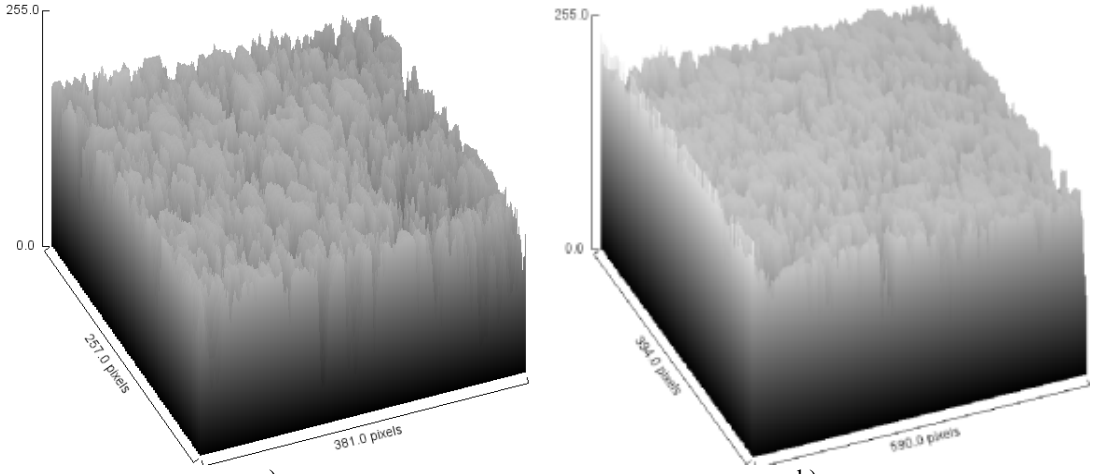

a) b)

Fig. 2. *3D image of the polished surface of samples in cycle 1, obtained using the Image J software: a) P_1; b) P_2*

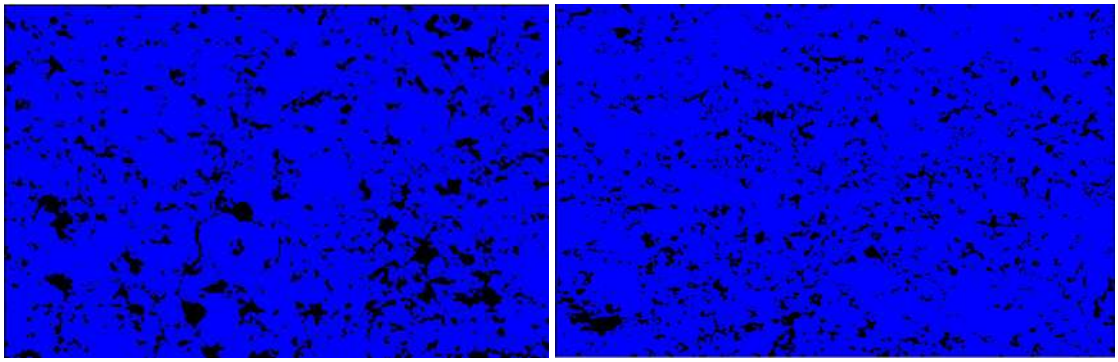

a) b)

Fig. 3. *Image analysis technique using the Image J software to detect porosity for samples in cycle 1: a) P_1; b) P_2*

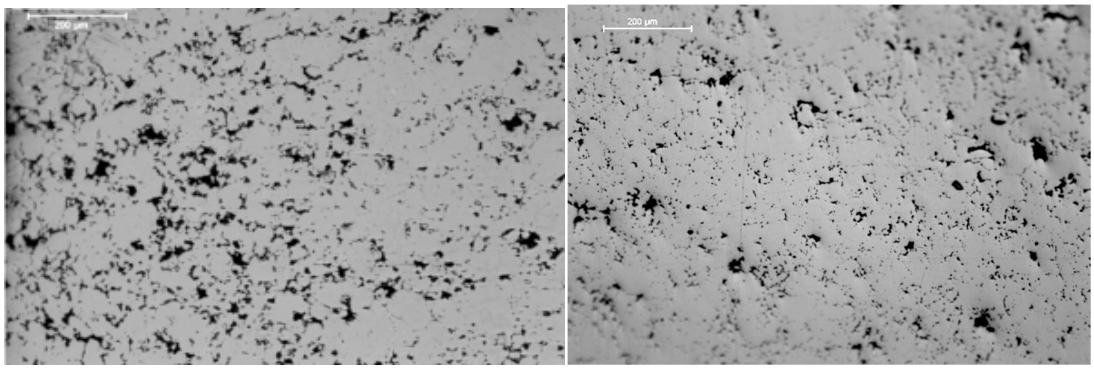

a) b)

Fig. 4. *Optical micrographs of polished surface of samples in cycle 2 of sintering (120 minutes): a) P_1; b) P_2*

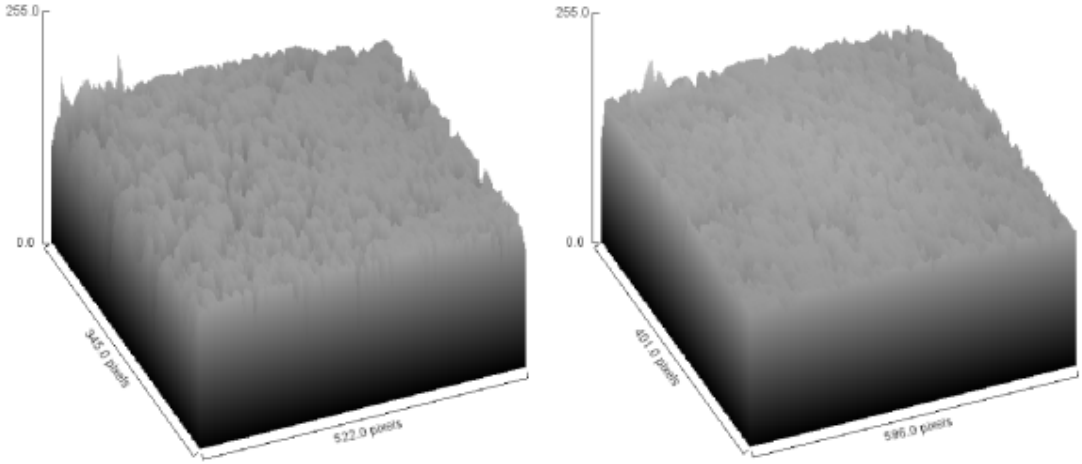

a) b)

Fig. 5. *3D image of the polished surface of samples in cycle 2, obtained using the Image J software: a) P_1; b) P_2*

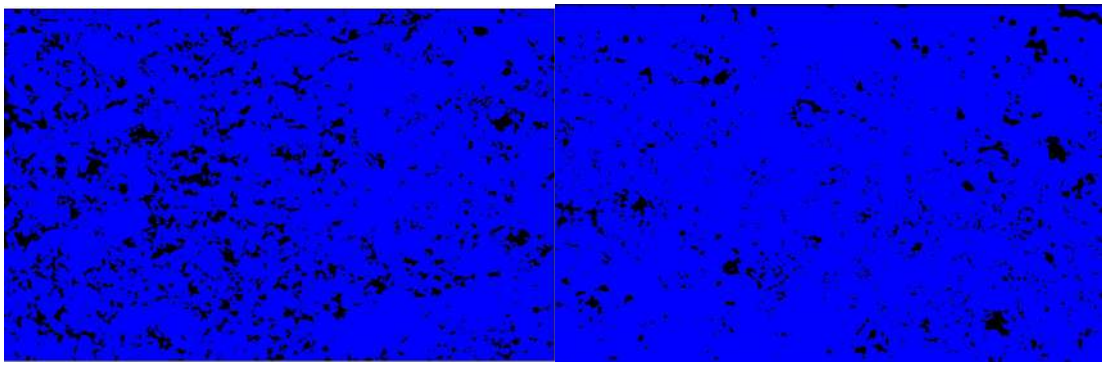

a) b)

Fig. 6. *Image analysis technique using the Image J software to detect porosity for samples in cycle 2: a) P_1; b) P_2*

4. Conclusions

The porosity in P/M parts is correlated to processing parameters such as green density, alloying elements, particle size distribution of the powders, sintering temperature and time.

An increase in the sintered density is correlated with a lower pore fraction, smaller pore size, and more spherical pore shape. Decreased pore size was correlated with an increase in the sintering time [12-16].

The pores in the sample with the lowest density (P_1) appeared to be much larger and more irregular than the pores in the other alloyed sample (P_2).

The porosity measured by image analysis using the *Image J* software is ranging from 10.53% for 7.10 g/cm^3 to 14.14% for 6.93 g/cm^3 in the sintered state. These values were similar to the porosity values computed from the sintered density of the alloys.

References

[1]. U. Engstrom, C. Lindberg, J. Tengzelius, *Powders and processes for high performance PM steels*, Powder Metallurgy, vol. 35, no. 1, p. 67-73, 1992.
[2]. C. Lindberg, *Sintered high strength materials*, Advances in P/M & Particulate Materials, vol. 5, p 107-114, 1992.
[3]. F. Chagnon, C. Gelinas, Y. Trudel, *Development of high density materials for P/M applications*, Advances in P/M & Particulate Materials, vol. 3, p. 199-206, 2004.
[4]. R. Haynes, *Astudy of effect of porosity content on ductility of sintered metals*, Powder Metall, vol. 20, p. 17-20, 1977.
[5]. R. Bourcier, D. Koss, R. Smelser, O. Richmond, *The influence of porosity on the fracture of alloys*, Acta Metall, vol. 34, p. 2443-53, 1983.
[6]. X. Deng, G. Piotrowski, N. Chawla, K. Narasimhan, *Effect of pore clustering on the mechanical behavior of powder metallurgy (P/M) steels*, P/M Sci Technol Briefs, vol. 6, p. 5-10, 2004.
[7]. K. Christian, R. German, *Relation between pore structure and fatigue behavior in sintered iron-copper-carbon*, Int J Powder Metall, vol. 31, p. 51-61, 1995.

[8]. T. M. Cimino, A. H. Graham, T. F. Murphy, The *effect of microstructure and pore morphology on mechanical and dynamic properties of ferrous P/M materials*, Advances in P/M & Particulate Materials, vol. 3, p 13-33/13-43, 1998.
[9]. B. Lindqvist, *Influence of microstructure and porosity on fatigue properties of sintered steels*, Metal Powder Report, vol. 44, p. 443-448, 1989.
[10]. W. D. Angela, L. Tellez, J. F. Alcala, E. Martinez, V. F. Cedeno, *Effect of copper on the mechanical properties of alloys formed by powder metallurgy*, Materials and Design, vol. 58, p. 12-18, 2014.
[11]. F. Chagnon, Y. Trudel, *Effect of density on mechanical properties of sinter-hardened materials*, Advances in P/M & Particulate Materials, vol. 3, p 12-119/12-125, 1988.
[12]. H. Gonobadi, *Physical and mechanical characteristics of heat treated PM parts, infiltrated by copper*, Life Sci J, vol. 10, p. 86-91, 2013.
[13]. F. Chagnon, Y. Trudel, *Effect of sintering parameters on mechanical properties of sinter hardened materials*, Advances in P/M & Particulate Materials, NJ, vol. 2, p 14-97/14-106, 1997.
[14]. R. J. Causton, J. A. Hamil, S. O. Shah, *Properties of heat treated P/M alloy steels*, Advances in P/M & Particulate Materials, vol. 4, p 61-96, 1993.
[15]. A. Piotrowski, G. Biallas, *Influence of sintering temperature on pore morphology*, *Microstructure and Fatigue Behavior of Mo-Ni-Cu Alloyed Sintered Steel*, Powder Metallurgy, vol. 41, no. 2, p. 109-114, 1998.
[16]. Z. Brytan, L. A. Dobrzański, M. Grande, M. Rosso, *The influence of sintering time on the properties of PM duplex stainless steel*, JAIMME, vol. 37, p. 387-396, 2009.

THE ANNALS OF "DUNAREA DE JOS" UNIVERSITY OF GALATI
FASCICLE IX. METALLURGY AND MATERIALS SCIENCE
N°. 4 – 2014, ISSN 1453 – 083X

SUPERFICIAL HARDENING WITH PULSE LASER APPLIED TO ASTM A537 HSLA STEEL

Nelu CAZACU, Bogdan Silviu VRABIE
"Dunarea de Jos" University of Galati
e-mail: nelu.cazacu@ugal.ro, vrabie.bogdan10@gmail.com

ABSTRACT

The surface hardening with YAG:Nd pulse laser is used to obtain a set of surfaces with different properties and it is based on the formation of a very fine martensite.

The paper has been elaborated based on laboratory experiments on samples of A537 (HSLA steel).

KEYWORDS: pulse laser, YAG:Nd, hardening, surface treatment

1. Introduction

Laser hardening (LH) became an important technology to obtain superficial coatings with high hardness, which could increase the utilization time of some parts [1], due to the possibility to concentrate the energy on controlled surfaces and thus to obtain high density energies.

The details of the factors are shown in Fig. 1:

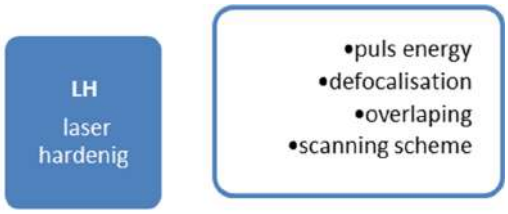

Fig. 1. *Factors influencing the LH process*

In steels:

- laser hardening leads to the formation of very fine martensite;
- nitrocarburizings in fluidized bed is an effective method.

The interaction of laser radiation with a solid is an important point of concern, initially in theory [2] and lately with technological applications [3].

Notations and Abbreviations
HSLA steel – High Strengh Low Alloy
LH - Laser Hardening,
SE – Surface Engineering,
YAG:Nd – Yttrium Aluminum Garnet, Neodimoium doped

A sum of elementary processes is conducted at very high speed leading to the reorganization of atoms in a solid substance in response to the excitation energy for short periods of time. The energy of the laser radiation and high heating and cooling rates result in substantial changes in the structure and material properties of the surface layer. Within certain limits and under adequate control of the influencing factors, [2], this interaction may be useful in SE technological applications.

2. Experimental

2.1. Equipment

For the experiments we used the equipment existing in the laboratories of the Faculty of Metallurgy and Materials Science, *Dunarea de Jos* University of Galati. Pulse Laser installation KVANT 17 (YAG: Nd) is a facility dedicated to welding and cutting materials where these operations are difficult to achieve with other methods or other methods are not available.

Fig. 2. *YAG laser system image: pulsed Nd (KVANT 17)*

Fig. 3. *YAG laser system image: pulsed Nd (KVANT 17)*

The main features of the system are: active medium solid glass Y3Al5O12 (yttrium aluminum garnet) laser glass size: 6.3 mm 100 mm diameter, 1.06 μm wavelength (IR) pulse duration 2 ... 5 ms 1 ... 20 Hz operating frequency. Object focal distance 50 mm equivalent at maximum focalization diameter 0.3 ... 1.3 mm, pulse energy min. 8J, scanning surface 400 mm^2 (20 mm x 20 mm), 2 functional units simultaneously.

Fig. 4. *Interaction of laser radiation with sample and intense sparks due to interaction*

2.2. Samples

For the experiments we have used A537 steel samples characterized by:

- material: A537 (normalized condition);
- shape: disc two sides prepared;
- size 27 mm x 44 mm x 12.38 mm;
- initial properties;
- status of the surface.

Deviations from sample to sample should be minimal.

The experiments were carried out taking into account the following factors of influence cumulated for all technological operations. Depending on previous experience, there is a hierarchy of factors influencing the light of the objective function (out).

Table 1. *Chemical compositions of A537 –ASTM A537(HSLA steel)*

Element	Width, mas %		comments
	on liquid	on solid	
Carbon	max. 0.24	max. 0.24	
Mangan	0.70 … 1.35	0.64 … 1.46	< 40 mm width
	1.00 … 1.60	0.92 … 1.72	> 40 mm width
Phosfor	max. 0.035	max. 0.035	
Sulf	max. 0.035	max. 0.035	
Siliciu	0.15 … 0.50	0.13 … 0.55	
Copper	max. 0.35	max. 0.38	
Nichel	max.0.25	max. 0.28	
Cromium	max. 0.25	max. 0.29	
Molibdenium	max. 0.08	max. 0.09	

Table 2. *Properties of the steel according to the state of A537 heat treatment (ASTM)*

Grade	Heat treatment	Width	Yield (min)	Tensile strength (min)
u.m.	-	mm	Mpa	Mpa
1	Annealing	< 65	345	485
		65 … 100	310	450
2	quenching and tempering	< 65	415	550
		65 … 100	380	515
		100 … 150	315	485
3	quenching and tempering	< 65	380	550
		65 … 100	345	515
		100 … 150	275	485

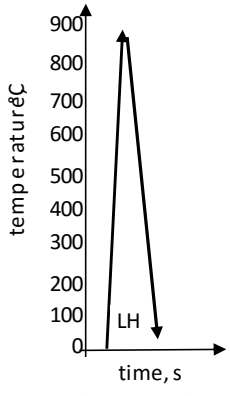

Fig. 5. *Cycle quenching and tempering heat treatment applied to the A537 steel*

2.3. Testing regimes

The matrix experiment has to take into account these factors and their hierarchy, even if a procedure is not yet developed for determining the weight factors on the process quality and regimes. The steel used is part of HSLA steel. The initial state of the material is normalized condition (delivery).

3. Results and discussions

The investigations highlighted changes in structure, properties and performance.

The macroscopic analysis serves to highlight the changes in the surface morphology of the treated samples. Pictures of the surface morphology are mainly about the different regimes LH laser activation and morphological changes (craters, waves, scales, modes of vibration, uneven heating, etc.). In Fig. 6 are presented the samples after LH and in Fig. 7, are presented the same samples after FBNC. These samples present in the end a dark gray coloration. To allow the hardness tests, a superficial polishing was realized using fine abrasive paper (>1200).

Optical microscopy (metallographic) highlights superficial changes, knowing that treated surfaces have a specific texture due to the interaction laser / material.

Usually, the samples surface must be processed uniformly and continuously implying an overlap of 10 ... 30% of traces for each interaction (Fig. 5). An increase in the intensity of the laser spot and a reduction of defocus have the effect of increasing the depth and reduce surface traces. The presence of a strong local melting (Fig. 8) leads to local hardening mechanism by recrystallization at high speed.

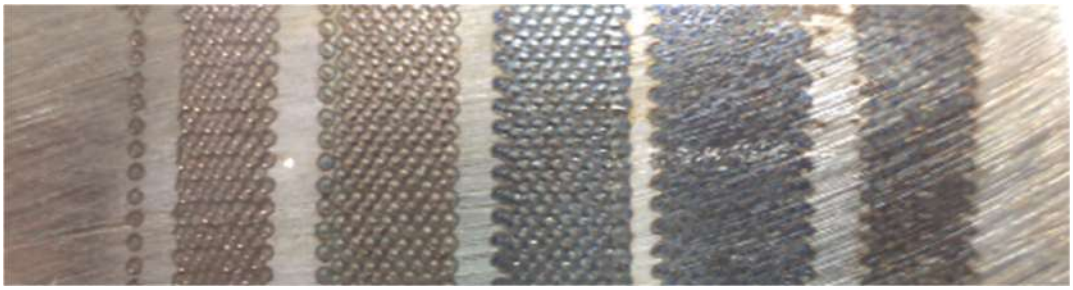

Fig. 6. *Image of the area after LH*

This hardening mechanism is present in most samples (Figs. 8-14).

Hardening by local quenching is shown in Fig. 13 and partially in Fig. 14. The staining surface in the presence of oxygen in the air is dependent on surface temperature obtained after interaction with the focused spot of laser radiation. At a macroscopic scale, average surface hardness is obtained, as a weighted average of local hardness obtained by one of two mechanisms.

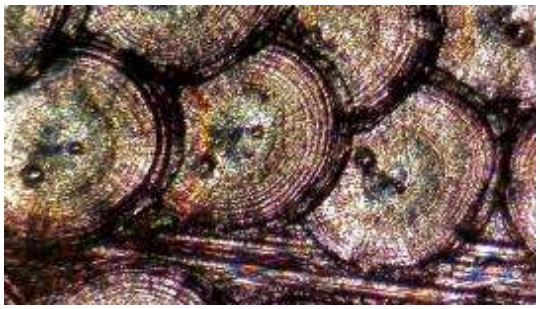

Fig. 7. *LH sample after the 1a regime (length of the image corresponds to 1.2 mm)*

Fine martensite formations and possible fine dispersion of hard nitride precipitates are highlighted.

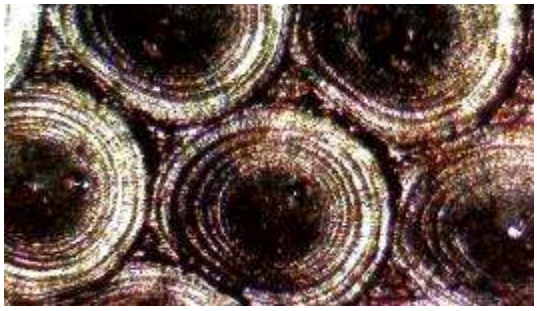

Fig. 8. *LH sample after the 2b regime (length of the image corresponds to 1.2 mm)*

Fig. 9. *LH sample after the 3a regime (length of the image corresponds to 1.2 mm)*

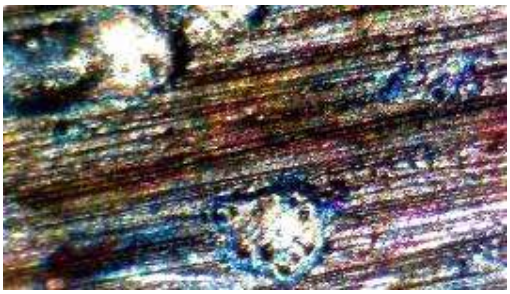

Fig. 10. *LH sample after the 4a regime (length of the image corresponds to 1.2 mm)*

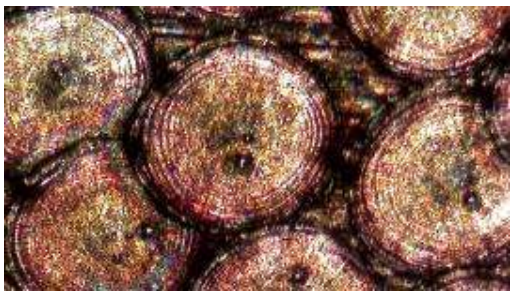

Fig. 11. *LH sample after the 5a regime (length of the image corresponds to 1.2 mm)*

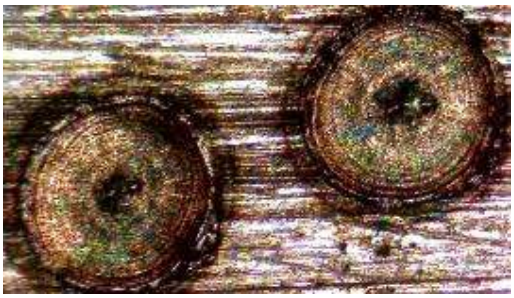

Fig. 12. *LH sample after the 6b regime (length of the image corresponds to 1.2 mm)*

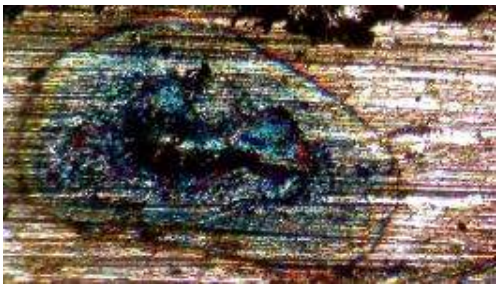

Fig. 13. *LH sample after the 7a regime (length of the image corresponds to 1.2 mm)*

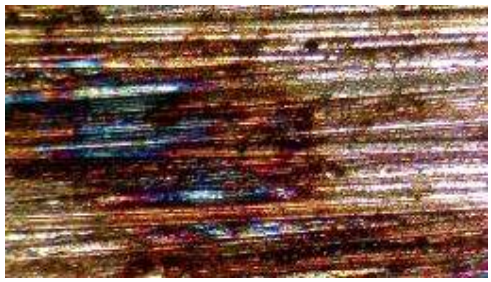

Fig. 14. *LH sample after the 8a regime (length of the image corresponds to 1.2 mm)*

3.1. Surface hardness

Surface hardness is the main technological feature being measured and obtaining a high hardness is a condition to reduce the wear of treated metallic materials.

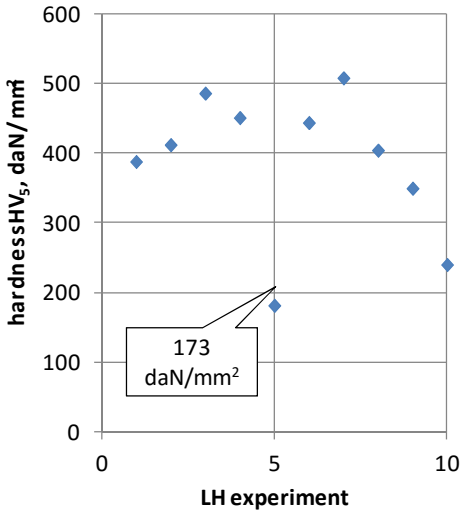

Fig. 15. *Variation of hardness over surface of A537 steel samples after laser hardening (LH)*

Table 3. *Experimental matrix for A537 laser hardening (LH)*

experiment	Ox steps	puls	delay	defocalisation	mean Hardness HV_5	Battery voltage
m.u.	-	-	s	mm	daN/mm^2	V
1	1	1	1	0	387	1000
2	1	1	1	2.5	411	1000
3	1	1	1	5	485	1000
4	1	1	1	7.5	450	1000
5	1	1	1	9	181	1000
6	4	1	1	9	443	1000
7	4	1	1	7.5	507	1000
8	4	1	1	5	403	1000
9	4	1	1	2.5	349	1000
10	4	1	1	0	239	1000

Tabel 4. *HVD in surface hardness daN/mm^2 laser hardened samples A537*

experiment no.	d_1	d_2	d_3	HV_5 (1)	HV_5 (2)	HV_5 (3)	HV5 med	observations
m.u.	mm	mm	mm	daN/mm^2	daN/mm^2	daN/mm^2	daN/mm^2	-
0	0.231	0.232	0.231	174	172	174	173	initial hardness (after annealing)
1	0.185	0.140	0.149	271	473	418	387	
2	0.149	0.189	0.129	418	260	557	411	
3	0.150	0.145	0.124	412	441	603	485	
4	0.109	0.190	0.172	780	257	313	450	
5	0.230	0.230	0.220	175	175	192	181	
6	0.148	0.150	0.137	423	412	494	443	
7	0.128	0.135	0.144	566	509	447	507	
8	0.129	0.168	0.169	557	329	325	403	
9	0.174	0.145	0.176	306	441	299	349	
10	0.209	0.184	0.200	212	274	232	239	

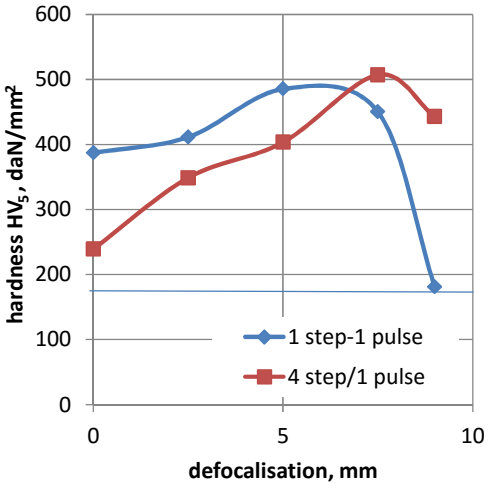

Fig. 16. *Defocusing influence over surface Hardness of A537 steel samples after LH*

3.2. Microhardness in section

Getting a slow transition structure and properties is a condition that is not beyond the breaking strain layer and produces exfoliation. Checking the property of the superficial layer is done by the Knoop or the Vickers microhardness tests.

Microhardness variation can be correlated with treatment regimes.

4. Conclusions

1. The hardness after treatment is higher than the initial hardness (173 daN/mm^2) of samples for all experiments (Fig. 15). Changing the superficial hardness shows that interactions between laser radiation processes and the sample surface (steel A537) were present in all regimes.

2. Changing the setting levels for influence factors (number of successive steps, defocus the laser spot, etc.) leads to changing the surface topology (Fig. 8 ... Fig. 14) and surface properties (hardness).

3. Changing the number of successive steps to a pulse, has the effect of altering the final hardness (Fig. 16) by changing the heat exchange with the substrate material. Using distant pulses results in a higher final hardness (up to 507 daN/mm^2). The phenomenon is due to the thermal diffusivity of the material that allows better cooling after an interaction, and thus to a better subcooling for martensitic transformation or recrystallization.

4. Differences between experimental regimes are found in a curve shape regarding the change and modification useful in applications ranges (Fig. 16). A high hardness is associated with fewer pulses and a smaller range of defocus. A low hardness is obtained from closer pulses and a higher range of defocus.

References

[1]. De Kock J., *Lasers Offer Unique Heat Treating Capabilities*, Industrial Heating, Vol. oct., 2001.
[2]. Ursu I., *et al.*, *Interacţiunea radiaţiei laser cu materialele.* Bucureşti: Editura Academiei, 1986.
[3]. Ganeev R. E., *Low power hardening of steels*,Journal of Materials Processing Technology, p. 414-419, 2002.
[4]. Cazacu Nelu T., *Cercetari privind tehnologia de tratament termic in strat fluidizat pentru semifabricate siderurgice si piese (teza de doctorat)*, "Dunarea de Jos" University of Galati, 2000.
[5]. Pye David, *Diffusion Surface Treatment Techniques. A Review*. 2001.
[6]. Samoila C., Ionescu M. S., Drugă L., *Tehnologii şi utilaje moderne de încălzire.* Bucureşti, Editura Tehnică, 1986.
[7]. Samoilă C., Drugă L., Stan I., *Cuptoare şi instalaţii de încălzire.* Bucureşti, Editura Didactică şi Pedagogică, 1983.
[8]. Popescu Nae, Gheorghe C., Popescu O., *Tratamente termice neconvenţionale*, Bucureşti, Editura tehnică, 1986.
[9]. Weber Marvin John., *Handbook of Lasers*, Lawence Berkeley National Laboratory, University of California, Berkeley, California, CRC Press LLC, 2001.

THE ANNALS OF "DUNAREA DE JOS" UNIVERSITY OF GALATI
FASCICLE IX. METALLURGY AND MATERIALS SCIENCE
N°. 4 – 2014, ISSN 1453 – 083X

IMPROVING SLAB QUALITY THROUGH CONTROL OF COOLING PARAMETERS IN CONTINUOUS CASTING PLANTS

Marian BORDEI, Ștefan DRAGOMIR
"Dunarea de Jos" University of Galati, Romania
e-mail: mbordei@ugal.ro

ABSTRACT

Coupling the continuous casting installations with the rolling ones is a modern process that brings considerable economic benefits. During the continuous casting process of steel slabs, necessary technological conditions must be met in order to obtain some semi-finished products with minimum probability of defect appearance, under the conditions of a maximum amount of heat conservation in development without negatively affecting the productivity of the continuous casting machine.

KEYWORDS: slab quality, cooling parameters, continuous casting

1. Introduction

The conditions which must be achieved by the continuous casting installations, in order to be correlated with the rolling ones (for direct rolling), are the following:

- flawless casting (especially surface casting);
- reducing the thickness of continuous casting slabs;
- maintaining the slab temperature to values over the range of plastic deformation.

In this sense, the temperature conditions for a continuous casting plant can be defined as follows:

- *initial conditions*: at entrance, the steel should be as "cool" as possible (10-30 °C distributor overheating);
- *final conditions*: at exit, the slabs should be as "hot" as possible (approx. 1200 °C) to be rolled directly.

On the surface, heat is removed by contact with a solid cold surface (in the mold) and by spraying with water, air, air-mist (in the secondary cooling zone).

The conditions of steel solidification during continuous casting differ from those during ingot casting by:

- higher cooling speed, especially at the surface, due to the contact with the walls of the mold and the direct spraying in the secondary cooling zone;
- high metallurgical length, which creates a high static pressure in the liquid metal cone;
- smaller casting sections with higher ratio lateral surface/volume, which favors a more rapid evacuation of heat;
- a more sensitive connection between the mechanical strength and the tensions in the solidified crust; overcoming this balance at the expense of the mechanical strength is more prominent in case of curved wire casting, leading to cracks, especially on the surface.

The heat extracted by conduction (through solidified crust – during cooling at the contact with the surface of the mold) is the outer limit of the product cooling, the specific thermal power being, at the beginning of solidification, 2-5 MW/m^2.

The shorter the period of time between the final moment of casting and the beginning of rolling, the higher the temperature of the semi-finished product (therefore, an energy gain). This stage can be reduced by eliminating the repair stage, which involves ensuring a consistently good quality of the continuous casting of semi-finished products. In addition, the temperature of the semi-finished product can be increased by setting some appropriate technological conditions (casting speed, primary and secondary cooling).

In this situation, it may be able to transfer, in hot state, the continuous casting semi-finished products.

The effects are the following:

- reducing the fuel consumption with the appropriate heating rate from ambient to rolling temperature;
- reducing metal losses caused by the scale obtained during the warming of the semi-finished products and defect repair;
- increasing the productivity of the casting plant by increasing the casting speed.

2. Analysis of the main parameters of the continuous casting process

2.1. Overheating liquid steel

Overheating the liquid steel (the difference between the steel temperature and the liquid temperature) is set in the distributor; the overheating must be as small as to prevent the formation of precipitates and to obtain a minimum interdendritic segregation (large equiaxial zone).

The control of the steel temperature in the distributor, meaning the decrease of overheating and maintaining it within narrow limits, has the following effects:

- increasing the casting speed, which results in the improvement of the semi-finished product quality and the increase in productivity of the machine;
- decreasing the exhaust temperature from the processing unit, with implications for energy consumption and refractory materials;
- improving the casting structure by reducing the area occupied by columnar crystals and obtaining a homogeneous structure.

In the experiments that were carried out to optimize the moulding process we followed the variation of the temperature in the distributor for 66 charges from the four groups of steel specified in Table 1.

At the charges followed, the temperature system practised in the distributor was generally low in comparison with the brand technological instructions presented in Table 2.

Table 1. *Temperature variation in the distribution of some steel charges*

Steel group	Charge no.	Temperature in the mold, [°C]		
		minim	maxim	average
I	15	1530	1557	1545
II	22	1527	1554	1541
III	17	1520	1549	1537
IV	12	1522	1555	1535

Table 2. *Comparison of temperature systems from technological instructions and experimental*

Steel group	Temperature in the distributor, [°C]		
	calculate (T_l + 15-30 °C)	recommended in technological instructions	experimental
I	1545-1560	1545-1555	1530-1557
II	1540-1555	1540-1550	1527-1555
III	1535-1550	1535-1545	1520-1549
IV	1525-1540	1525-1535	1522-1555

Several temperatures below the permissible minimum and further from the maximum limit were recorded. The average temperature value in groups, at the charges followed (except group IV), was at the lower limit of the range indicated by technological instructions.

The analysis shows that, while the cooling rate does not lead to the entry of the steel in fragile areas, the quality of the slab is impaired, particularly, by the temperature in the distributor (the overheating of the liquid steel), the metal efficiency is negatively affected by the interruptions in casting, first of all, because of too low temperatures in the distributor (Figs. 1-4).

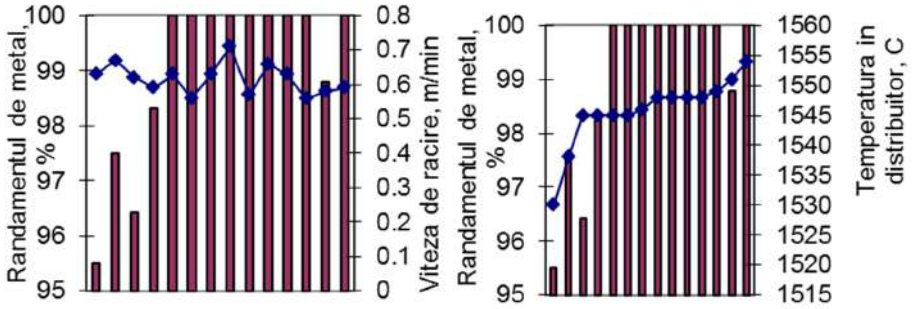

Fig. 1. *Metal efficiency depending on cooling and temperature rates of the steel in the distributor (for steels in group I)*

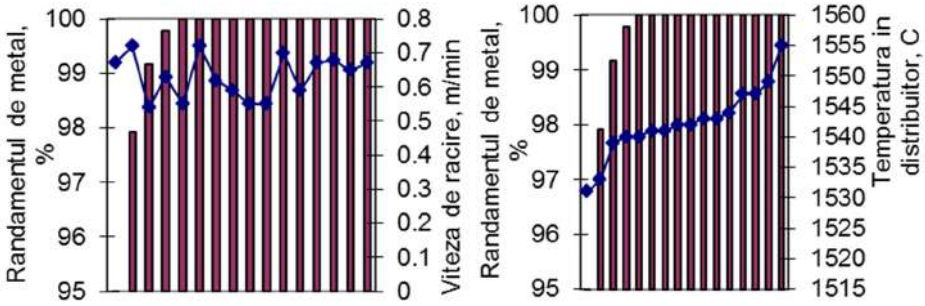

Fig. 2. *Metal efficiency depending on cooling and temperature rates of the steel in the distributor (for steels in group II)*

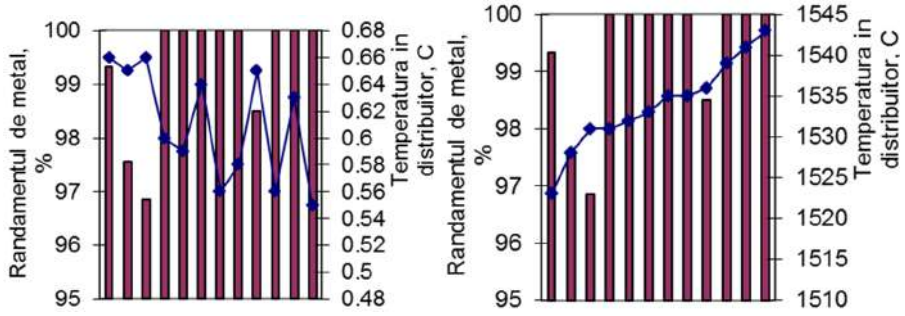

Fig. 3. *Metal efficiency depending on cooling and temperature rates of the steel in the distributor (for steels in group III)*

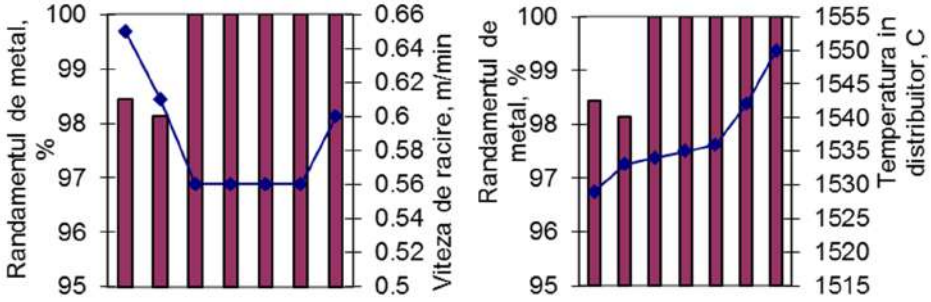

Fig. 4. *Metal efficiency depending on cooling and temperature rates of the steel in the distributor (for steels in group IV)*

3. Conclusions

The intensity of the axial segregation depends on the way the solidification takes place. Short solidification times and low overheatings are favorable to the reduction of the axial segregation with beneficial effects in terms of reduction of carbon, sulphur and phosphorus segregations.

To obtain a proper quality, it is required that the overheating 15-25 ºC in the distributor to be reduced so that the waste overheating at entry in the mold to be only 1-7 ºC, which can be achieved by using tubular jet nozzles (the role of heat exchanger and temperature controller).

THE ANNALS OF "DUNAREA DE JOS" UNIVERSITY OF GALATI
FASCICLE IX. METALLURGY AND MATERIALS SCIENCE
N°. 4 – 2014, ISSN 1453 – 083X

POLICIES FOR ECONOMIC EFFICIENCY. PROVIDING UTILITIES IN PUBLIC ADMINISTRATION

Aurel Gabriel SIMIONESCU[a], Mariana Carmelia DRAGOMIR[b]
[a]"Constantin Brâncoveanu" University, Pitești, Faculty of Administrative Sciences and Communication, Braila
[b]"Dunarea de Jos" University of Galati, Cross-border Faculty of Humanities, Economics and Engineering Sciences, Cahul, the Republic of Moldova
e-mail: dragomircarmelia@gmail.com

ABSTRACT

The reality of the contemporary world has shown that there is an increasing interdependent power often turned into political pressure. Today, in Europe 25% of the imports of natural gas come from Russia. Therefore, reducing energy dependence by using all the internal resources of each country becomes a national policy priority. This and the conditions in which alternative energy sources and building envelopment procedures can lead to considerable savings especially in areas where the heating of the public institutions needs to be done for more than half a year. For example, the overall heating costs in schools meaning between 60-90 lei/student/year for about 3.3 million students, it is possible to reduce them with about 20%. In this context, for the 2014-2020 period, the public authorities have at their disposal an important tool in the P.O.R. respectively the measure of "supporting energy efficiency and the use of renewable energy in public infrastructure".

KEYWORDS: energy efficiency, renewable energy, envelope, public expenditure

1. Introduction

Energy consumption has greatly increased with technological development and the diversification of human activities. The limited resources versus the unlimited needs of society led eventually to a series of fractures in the process of ensuring the energy required in its various forms, from raw materials such as gas, oil, coal, uranium consumed in specialized units, to the use at an increasingly wider scale of renewable ones: hydro, wind, solar, etc.

Various energy policies were developed, trying as much as possible to ensure its energy from internal sources, depending on the specificity of the area and the resources available for each country in the world.

However, a substantial pressure is currently maintained by countries holding the resources, pressure that, in some cases, has even apolitical nature, due to the energy production costs involved depending on the available raw material.

A short analysis of the dependence of methane of European countries, the issue "on the agenda", shows that almost a quarter of gas consumption is provided by imports from Russia, 23% from Norway, 20% from various other non-European countries (Algeria, Qatar) and only 33.74% from internal production.

When it comes to Romania, the imports from Russia are around the European average, but we can say that, from this point of view, we are privileged; our internal resources ensuring 75.67% of the national demand [1].

Considering the costs induced by energy prices, the limited resources, the dependence on imports and the emphasized constraints to environmental protection, at EU level, in the Europe 2020 Strategy, a major target was formulated, the 20/20/20 objective, to reduce carbon emissions by 20% while increasing energy efficiency by 20% and providing at least 20% of energy from renewable sources.

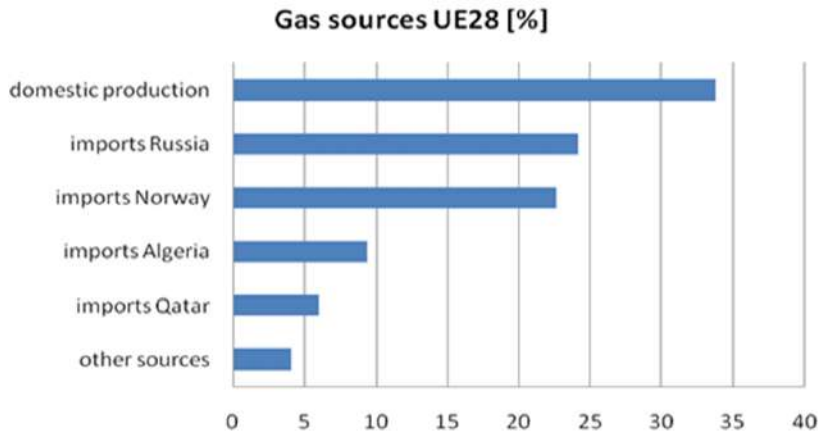

Fig. 1. *Gas sources in the EU 28*

2. Public policies on energy

"Meeting our energy goals could result in 60 billion euros less in oil and gas imports by 2020" [2]. "This is not only a financial saving but is essential for our energy security. If further progress in the integration of the European energy market is made, the GDP could increase by 0.6 to 0.8 percent" stated the Europe 2020 strategy. It is estimated that achieving the objective of having more than 20% energy from renewable sources could create more than 600,000 jobs, which is extremely important taking into consideration that the 10.5% unemployment in the EU has become alarming.

In these circumstances the role of public policies applied to the energy field becomes extremely important both in terms of reducing the consumption and in terms of providing facilities for the development of activities for energy production from renewable sources. The analysis of the classical categories of the national primary energy resources hows their limitation particularly in oil and gas, the resources of 2020 being virtually half of those of 2011.

The conclusion that can be drawn is that the energy production with the conventional sources of raw materials may not be sufficient over the next 20-40 years; the rest must be achieved by increasing the use of renewable energy sources.

Table 1. *Estimating the national reserves of oil and gas in Romania (2011-2020)*

YEAR	OIL million tons	GAS billion m^3
2011	60	134
2012	56	127
2013	52	120
2014	48	114
2015	45	107
2016	41	101
2017	38	95
2018	34	89
2019	31	83
2020	28	77
The considered premises in the estimation	Considering the depletion of the deposits, the oil production may register 2-4%annualdeclines. The degree of substitution of the exploitable reserves will not exceed15-20%	Considering the depletion of the deposits, the natural gas production can register annual declines of 2-5%. The degree of substitution of the exploitable reserves will not exceed 15-30%

"The dependence on import will depend on the discovery of new exploitable internal resources, the degree of integration of renewable energy and resources needed to increase efficiency" is shown in the Romanian Energy Strategy for the period 2007-2020 updated for the period 2011-2020 [3].

Thus the analysis of the potential of the renewable energy sources notes that Romania has developed an important segment in hydro, taking into account the natural potential that we have.

Also, a substantial increase in solar and wind energy in the recent years is observable. Given the fact that we basically started from zero in this field, the development can be seen as spectacular but far from fulfilling the potential that our country has.

Table 2. *Potential of Romania's national renewable sources*

Renewable energy source	Annual energy potential	Economic equivalent energy (thousand tep)	Application
Solar			
- **thermal**	$60x10^6$ GJ	1433	Heat
- **photovoltaic**	1200 GWh	103.2	Electricity
Wind	23000 GWh	1978	Electricity
Hydro in which: - **less than 10 MW**	40000 GWh 6000 GWh	3440 516	Electricity
Biomass and biogas	$318x10^6$ GJ	7597	Heat
Geothermal	$7x10^6$ GJ	167	Heat

From this point of view, the Energy Strategy for Romania, for the period 2007-2020 updated for the period 2011-2020, provides that in Romania steps will be taken specifically towards energy efficiency and renewable energy [4].

The actions targeting these are as will lead to the fulfillment of the objectives assumed by Romania in the environment field. Also very important, these actions will reduce our country's dependence on imported energy, the strategic national objective in the conditions of political and economic development today.

Directive 2006/32/EC, regarding the energy efficiency for final users, requires Romania to adopt significant measures in energy efficiency, including:

- The use of financial instruments to determine energy savings. It is inclusively considered the energy performance contracting.
- The purchase of equipment and technologies taking into account the priority of the defining elements for achieving energy efficiency.
- Conducting rigorous energy audits to industrial consumers, public and residential buildings. These must determine measures to reduce energy consumption and lead to the realization in 2016 of an economy through interventions at both existing buildings and at the new ones, by upgrading or creating new installations in residential areas and in the tertiary sector.

Table 3. *Estimated energy savings by sector in 2016*

SECTORS	Savings in 2016 Mil. Tep
Total Consumption, in which:	1.992
- by investing in facilities, existing buildings	1.047
- by making/building new installations, buildings	0.945
Residential, total, in which:	1.247
- investment in existing buildings	0.899
- the development of new buildings	0.348
Tertiary, total, in which:	0.085
- investment in existing buildings	0.007
- the development of new buildings	0.078

The National Program for thermal rehabilitation of buildings, the support of energy efficiency programs as well as the fiscal and the financial incentives to achieve energy efficiency projects are some of the implemented measures in the future [5].

The funding of these investments is an important problem, particularly concerning the financial effort and also supporting it for a relatively short time while the effects are observed gradually.

The main sources of funding are expected to come from:

- the state budget and local budgets, as a result of the national programs or local initiatives;

- on the basis of performance contracts signed with producers and energy service providers;
- financial loans obtained from foreign institutions WB, EBRD, EIB;
- co-financing from structural funds.

Considering the national budget, the local budgets and also the constraints related to loans in the banking system, accessing European programs appears to be the best solution to solve, at least partially, a series of actions in the field.

Thus, the priority axes "Energy efficiency in public buildings" and "Supporting urban development" are provided in the 2014-2020 Regional Operational Program, with the topic "supporting the transition towards alow-carbon economy in all the sectors "and as an investment priority" supporting the efficiency of energy and the use of renewable energy in public buildings and public infrastructure including housing"; these actions aim at improving the efficiency of energy in public buildings and public lighting system. The amount allocated exceeds 1.1 billion Euros and will be a real challenge for the public authorities.

It is estimated that the energy performance of buildings in Romania is low; buildings are responsible for about 36% of energy consumption. In this context the potential of saving for the buildings owned by public authorities is significant, averaging at 38% for heating and 23% for electricity [6].

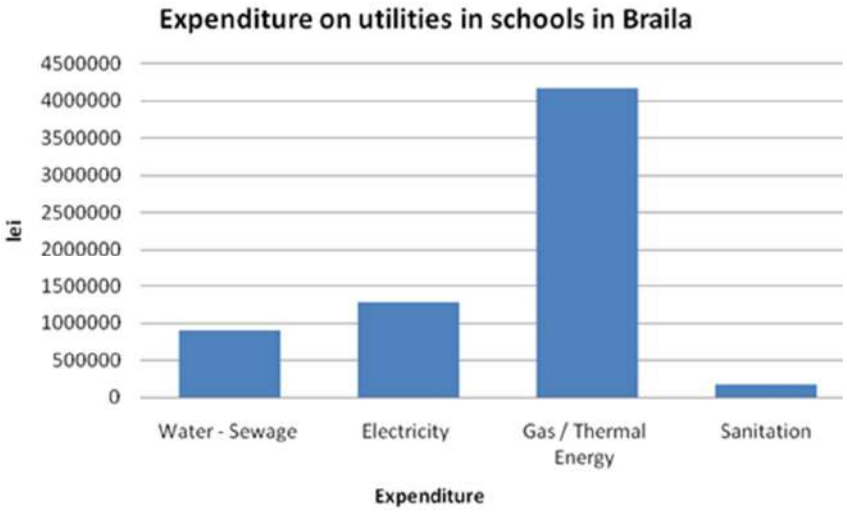

Fig. 2. *Expenditure on utilities in schools in Braila*

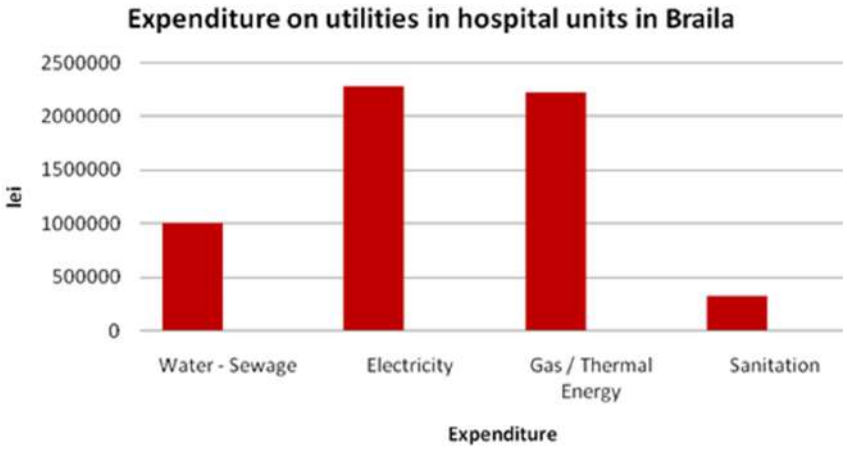

Fig. 3. *Expenditure on utilities in hospital units in Braila*

A detailed examination of a large municipality-Braila, reveals that all the utilities expenses from schools were over 6.5 million lei in 2013, from which 4.1 million was spent to provide heat either from the central heating system or on its own, the share of these expenses being 64%.

The same analysis for hospitals shows that, from a total expenditure of approx. 6.1 million lei, the cost of heating and hot water was 2.2 million lei, respectively 36.34% [7].

Thus, a 30% reduction of budget expenditures for providing heat and hot water in these institutions can mean annual savings of nearly 2 million.

If we analyze the electrical power consumption, at the school level, this means about 1.3 million lei, or 20% of the total amount paid for utilities, and in hospitals 2.3 million lei, 37.25% of total utilities payments, such that a reduction of these expenses by 20% would mean saving 720,000 lei annually.

In this respect Axis 3 of 2014-2020 ROP mentions a number of actions that can be carried out in public buildings and which can be considered as examples for implementing energy efficiency measures. Some of these actions are:

• improving the thermal insulation of the building, including measures to strengthen it;

• rehabilitation and modernization/upgrading of the facilities for producing and transporting heat, AC, hot water, etc.;

• intelligent power management including the changing of electric lighting by using lighting with high energy efficiency and long life;

• use of renewable energy sources in particular for providing heating and hot water.

4. Conclusions

There are significant sums for local budgets that may be made available for various activities, and also to support European co-funded projects.

In these circumstances the local authorities must use all their opportunities to complete the required projects so when signing the partnership Romania - the EU funding admission becomes operational, in order to be able to access the EU available funding for this axis.

Creating an "Efficient Europe in terms of use of resources" will allow for a decoupling of economic growth from the existing limited resources, the increase of the degree of the use of renewable energy resources and promoting actions and activities characterized by energy efficiency.

Improving the efficiency of energy in public buildings will lead not only to reduced energy consumption and costs, but will also cause a growth particularly in the construction industry and local industry, influencing also the research and the innovation in the field.

The use of the Regional Operational Program to finance such interventions in the public and providing incentives and tax with the use of all resources available to public authorities can help to achieve important saving goals assumed by Romania in energy efficiency and environment protection with a significant impact on the whole economy and social life for the next 40-50 years [8].

Acknowledgement

The work of Carmelia Mariana Dragomir was supported by Project SOP HRD - PERFORM /159/1.5/S/138963", project co financed from ESF of EC, the Romanian Government, and "Dunarea de Jos" University of Galati.

References

[1]. *,** *"Europe 2020 - A strategy for smart, sustainable and inclusive growth"* – Brussels, 2010.

[2]. WBGU, ***"****World in Transition – Future Bioenergy and Sustainable Land Use"*, German Advisory Council on Global Change (WBGU), Earthscan, London, UK, 2009.

[3]. Environmental indicator report 2012, *"Ecosystem resilience and resource efficiency in a green economy in Europe EEA"*, Copenhagen, 2012.

[4]. REN21, *"Renewables 2010 Global Status Report. REN21 Renewable Energy Policy Network for the 21st Century"*, Paris, France. Reprinted with permission from REN21.

[5]. Territorial Agenda of the European Union in 2020, *"Towards a smart, sustainable and inclusive of Diverse Regions"*, Gödöllő, Hungary, 2011.

[6]. *Romanian Energy Strategy for the period 2007 to 2020 updated for the period 2011-2020.*

[7]. UNEP, ***"****Global Trends in Sustainable Energy Investment 2009: Analysis of Trends and Issues in the Financing of Renewable Energy and Energy Efficiency"*, United Nations Environment Programme, Paris, France, 2009.

[8]. Commission of the European Communities, *"Communication from the Commission - The support of electricity from renewable energy sources – Brussels"*, COM(2005) 627 final.

THE ANNALS OF "DUNAREA DE JOS" UNIVERSITY OF GALATI
FASCICLE IX. METALLURGY AND MATERIALS SCIENCE
N°. 4 – 2014, ISSN 1453 – 083X

ANALYSIS FREQUENCIES OF A VIBRATION-TYPE STRUCTURE HALL

Ionel PETREA
"Dunarea de Jos" University of Galati, Romania
e-mail: ipetrea@ugal.ro

ABSTRACT

Its main purpose was to identify natural vibration frequencies for a warehouse type structure in order to avoid resonance phenomena of the structure. The analysis is performed using the finite element analysis module of the CATIA system.

KEYWORDS: Von Mises stress, displacement field, restrictions, loads

1. Introduction

The finite element method (FEM) is one of the best methods of doing calculations and simulations in engineering.

CATIA systems contains Generative Structural Analysis modules, which is a suitable for advanced finite element analysis.

The steps in a finite element analysis are as follows:

- three-dimensional modeling of components assembled using CATIA Part Design and CATIA sketcher modules;
- insert all component parts using CATIA Assembly Design module;
- application of a material to the assembly components;
- accessing CATIA Generative Structural Analysis module and determination of the type of analysis;
- definition of nodes and elements (a process called meshing) and it's editing;
- setting restrictions;
- adding loads for the model;
- performing analysis calculations;
- visualization and interpretation of the results.

Hall-type structures are characterized by rigidity, being made generally of elements made of steel or wood. The identification of natural vibration frequencies is particularly important in order to avoid, through the design process, the frequent earthquakes, thereby avoiding the appearance of resonance structure in case of earthquakes, a phenomenon that can lead to partial or total destruction of the hall.

The Hall type structure in Figure 1 is composed of parts made of wood, hardened and joined together by elements made of steel.

The analysis is shown in Figure 2. To analyze the natural vibration frequencies a rigid connection between elements is considered and the foundation is modeled through a restriction that requires the cancellation of 6 degrees of freedom possible embedding surface.

The analyzed subassembly consists of elements made from oak (longitudinal elastic modulus E = 1.32 x 10 N/mm^2 and density ρ = 753 kg/m^3) and assembled reinforced by elements made of steel (modulus of elasticity E = 2.1 x 10^5 N/mm^2 and density ρ = 7860 kg/m^3).

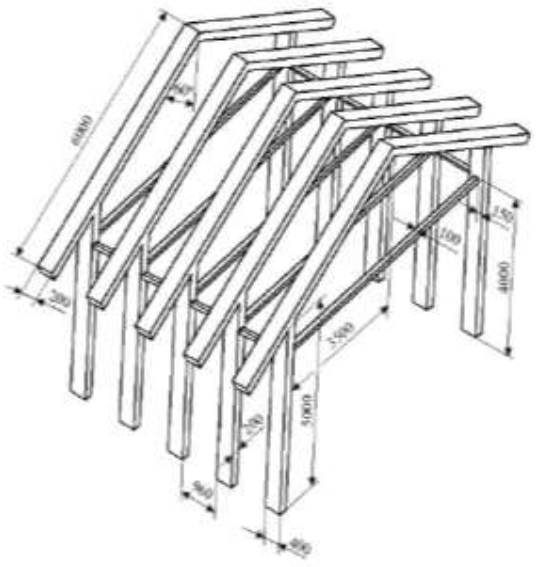

Fig. 1. *Hall type structure*

2. Geometric modeling

The geometric design of the main structure (wood) is obtained in the Sketcher module (Figure 2).

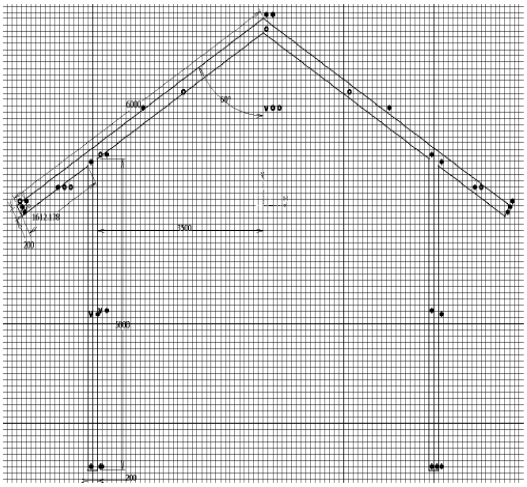

Fig. 2. *Outline of the main structure*

The main structure is obtained by extruding a 400 mm (thickness structure) profile previously created (Figure 4).

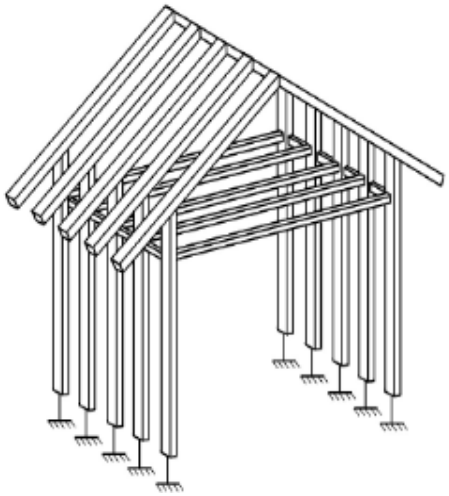

Fig. 3. *The finite element analysis*

Fig. 4. *Main structure*

The element geometric relationship between structures made of wood is obtained in the Sketcher and Part Design module (Figure 5). The geometric design of the reinforcing element is shown in Figure 6.

Fig. 5. *Connection element*

Fig. 6. *Reinforcing element*

The insertion of the component parts is made in the CATIA Assembly Design module (Insert/Existing Component) (Figure 6).

The assembly is created using geometric constraints between components (Contact Constraint and Coincidence Constraint).

Fig. 7. *Assembly structure*

Application of material using Apply Material icon. Entering the values of material characteristics required for the finite element analysis is performed using the CATIA environment library materials, to choose from:

- Metallic material group steels (Steel), which changes the values of the elastic modulus (Young's modulus) and Poisson coefficient, taking into account the values given as input.

- Material ranging from wood (Wood), Group oak wood (Oak), for which the modulus of elasticity (Young's modulus) and Poisson coefficient are accepted.

3. Finite element analysis

Accessing CATIA Generative Structural Analysis module and setting the type of frequency analysis allows for the analysis of the vibration modes of the structure in terms of imposing rigid type connections between components and considering a database connection to cancel the 6 degrees of freedom associated with the possible points.

The definition of nodes and elements (a process called meshing) determines the size of finite element (Size), the maximum tolerance between discretized model and real model used in the analysis (Absolute sag) type element (element type), etc. For this, a double click is executed on "Mesh tetrahedron OCTREE" sub-item found in the specification tree.

Figure 7 presents the specification tree and the dialog with the same name, which contains the finite element size (30 mm), minimum tolerance (6 mm) and the type of the element as parabolic.

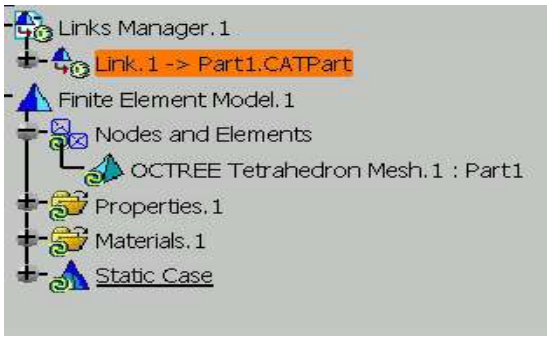

Fig. 8. *Discretization of the part model*

Restrictions definitions

The connections between elements is achieved through a connection type Rigid Connection, applying the geometric constraints generated module assembly, faces common in contact.

The contact imposed based model is defined by canceling the 6 degrees of freedom associated potential surfaces Contact element wood foundation (Clamp) (Figure 8).

The effective step analysis calculation is done using the *"Compute"* icon.

The display and interpretation of results is achieved, with the help of *Image* on the toolbar. In Figure 9 the specification tree is exemplified, containing a list of three images and their icons.

Figure 10 displays the corresponding results Von Mises stress (values of a scalar field energy density obtained from the volume of strain).

The numerical values of these stresses are displayed along with the Von Mises stress. Also, the nodes location is displayed where minimum and maximum values of these tensions are located.

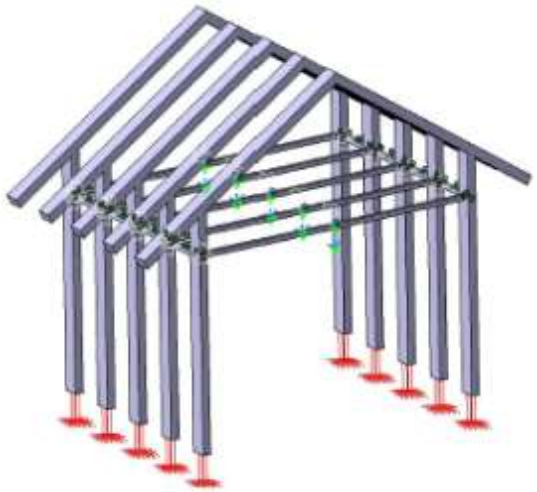

Fig. 9. *Restrictions definitions*

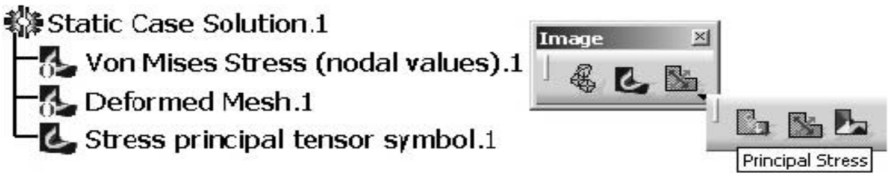

Fig. 10. *Tools of image display and the corresponding menu tree*

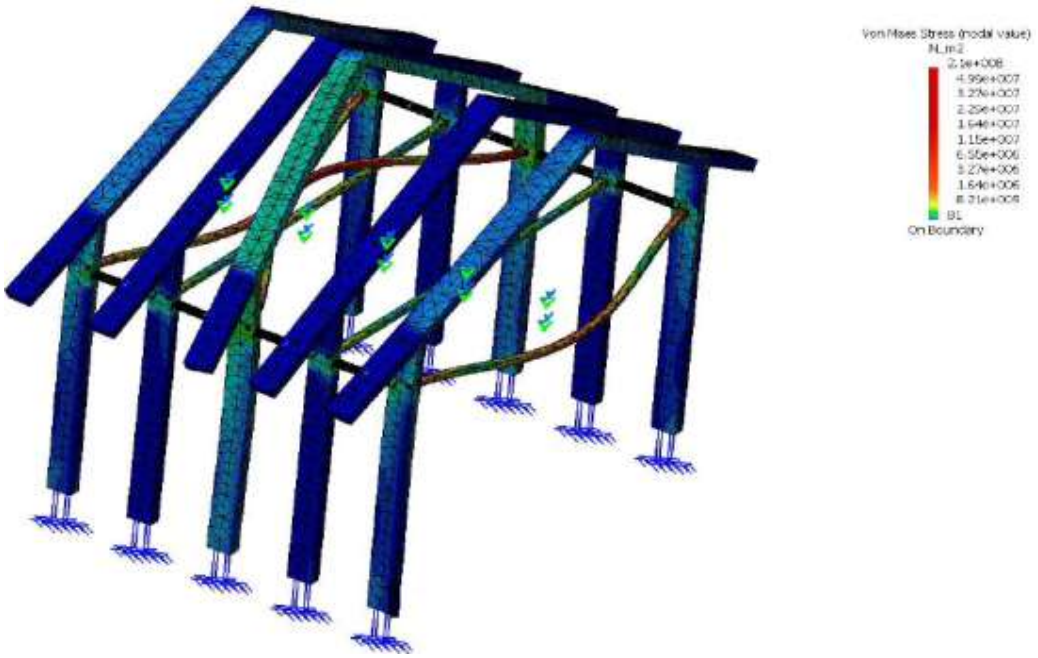

Fig. 11. *Result of Von Mises stress and indication of extreme stress*

4. Conclusions

The analysis of displacement and stress fields shows that the analyzed subassembly is a rigid structure with high peak voltages stiffeners (maximum Von Mises equivalent stress is 210 MPa). To avoid structural or technological damage, adopt constructive measures (increase cross section of stiffeners and/or use of materials with superior mechanical properties).

Identification of natural vibration frequencies is useful in order to avoid the phenomenon of resonance.

References

[1]. Ionuț Gabriel Ghionea, *Proiectare asistata în CATIA V5 – Elemente teoretice şiaplicaţii*, Editura BREN, Bucureşti, 2007.
[2]. Mihai Tiberiu Lates, *Metoda elementelor finite. Aplicaţii,* Editura Universitatii Transilvania din *Brasov*, 2008.

THE ANNALS OF "DUNAREA DE JOS" UNIVERSITY OF GALATI
FASCICLE IX. METALLURGY AND MATERIALS SCIENCE
N°. 4 – 2014, ISSN 1453 – 083X

FUNCTIONAL MODEL OF SAVONIUS TYPE VERTICAL AXIS WIND TURBINE WITH PERIODIC COUPLING OF ADJACENT VERTICAL BLADES

Nelu CAZACU, Catalin Bogdan LUCACI
"Dunarea de Jos" University of Galati
e-mail: nelu.cazacu@ugal.ro, catalin.bogdanlucaci@gmail.com

ABSTRACT

The field of HAWT (Horizontal Axis Wind Turbines) regarding the use of wind energy (WE) as a renewable energy source (RES) is well researched and the results are covering both the power range and efficiency. Deficiencies observed during high wind speeds affect the investment costs. Savonius is a VAWT (Vertical Axis Wind Turbine) used for low wind speed, with low costs and low efficiency. The study proposes a conceptual model of Savonius type of VAWT (SWT) meant to increase the efficiency by reducing the resistance of the returning blade. SWT conceptual models were studied and analyzed and then a MC was elaborated and a MF and MM have been developed. An ME was made based on the MC and MF, which was used in wind tunnel experiments. The starting torque, the power factor, the efficiency, the speed and the output voltage of the generator were investigated. The results confirm the viability of the model and its resources to increase efficiency.

KEYWORDS: wind energy, VAWT, Savonius, coupled blades

1. Introduction

A classification of WT based on the rotation axis position leads to HAWT, which are the most widespread, and VAWT, less prevalent and less effective.

The literature recognizes that the main advantage of vertical axis wind turbines, namely the lack of wind direction dependence, leads to some simplifications in the handling of the problem.

A graphical representation of the power coefficient Cp, presented in many studies, leads to fields of application of various types of wind turbines depending on wind speed vi or speed coefficient λe. The diagram highlights the existence of the relative speed as an important element in the design and operation of a wind turbine:

Notations
v_v - wind speed input (to infinity) m/s
u - peripheral speed at the top the blade, m/s
R - the radius of the disc base, m
c - overlap, m
d - width of blade, m
h - height of blade, m
ω - angular speed, radians/s
λ - coefficient of speed (speed index)
Cp - power index
n - number of blades on the floor
m - number of floors

Abbreviations
WE – wind energy
WT – wind turbine
VAWT – vertical axes wind turbine
HAWT– horizontal axes wind turbine
SWT – Savonius Wind Turbine
SBWT – Savonius-Benesh Wind Turbine
SWT-API – SWT with Alternating pocket/interval
RES – Renewable Energy Sources
d.c. – direct current
Re – Reynolds number

$$\lambda_e = \frac{v}{v_i} \quad (1)$$

The tangential speed at the blade tip is dependent on angular velocity and the radius of rotation:

$$v = \omega R \quad (2)$$

The Savonius type wind turbine (SWT) has a low power coefficient (max. 18%) and λe max 1.5, which shows low rotation speed and also small tangential speed at the blade tip (Menet, and *et al.*).

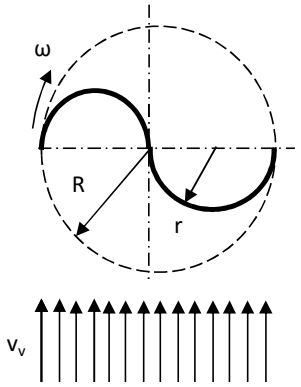

Fig. 1. *Section through Savonius Wind Turbine (SWT)*

SWT theory explains this by the braking effect of the blade during the return. One method to reduce the resistive return effect is to move the air stream after the mechanical work is done from the pressure side to the return side.

FEM simulations (Menet, and *et al.*) highlight the causes of SWT low efficiency, i.e. gas-dynamic braking determined by adverse changes in the pressure.

The operation of this type of wind turbine is characterized by changing the rotation angle of the torque generated by a pair of pales, in the original and simplest situation.

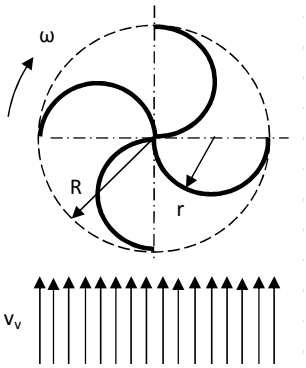

Fig. 2. *SWT with four semicilindrical blades*

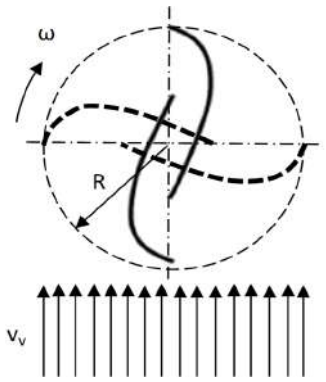

Fig. 3. *SWT with Benesh airfoil: one real pair of blades and fictive second pair of blades*

Fig. 4. *Variation of couple to axe for SWT (Menet, et al.)*

2. Experimental

The objectives in this paper are:
- increasing the wind speed range;
- increasing the efficiency;
- reducing the resistance of the returning blade;
- changing the blade profile.

The reference literature offers a great number of conceptual (theoretical) models and experimental models. They are based on a SWT or VAWT, so called "S wind turbine" because of the specific blade section profile.

The CM proposed in this paper is a SWT model modified to reduce the drag resistance of reverse blade without using control screens that reduce the main advantage of SWT i.e. the independence from wind speed.

The development of a conceptual model containing elements of novelty is possible after a complete and critical analysis of data from the relevant literature and beyond. The interest in the construction of cheap wind turbines for families is high where an RES exists.

The premises for SWT use are as follows:
- VAWT type;

- independence from wind speed;
- operation at low wind speeds;
- great solidity coefficient;
- great surface;
- problems during storms and wind blasts.

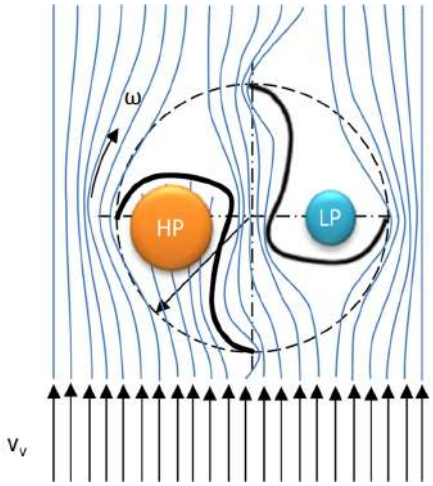

Fig. 5. *Alternating "pocket/interval" (API) for SWT with coupling blades (superior level)*

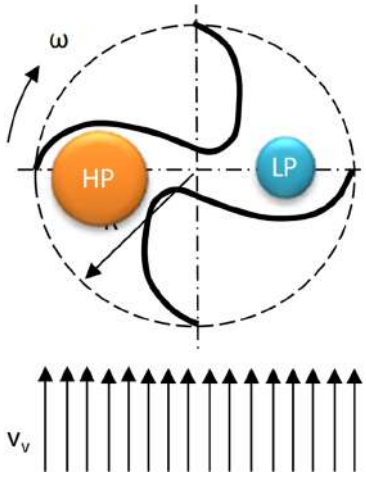

Fig. 6. *Alternating "pocket/interval" (API) for SWT with coupling blades (inferior level)*

The following factors of influence shall be noted:

SWT operates based on the forces of wind (D-Draft force).

The driving torque is given by the force Draft at a given time and the force arm.

Reducing the blade surface and increasing the radius is a solution for increasing the axis torque.

The torque and blade angle shall be rendered uniform with wind speed by two methods.

An advantage is increasing the number of blades, while a disadvantage will be a uniform torque, increasing inertia, mass will also be increased.

Blades staggering by reducing the height and creating stages (Helix).

Measurements and simulations show that a disturbed zone is produced in the SWT area, with local increases/decreases of the pressure, and hence the formation of local currents (vortices), reducing the efficiency of the system. As a Drag-type system, SWT efficiency increases with reducing the pressure difference.

In principle, the conceptual model is based on creating a gas-dynamic channel between two pairs of blades with approximate Benesh (Benesh, 1988) structure and layout, which provides a fast equalization of pressures.

When 2, 3 or 4 pairs of blades may be used with changing the distances, this will involve the smooth operation of the gas-dynamic turbine.

In principle, the following effects occur:

- reduction of the variability of a torque around a rotation axis due to a lower differential pressure (pressure/depressure).
- uniformization of torque to axis as a result of superposition of several blades.
- increase in the starting torque due to the constant wind speed.
- torque uniformization.

3. Functional Model

The CM proposed that SWT starts from the use of pairs of blade in continuous or overlaying a gap case. The different behavior of the pair of blades in a lower wind speed gives the difference of force, coupled forces and finally a rotation.

Increasing the torque on the back masking blade is useful but the advantage of independence from wind direction will be lost.

If SWT has two blades the torque varies with the rotation angle measured from the direction of the wind (Menet reference).

Wind is a variable load and efficiency is low.

The CM proposed uses physical coupling and gas dynamics of the 4 vertical blades of the SWT. The coupling is made between adjacent blades and thus creates a succession "pocket/range" both diametrically high and using the opportunity to increase the pressure behind the blade through the front airflow created by the constructive interval.

The MM (mathematical model) of wind energy, widely available in literature, takes into consideration the kinetic energy of a moving air stream, using Betz's calculations to obtain an energy conversion before and after the wind rotor (v) to have a certain value. When the wind speed after rotor v = 0, the

wind cannot pass through the rotor blades; when the wind speed brake rotor is not 0, energy transformation will take place.

The optimum value brake wind is obtained to value ratio: $\frac{v_3}{v_1} = \frac{1}{3}$.

We obtain values corresponding to this optimum value of power coefficient (aerodynamic efficiency).

$$c_p = \frac{16}{27} = 59.3\%$$

The plan has the speed wind rotor $v_2 = \frac{2}{3} \cdot v_1$.

Particularly, in the case of vertical axis wind turbines, Betz's limit has a value up to 14.81%.

The conversion of wind energy can be made according to the following schemes:

Wind Energy>Work>Electric Energy

VAWTs are generally of the "Drag-force" type, i.e. push or wind drag. This means that, if a body is in a system with the central axis of rotation under the influence of the wind, a pushing force is created, which, in turn, generates a torque towards axis, pushing force is for an object fixed on the surface placed in the path of an air flow:

$$\frac{F}{A} = \frac{1}{2} p v^2 C_D \quad (6)$$

C_D is defined as an important parameter when it comes to wind resistance. The power lost by wind, namely the power gained by the body, is as follows:

$$P = \frac{1}{2} p v^3 C_D A \quad (7)$$

In case of "Drag-force" wind turbines, the relative speed is as follows:

$$v_r = v_0 - u \quad (8)$$

Where v_v - wind speed, m/s; u – tip blade speed, m/s:

$$\frac{P}{A} = \frac{1}{2} (v_v - u)^2 C_D u \quad (9)$$

The power extracted at SWT axis is given by the formula:

$$P = C_p \rho_a H v_i^3 \quad (3)$$

The axis torque is as follows:

$$P = C_m \rho_a R^2 H v_i^2 \quad (4)$$

Air density affects the power and this influence is determined by the relation:

$$\rho_a = \frac{353.049}{T} e^{-0,034 \frac{Z}{T}} \quad (5)$$

The power conversion efficiency is defined by the extracted power related to wind power.

$$\eta = \frac{P}{P_v} = \frac{\frac{1}{2}\rho (v_v - u)^2 C_D u A}{\frac{1}{2}\rho A v_v^3} \quad (10)$$

$$\eta = \frac{(v_v - u)^2 C_D u}{v_v^3} \quad (11)$$

4. Experimental condition

An experimental wind tunnel with the following characteristics was used for experiments:

• anchoring the experimental model (ME) of VAWT;

• allowing easy exchange of EMs;

• allowing measurement of sensor location (force, speed, pressure).

The experiment performed a number of experimental models that changed the limits of a number of factors.

The purpose of the experiments is to verify the assumptions mentioned and then to find mathematical expressions that give theoretical explanations.

The construction is made of two steel plates, the lower and upper columns and 6 of the work 2 (M8) and 4 abutment and stiffening (M6):

• motherboard dimensions: 282 x 235 mm;

• height: 498 mm.

VAWT experimental models are supported on two rails 300 x 40 x 8 mm. When operating, these columns can be fixed with nuts and washers. The center bearings are fixed and centering devices ME discs.

A simple and efficient anemometer was made from a table tennis ball and a pendulum application.

The experimental metal frame presented in Figure 7has the following functions:

- to allow the anchorage of the EM of VAWT;
- to allow easy change of EMs;
- to allow the placement of measurement sensors (force, speed, pressure).

Experimentally, a number of experimental models shall be made, where the number of factors shall be changed in the established limits.

The purpose of the experiments is to verify the mentioned assumptions and then to find mathematical expressions.

It is a four blade model SWT modified by alternate coupling of blades on pocket/range section and ½ height alternating pocket/interval (API). A number of EMs have been built on the CM to verify functionality and performance.

Fig. 7. *Alternating "pocket/interval" blade over diametral and axial for EM of SWT*

The EM characteristics are:
- type with changes SWT API;
- number of blades: 4;
- number of horizontal pockets: 2;
- number of intervals horizontally: 2;
- number of vertical alternation: 1;
- maximum diameter: 0,150 m;
- blade height: 0.390 m;
- airfoil: approx. Benesh;
- airfoil material: PE cellulated;
- blade material thickness: 0.003 m.

5. Results and discussion

The wind speed influence over the open loop turbine rotations is the simplest experiment. The wind turbine is attached on a support frame containing centered axial bearings which allow the setting of EMs with heights of 50...495 mm and maximum diameters of 250 mm.

Table 1. *Values of wind speed versus wind energy*

exp. no.	wind speed	wind energy	wind power	wind specific power	Bets limit 14.81%
u.m.	m/s	J	W	W/m^2	W
1	3.62	98.13	1.64	27.96	0.24
2	3.98	130.42	2.17	37.16	0.32
3	3.35	77.77	1.30	22.16	0.19
4	2.88	49.42	0.82	14.08	0.12
5	2.37	27.54	0.46	7.85	0.07
6	2.14	20.27	0.34	5.78	0.05
7	2.12	19.71	0.33	5.62	0.05
8	1.83	12.68	0.21	3.61	0.03
9	1.81	12.27	0.20	3.49	0.03
10	1.62	8.79	0.15	2.51	0.02
11	0	0	0	0	0

In the wind speed range of 0...4.5 m/s and when there is no load, the variation of the axis speed and the wind speed are shown in Fig. 4.

In Fig. 5 are shown the variations of Re which has a constantly growing number of wind speed (Fig. 11) and specific speed (Fig. 14) in the range of wind speeds used in the experiments. The Re number is a constantly growing number of wind speeds (Fig. 11) and specific speeds (Fig. 14) in the range of wind speeds used in the experiments.

The efficiency of the SWT EM with "pocket/Interval" coupled blades is shown in Figs. 8 and 9. A maximum efficiency around 0.12 was obtained for wind speed around 2 m/s and λ_e between 2.23 and 0.39.

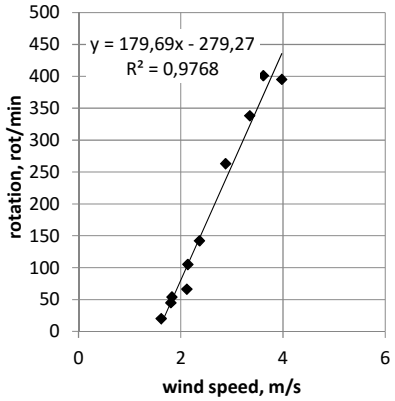

Fig. 8. *EM speed variation with wind speed*

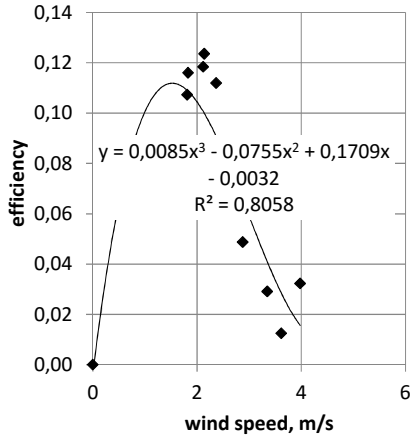

Fig. 9. *Wind speed influence over efficiency*

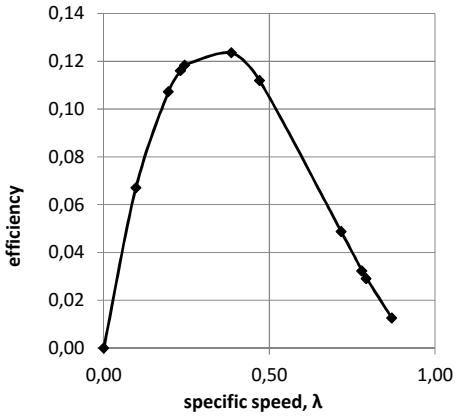

Fig. 10. *Specific wind speed influence over efficiency for EM*

Table 2. *Values regarding speeds of rotating components and the obtained power*

u.m.	rot/min	rot/s	Hz	rad/s	m/s	-	-	W/m²	W	-
1	401	6.68	6.68	41.97	3.15	0.87	64242	0.35	0.021	0.01
2	395	6.58	6.58	41.34	3.10	0.78	63281	1.20	0.070	0.03
3	338	5.63	5.63	35.38	2.65	0.79	54149	0.64	0.038	0.03
4	263	4.38	4.38	27.53	2.06	0.72	42134	0.69	0.040	0.05
5	142	2.37	2.37	14.86	1.11	0.47	22749	0.88	0.051	0.11
6	105	1.75	1.75	10.99	0.82	0.39	16821	0.71	0.042	0.12
7	66	1.10	1.10	6.91	0.52	0.24	10573	0.66	0.039	0.12
8	54	0.90	0.90	5.65	0.42	0.23	8651	0.42	0.025	0.12
9	45	0.75	0.75	4.71	0.35	0.20	7209	0.37	0.022	0.11
10	20	0.33	0.33	2.09	0.16	0.10	3204	0.17	0.010	0.07
11	0	0	0	0	0	0	0	0	0	0

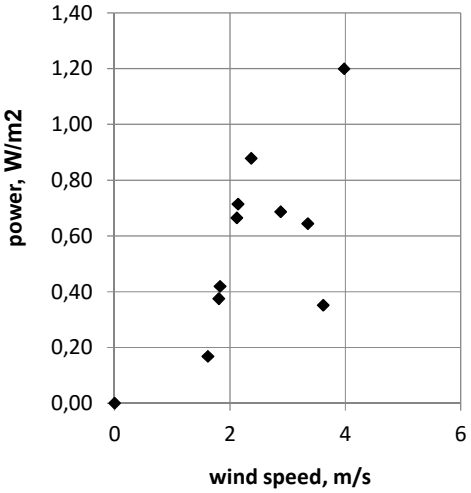

Fig. 11. *Power dispersions with wind speed for EM*

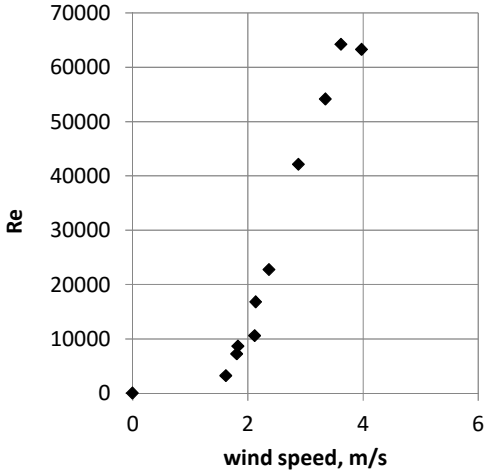

Fig. 12. *Re number variation with wind speed*

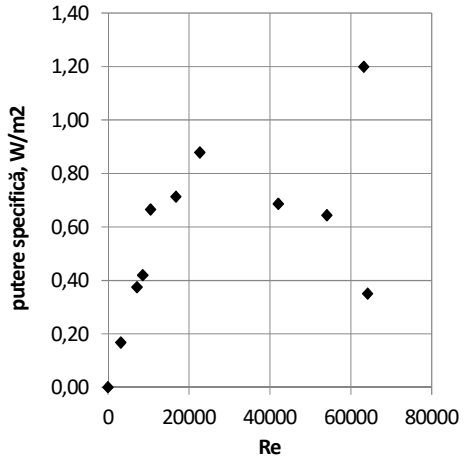

Fig. 13. *Specific power with Re number for EM*

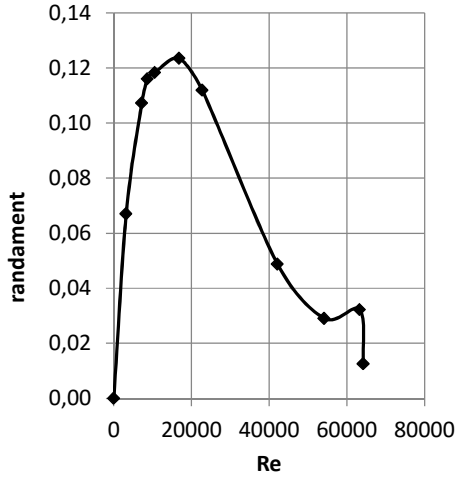

Fig. 14. *Efficiency with Re number for EM*

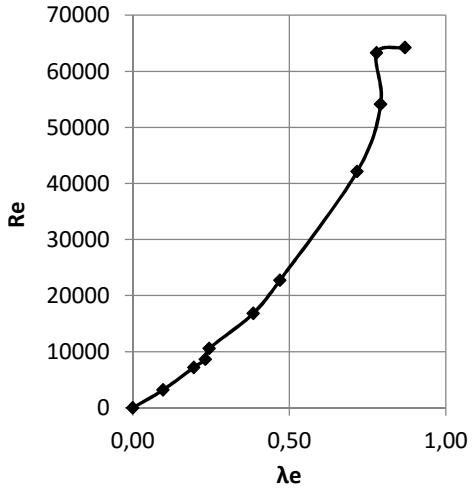

Fig. 15. *Re number variation with λe*

6. Conclusions

In the tests conducted in the wind tunnel, it is observed that the model developed has acceptable behavior.

The concept initially described is checked in the experimental model to have a rotating uniformity and more functionality is explained by the flow channels of "pocket/interval".

The EM was tested in no load conditions. An efficiency of 12 % was achieved for a range of wind speeds between 1.83 ... 2.14 m/s and λe = 0.23 ... 0.39.

Reynolds number continues to increase with wind speed aprox. 65000 (Fig. 12) and depending λe (λe = 1) drive situation shown in Fig. 15.

The maximum efficiency model for Re is obtained at about 20000 (Fig. 14) and a relative speed of 0.35.

References

[1]. Babu Suresh K., *et al.*, *The material selection for typical wind turbine blades using a madm approach& analysis of blades*, Conference, Chania, 2006.
[2]. Anthony Jiju, Book.
[3]. Archer Cristina L., Jacobson Mark Z., *Evaluation of global wind power*, Journal of geophysical research, 2005, Vol. 11.
[4]. Argaw N., Foster R., Ellis A., *Renewable Energy for Water Pumping Applications in Rural*, Report, Colorado, NREL, National Renewable Energy Laboratory Villages, 2003, p. 117.
[5]. Benesh A., *Wind turbine system using a vertical axis Savonius-type rotor*, US Patent 4784568, Journal, 1988.
[6]. Benesh A., *Wind turbine system using a vertical axis Savonius-type rotor*, Patent: 4784568, US, 1988.
[7]. Bianchi Fernando D., De Battista Hernán and Mantz Ricardo J., *Wind Turbine Control Systems. Principles, Modelling And Gain Schedu*.., Book: Springer, 2007, p. 219.
[8]. Blackwell B., *Wind tunnel performance data for two bucket savonius rotors*, Book, 1977.
[9]. Burton Tony, *et al.*, *Wind Energy Handbook*, Book, John Wiley & Sons, Ltd, 2001, p. 463, ISBN 0 471 48997 2.
[10]. Dumitrescu H., Georgescu A., *Calculul elicei, Cap. 4 Elicea eoliana*, Editura Academiei Romane, 1990.
[11]. Gardner Paul, *Wind Energy - The Facts*, Vol. 1 – Technology, Book.
[12]. Hansen Martin O. L., *Aerodynamics of Wind Turbines*, 2nd ed., Earthscan, 2008, Book, ISBN 978-1-84407-438-9.
[13]. Hau Erich, *Wind Turbines, Fundamentals, Technologies, Applications, Economics*, Book, Springler, 2006.
[14]. Houghton E. L., Carpenter P. W., *Aerodynamics for engineering students*, 5th ed., Oxford: Butterworth Heinemann, 2003.
[15]. Ivanko J., *Alternative Energy - Farming Sun Wind*, Book: www.solartoday.org, 2005.
[16]. Joachim Peinke, Schaumann Peter, Barth Stephan, *Wind Energy Collocvium*, Book: Springer, 2007.
[17]. Johnson G. J., *Wind Energy Systems*, Book: Manhattan, KS, 2001.
[18]. Koller Julia, Koppel Johann, Peters Wolfgang, *Offshore Wind Energy Research on Environmental Impacts*, Book, Berlin Heidelberg: Springer-Verlag, 2006.
[19]. Kreith Frank, Goswami Yogi D., *Handbook of Energy Efficiency and Renewable Energy*, Book: Taylor & Francis CRC, 2007.

[20]. Kyozuka Y., Akira H., *An Experimental Study on the Darrieus-Savonius Turbine for the Tidal Current Power Generation*, Conference, Osaka, 2009.
[21]. Lund Henrik, *Renewable Energy Systems - The Choice and Modeling of 100%*, Book: ELSEVIER Inc., 2010.
[22]. Manwell J. F., McGowan J. G., Rogers A. L., *Wind Energy Explained. Theory, Design and Application*, Book: John Wiley & Sons Ltd, 2002, p. 590.
[23]. Mathew Sathyajith, *Wind Energy Fundamentals, Resource Analysis and Economics*, Book: Springer, 2006.
[24]. Menet J. L., Bourabaa N., *Increase in a savonius rotor efficiency*, Book, 2003.
[25]. Nelson V, *Wind Energy. Renewable Energy and the Environment*, Book: Taylor & Francis Group LLC, 2009.
[26]. Nybroe Klaus, *Basic Blade Design*, Book: old.windmission.dk.mht.
[27]. Pasqualetti M. J., Gipe P., Righter R. W., *Wind Power in View Energy Landscapes in a Crowded World*, 1st ed., Book: Academic Press, 2002.
[28]. Patel M. R., *Wind and Solar Power Systems*, Book: CRC Press, 1999.
[29]. Piggot H., *PMG construction manual*, Book.
[30]. Piggot Hugh, *Small Wind Turbine Design Notes*, Book, 1998.
[31]. Piggot Hugh, *Wind Rotor Blade Construction*, Book.
[32]. *,** *Renewable Energy Focus Handbook*, Book: Academic Press-Elsevier, 2009.
[33]. Saha U. K., Rajkumar M. J., *On the performance analysis of Savonius rotor with twisted blades*, Journal Renewable Energy, 31, 2006.
[34]. The European Wind Energy Association, *Wind in power*, 2010 European statistics, Report 2011.
[35]. Zigman A., *Optimization of a Savonis Rotor Vertical-Axes wind turbine*, Book, Massachussets: MIT, 2007.

THE ANNALS OF "DUNAREA DE JOS" UNIVERSITY OF GALATI
FASCICLE IX. METALLURGY AND MATERIALS SCIENCE
N°. 4 – 2014, ISSN 1453 – 083X

EXPERIMENTS ON BALLISTIC TESTS FOR IMPROVING PERFORMANCE OF A NEUTRALIZING GAS DYNAMICS SYSTEM

Vasile BĂLAN[1], Marian BORDEI[2*]
[1]Tehnical Military Academy of Bucharest
[2]"Dunarea de Jos" University of Galati, Romania
[*]Corresponding author
email: mbordei@ugal.ro

ABSTRACT

Neutralizing improvised explosive devices (handmade) by mechanical separation of the elements which are part of their composition can be achieved by the following methods:

- generation of shock waves by means of the impact method between a projectile or a jet formed from diverse disrupting backgrounds and the improvised explosive device. It is known that after impact we must have at the interface projectile (jet)–target the same pressure and material speed; they characterize the equilibrium that is established at the interface;

- generation of shock waves by detonating explosives placed in direct contact with parts subject to shock. This method is destructive and it must take into account the combined effects of explosive load that we want to neutralize and cargo of explosives used in neutralization; it can be used only in special places which can provide a range of effective safety;

- generation of shock waves using lasers; at this stage, this method is only used in laboratories through fundamental research.

The most used method for neutralization of an improvised explosive device is the first one. The neutralization systems (gas-dynamics systems) that propel the kinetic projectiles using explosives are used to transmit large shocks to various inert or reactive targets. These shocks have a significant impact on the targets, transmit changes in state and kinematic parameters, leading to either dismantling of targets or initiating explosive charges receivers. Initiating the explosive to the receiver detonation devices that can be parts of improvised explosive devices happens because the incident shock wave has exceeded the critical threshold of initiation. The initiation of detonation is, generally, an undesirable event, as explosive charge mass, although part of it, may not make it possible to take appropriate safety distances and thus material damage and human injury can be induced.

Given the complexity of improvised explosive devices, the impossibility of knowing the exact explosive charges and the initiation ones in their composition, we cannot say that there existsa neutralizing thruster jet to meet all technical requirements specified above. In an attempt to simplify and systematize the study, we are going to present a summary classification of explosive jet engines means, capable of being used to neutralize improvised explosive devices.

KEYWORDS: ballistic, neutralizing gas dynamics system

1. Propelling jets with gas-dynamics devices, using deflagration of colloidal powder

Disruptors with water jet have been used since the Second World War by British sappers when they had to find a way to defuse aviation bombs with delay mechanisms, which were found in great number in Europe, as an alternative to the use of detonating wicks. At the end of the war, the disrupters demand dropped until the 70s, when Canadians used them because of bombs placed by the Quebec Liberation

Front - a terrorist group. Initially, they were used in hand until a modern disruptor was invented which, placed on a tripod, could be used remotely.

Research programs have been developed by various companies, which have sought to respond to the current needs. Recently, due to new threats, tests were also made for neutralizing bombs which contain harmful agents (nuclear, chemical or biological). Reboundless disruptor is another innovation that can be used on remote controlled robots. There are calibre-disruptors 12.5 mm and 20 mm, and 12.5 mm versions, 20 mm, 29 mm.

Although the targets are very different, they can be successfully used for neutralization. Given the events, also studied is the possibility of using them for the packages with hard walls, by using projectiles. Disruptors of 12.5 mm were successfully used to neutralize mines with external warheads, being considered a leader in this technology. It can be used manually or mounted on the robot. It is power supplied to the 24V/1A, and may be used from the battery of the robot. The preparation time for drawing is 2.5 minutes. The maximum firing distance is 3 m.

If we add the fact that the distruptors are "collective weapons systems" and through them a "hidden" struggle is led with the most varied and dangerous targets, we can conclude that the importance of their projection is motivated.

It is in the interest of the intervention forces to know the weapons and ammunition they are confronted with. This information can give them confidence that the system used is effective, safe and more than that it is not used against their own forces.

In other words, the system needs to be dismantled using physical or functional improvised explosive device and it should not be opened unintentionally. This is possible only through proper knowledge of its properties.

2. Determination of existing ballistic cartouche

To determine the performance characteristics of the disruptor, experimental studies and shootings were made.

We determined:

- initial velocity of the projectile (agent of disruption being water);
- variation of the pressure in the pipe with respect to time;
- geometry of the water jet;
- influence of various parameters on the operation of the disruptor (plugs, the amount of water etc.);
- intensity of the sound wave emitted from the operation of the system.

The experimental configuration used to determine the ballistic characteristics, initial velocity and pressure is shown schematically in Figure 1.

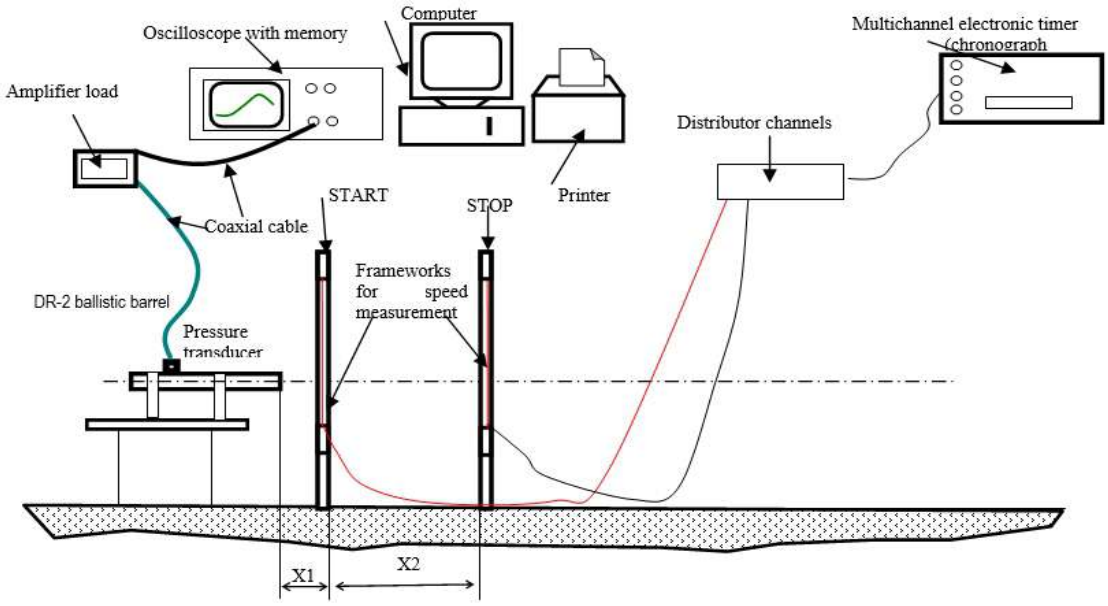

Fig. 1. *Scheme of the experimental set*

3. Experimental test results

As regards the ballistic tests, we considered: materials used, initial conditions, jet speed, pressure, noise level. Pictures of the geometrical configuration of the water jet propelled by the disruptor during shooting, for first shooting, are presented in Figure 2.

Shooting 1
Image water jet after 40 ms

Shooting 1
Image water jet after 80 ms

Shooting 1
Image water jet after 120 ms

Shooting 1
Image water jet after 160 ms

Shooting 2
Image water jet after 40 ms

Shooting 2
Image water jet after 80 ms

Shooting 2
Image water jet after 120 ms

Shooting 3
Image water jet after 40 ms

Shooting 3
Image water jet after 80 ms

Shooting 4
Image water jet after 40 ms

Shooting 4
Image water jet after 80 ms

Shooting 5
Image water jet after 40 ms

Shooting 5
Image water jet after 80 ms

Shooting 6
Image water jet after 40 ms

Shooting 6
Image water jet after 80 ms

Shooting 7
Image water jet after 40 ms

Shooting 7
Image water jet after 80 ms

Fig. 2. *Analysis of the geometrical configuration of jets: images of the water jet*

4. Conclusions

Analyzing the used cartouche configuration and given the deficiencies found, the following assumptions can be made:

- The colloidal powder used is Vufl, which explains the incomplete combustion of powder granules in some cases (especially when not using plugs).

- The use of retaining plugs of the disruption agent has an important role in the interior ballistics of the cartouche, but they are propelled at high speed along with the stream of the disruption agent; if water is used, the characteristics of the shock induced in different targets are amplified by the shock characteristics of the materials which the corks are made of; we can say, therefore, that the initiation of the explosive caps is produced by the action of the plugs and not by the water jet.

- It is possible to provide an adequate initial speed to the stream of water propelled by the disruptor if a new type of colloidal powder is used, easily inflammable and a high combustion speed; this can ensure the complete combustion of the powder grains before they enter the water column disposed in the disruptor pipe.

- In order to ignite the flinging load, it is possible to imagine another damper with combustion temperatures higher than those given by the black powder used in the electric damper of the cartouche in operation.

- Sealing the cartouche has a major importance in developing the phenomena following its subsequent ignition; it is possible to replace the existing stopper plug (plastic) with a different constructive solution, for example by means of a glass (stopper) with a very small weight, which can be assembled to the cartouche by means of an epoxy resin; this solution can solve the problem of the cartouche tightness in a proper manner, without inducing significant shocks to the targets.

Given the assumptions presented, the following results were obtained:

- exploration of the possibility of replacing the cartouche cal. 12.7 mm commonly used;

- study of the ballistic characteristics of the existing cartouche:

- initial speed of the jet and its geometric configuration;

- pressure value in loading chamber versus time;

- noise level produced at the load flinging initiation;

- identification of a powder for the load flinging whose combustion is complete;

- determining the load flinging mass ensuring ballistic performance similar to existing cartouche (initial speed while preserving the maximum level of pressure);

- replacement of the electric primer by using a new ignition composition, charged in a different configuration;

- finding a viable solution for the new cartouche seal;

- complete removal of restraint plugs of the disruption agent in the disruptor pipe;

- interaction between water jet propelled through the new cartouche with an electric detonator (as a possible component of an explosive device); the latter should not be initiated.

References

[1]. Goga, D.A., *Probleme speciale de detonică*, Editura Academia Tehnică Militară, Bucureşti, 2008.
[2]. Kinney, G.F., Graham, K.I., *Explosive Shocks in air*, Second Edition Poringer–Verlag Berlin Heidelberg, New York Tokyo, 1985
[3]. Kistiakovsky, G. B., Wilson E. B., *Teoria hidrodinamică a detonaţiei şi undele de şoc*, Report 114,1941
[4]. Thevenin, M., *Metode moderne în pirotehnie şi detonică*, Paris, 1972
[5]. Voicu V., *Sisteme clasice pentru neutralizarea dispozitivelor explozive artizanale utilizate de specialişti din alte ţări*, a XIX – a Sesiune de Comunicări Ştiinţifice cu participare internaţională „NAV – MAR – EDU 2005", Constanţa, 2005
[6]. Voicu V., *Studiul dispozitivelor explozive artizanale şi al mijloacelor de neutralizare a acestora*, Referat 3, Academia Tehnică militară, Bucureşti, 2002
[7]. Voicu V., *Studiul teoretic şi experimental al propulsiei jeturilor de neutralizare prin deflagraţia pulberilor*, Bucureşti, Revista Tehnică Militară nr. 2, 2004.
[8].***, http://www.internationalindustries.net/Proparms/index.htm
[9]. ***, http://www.antennasystems.com/disrupters/0201102.html.
[10]. ***, http://www.proparms.com/site/product_6.html.
[11]. ***, http://www.nrm.qld.gov.au/mines/explosives/incidents.html.
[12]. ***, http://www.fbi.gov/publications/terror.

MANUSCRISELE, CĂRŢILE ŞI REVISTELE PENTRU SCHIMB, PRECUM ŞI ORICE CORESPONDENŢE SE VOR TRIMITE PE ADRESA:

MANUSCRIPTS, REVIEWS AND BOOKS FOR EXCHANGE COOPERATION, AS WELL AS ANY CORRESPONDENCE WILL BE MAILED TO:

LES MANUSCRIPTS, LES REVUES ET LES LIVRES POUR L'ECHANGE, TOUT AUSSI QUE LA CORRESPONDANCE SERONT ENVOYES A L'ADRESSE:

MANUSCKRIPTEN, ZIETSCHRITFTEN UND BUCHER FUR AUSTAUCH SOWIE DIE KORRESPONDENZ SID AN FOLGENDE ANSCHRIFT ZU SEDEN:

After the latest evaluation of the journals by the National Center for Science Policy and Scientometrics (**CENAPOSS**), as recognition of its quality and impact at national level, the journal will be included in the B^+ category, 215 code (http://cncsis.gov.ro/userfiles/file/CENAPOSS/Bplus_2011.pdf).

The journal is already indexed in:

EBSCO: http://www.ebscohost.com/titleLists/a9h-journals.pdf

Copernicus: http://journals.indexcopernicus.com/karta.php

The papers published in this journal can be visualized on the site of "Dunarea de Jos" University of Galati, the Faculty of Engineering, pages: http://www.sim.ugal.ro/Annals.htm, http://www.imsi.ugal.ro/Annals.html.

Publisher's Name and Address:
Contact person: Antoaneta CĂPRARU
Galati University Press - GUP
47 Domneasca St., 800008 - Galati, Romania
Phone: +40 336 130139, Fax: +40 236 461353
Email: gup@ugal.ro

Editor's Name and Address:
Prof. Dr. Eng. Marian BORDEI
Dunarea de Jos University of Galati, Faculty of Engineering

111 Domneasca St., 800201 - Galati, Romania
Phone: +40 336 130208
Phone/Fax: +40 336 130283
Email: mbordei@ugal.ro

AFFILIATED WITH:

- THE ROMANIAN SOCIETY FOR METALLURGY
- THE ROMANIAN SOCIETY FOR CHEMISTRY
- THE ROMANIAN SOCIETY FOR BIOMATERIALS
- THE ROMANIAN TECHNICAL FOUNDRY SOCIETY
- THE MATERIALS INFORMATION SOCIETY (ASM INTERNATIONAL)

Edited under the care of
FACULTY OF ENGINEERING
Annual subscription (4 issues per year)

Editing date: 15.12.2014
Number of issues: 200
Printed by Galati University Press (accredited by CNCSIS)
47 Domneasca Street, 800008, Galati, Romania